To the Graduate Council:

I am submitting herewith a dissertation written by Barbara Jane Sheppard entitled "The Role Of Calcium Channels In The Growth Regulation Of Normal And Neoplastic Neuroendocrine Lung Cells." I have examined the final copy of this dissertation for form and content and recommend that it be accepted in partial fulfillment of the requirements for the degree of Doctor of Philosophy, with a major in Comparative and Experimental Medicine.

Hildegard M. Schuller, Major Professor

We have read this dissertation
And recommend its acceptance:

Accepted for the Council:

Associate Vice Chancellor And
Dean Of The Graduate School

THE ROLE OF CALCIUM CHANNELS IN THE GROWTH REGULATION OF NORMAL AND NEOPLASTIC NEUROENDOCRINE LUNG CELLS

A Dissertation
Presented for the
Doctor of Philosophy
Degree
The University of Tennessee, Knoxville

Barbara Jane Sheppard, DVM, MS
May, 1999

Copyright @ Barbara Jane Sheppard, 1999
All rights reserved

Dedication

To my mother Martha Jane Serven (1936-1979)

Acknowledgements

It is a great pleasure to have an opportunity to thank in spirit if not in name the many people who have helped me to reach this point. This thank you is certainly extended to my PhD advisor Dr. Hildegard Schuller and my PhD Committee members Dr. Kevin Hahn, Dr. George Kabalka and Dr. David Slauson. I would also like to thank Michelle Williams whose technical expertise and encouragement has been invaluable, Brian Porter and Dr. Neil Quigley for conducting the cDNA band sequencing.

This work was supported by PHS grants RO1CA51211 and T32 ESO7285-04.

Abstract

The binding of nicotine or nicotine-derived carcinogenic nitrosamines at the alpha$_7$ nicotinic acetylcholinergic receptor (α_7-nAChR) on the surface of human small cell lung carcinomas (SCLC) and pulmonary neuroendocrine cells (PNEC) stimulates release of the autocrine growth factor 5-HT. The release and reuptake of 5-HT leads to cell proliferation. Thus, nicotinic agonists acting at the cell surface α_7-nAChR, which is a functional Ca^{2+} channel, initiate a mitogenic autocrine loop with growing evidence of downstream activation of intracellular kinase-driven signaling cascades involving the *raf* kinases . The central role of Ca^{2+} as a second messenger in kinase-driven signaling pathways strongly suggests that cellular tools for controlling Ca^{2+} movement, such as VOCC, are upregulated in SCLC cells derived from chronic smokers.

It was shown using flow cytometry that nicotine and the nicotine-derived carcinogenic nitrosamine nitrosamine 4-(methylnitrosamino)-1-(3-pyridyl)-1-butanone (NNK) treatment of SCLC-derived NCI-H69 cells stimulated the influx of extracellular Ca^{2+} through α_7-nAChR followed by Ca^{2+} movement through voltage-operated calcium channels (VOCC). The maximal Ca^{2+} influx was observed with much lower doses of NNK (100pM) compared to nicotine (1μM) indicating a much greater affinity of NNK for the α_7-nAChR. PNEC exposed to nicotine or NNK

demonstrated a much smaller amount of Ca^{2+} influx indicating that the neoplastic SCLC cells exhibit an increased responsiveness to both compounds.

This work demonstrated, using relative quantitative reverse transcription - polymerase chain reaction (RQ RT-PCR), high expression levels by untreated NCI-H69 cells of all three "L, N, and P" VOCC subtype cDNA targets examined. In contrast, fetal hamster PNEC demonstrated a significant expression of only the "P" subtypes. The NCI-H69 exhibited this greatly enhanced expression of all the VOCC subtypes due to the massive upregulation of the serotonergic autocrine mitogenic pathway following years of exposure to nicotine and nicotine-derived carcinogenic nitrosamines such as NNK and to the hypoxia of concurrent chronic lung disease. It was also shown that NCI-H69 display a subtype-dependent alteration in VOCC subtype expression levels when subchronically exposed to constant uninterrupted nicotine, NNK or hypoxia.

These findings strongly support the hypothesis that the NCI-H69 cell line derived from the SCLC of a chronic smoker demonstrated a massively upregulated ability to manipulate Ca^{2+} levels using the α_7-nAChR Ca^{2+} channel and VOCCs. Unique levels or patterns of VOCC expression by SCLC may provide clinically useful targets in the search for better diagnostic and therapeutic options with which to combat this aggressive tumor type.

TABLE OF CONTENTS

CHAPTER PAGE

PART 1. GENERAL INTRODUCTION AND OVERVIEW

1. GROWTH PROMOTION OF HUMAN SMALL CELL LUNG CANCER....2
2. VOLTAGE OPERATED CALCIUM CHANNELS.....11
3. PROJECT OVERVIEW – HYPOTHESES AND OBJECTIVES 18

APPENDIX 20

PART II. CALCIUM MOVEMENT

1. ABSTRACT.....28
2. INTRODUCTION.....30
3. MATERIALS AND METHODS 34
4. RESULTS 40
5. DISCUSSION 45

APPENDIX 53

TABLE OF CONTENTS

CHAPTER PAGE

PART III. CHARACTERIZATION OF VOLTAGE OPERATED CALCIUM CHANNELS

1. ABSTRACT 90
2. INTRODUCTION 92
3. MATERIALS AND METHODS 102
4. RESULTS 113
5. DISCUSSION 118

APPENDIX 132

PART IV. CHANGES IN THE EXPRESSION LEVEL OF VOCC IN RESPONSE TO NICOTINE, NNK OR HYPOXIA AS ASSESSED BY RELATIVE QUANTITATIVE RT-PCR

1. ABSTRACT..... 141
2. INTRODUCTION 143
3. MATERIALS AND METHODS 147
4. RESULTS 157
5. DISCUSSION 160

APPENDIX 163

TABLE OF CONTENTS

CHAPTER PAGE

PART V. OVERALL SUMMARY

1. SUMMARY 180

PART VI. REFERENCES CITED

1. REFERENCES CITED.....192

VITA 208

LIST OF TABLES

TABLE PAGE

Table 2-1: NCI-H69: Dose Response Studies With Nicotine 54
(Figure 2-1)

Table 2-2: NCI-H69: Dose Response Studies With Calcium in Buffer 55
At A Nicotine Concentration of 1 μM (Figure 2-2)

Table 2-3: NCI-H69: Inhibition Of Response To 1 μM Nicotine by 56
α-BTX (Figure 2-3)

Table 2-4: NCI-H69: Comparison Of Response To 1 μM Nicotine 57
With Membrane Depolarization By 50 mM KCl (Figure 2-4)

Table 2-5: NCI-H69: Dose Response Studies With NNK (Figure 2-5).....58

Table 2-6: NCI-H69: Inhibition Of Response To 5 nM NNK by 59
α-BTX (Figure 2-6)

Table 2-7: NCI-H69: Effect Of Chronic Exposure To 10% CO_2 60
On Dose Response To NNK (Figure 2-7)

Table 2-8: NCI-H69: Comparison Of Response To 30 nM NNK 61
In An Environment Of 5% and 10% CO_2 (Figures 2-8 and 2-11)

Table 2-9: NCI-H69: Inhibiting Effects of α-BTX On The Response 62
To 30nM NNK In An Environment Of 10% CO_2 (Figures 2-9 and 2-11)

Table 2-10: NCI-H69: Inhibiting Effects Of The N-type Calcium 63
Channel Blocker ω-Conotoxin (CTX) GVIA On The Response
To 30 nM NNK in 10% CO_2 (Figures 2-10 and 2-11)

Table 2-11: PNEC: Dose Response Studies With Nicotine 64
(Figure 2-12)

Table 2-12: PNEC: Dose Response Studies With Calcium in Buffer 65
At A NicotineConcentration of 1 μM (Figure 2-13)

LIST OF TABLES

TABLE PAGE

Table 2-13: PNEC: Inhibition Of Response To 1 μM Nicotine by 66
α-BTX (Figure 2-14)

Table 2-14: PNEC: Dose Response Studies With NNK (Figure 2-15) 67

Table 2-15: PNEC: Dose Response Studies With Calcium in Buffer 68
At A NNK Concentration of 1 nM (Figure 2-16)

Table 2-16: PNEC: Inhibition Of Response To 1 nM NNK by 69
α-BTX (Figure 2-17)

Table 2-17: PNEC: Inhibiting Effects Of The Broad Spectrum Blocker 70
Of Neuronal nAChR, Hexamethonium, On The Response To 1 nM
(Figure 2-18)

Table 3-1: NCI-H69: Saturation Binding With ^{3}H-desmethoxyverapamil 127
And Nifedipine

Table 3-2: NCI-H69: Competition Binding With ^{3}H-desmethoxyverapamil 129
And Nifedipine

Table 3-3: NCI-H69: Saturation Binding With ^{125} I-ω-Conotoxin GVIA 130
and ω-Conotoxin GVIA

Table 3-4: NCI-H69: Competition Binding With ^{125} I-ω-Conotoxin GVIA, ...131
ω-Conotoxin GVIA and ω-Conotoxin MVIIA

Table 3-5: PNEC: Saturation Binding With ^{3}H-desmethoxyverapamil 132
And Nifedipine

Table 4-1: Relative Quantitative Reverse Transcriptase-Polymerase 164
Chain Reaction (RQ RT-PCR): NCI-H69 and PNEC: Phosphorimager
Volume Density Report Raw Data By Rectangle

LIST OF TABLES

TABLE PAGE

Table 4-2: RQ RT-PCR: Comparison Of "L, N and P" Type 166
Calcium Channel Expression In Untreated PNEC And Untreated
NCI-H69 Expressed Relative To Untreated NCI-H69.

Table 4-3: RQ RT-PCR: Comparison Of "L" Type Calcium Channel 166
Expression In NCI-H69 And PNEC Treated With Nicotine, NNK
Or Hypoxia Expressed Relative To Untreated NCI-H69.

Table 4-4: RQ RT-PCR: Comparison Of "N" Type Calcium Channel 167
Expression In NCI-H69 And PNEC Treated With Nicotine, NNK
Or Hypoxia Expressed Relative To Untreated NCI-H69.

Table 4-5: RQ RT-PCR: Comparison Of "P" Type Calcium 167
Channel Expression In NCI-H69 And PNEC Treated With
Nicotine, NNK Or Hypoxia Expressed Relative To Untreated NCI-H69.

Table 4-6: RQ RT-PCR: Comparison Of "L, N and P" Type 168
Calcium Channel Expression In NCI-H69 Treated With
Nicotine, NNK Or Hypoxia Expressed Relative To Untreated NCI-H69.

Table 4-7: RQ RT-PCR: Comparison Of "L, N and P" Type 168
Calcium Channel Expression In PNEC Treated With Nicotine or
NNK Expressed Relative To Untreated NCI-H69.

Table 4-8: RQ RT-PCR: Comparison Of "P" Type Calcium 169
Channel Expression In PNEC Treated With Nicotine or NNK
Expressed Relative To Untreated NCI-H69.

LIST OF FIGURES

FIGURE PAGE

Figure 1-1: Serotonergic Mitogenic Pathway In Pulmonary Neuroendocrine Cells 21

Figure 1-2: Voltage-Gated Calcium Channels 22

Figure 1-3: Neuronal Calcium Channel Toxins 23

Figure 1-4: Genetic Basis of Voltage-Activated Calcium Channels in Neural/Neuronally derived Tissues 24

Figure 1-5: CDNA Sequenced from Alpha-1 Subunits of Voltage-Activated Calcium Channels 26

Figure 2-1: NCI-H69: Dose Response Studies With Nicotine (Table 2-1) 71

Figure 2-2: NCI-H69: Dose Response Studies With Calcium in Buffer At A Nicotine Concentration of 1 μM (Table 2-2) 72

Figure 2-3: NCI-H69: Inhibition Of Response To 1 μM Nicotine by α-BTX (Table 2-3) 73

Figure 2-4: NCI-H69: Comparison Of Response To 1 μM Nicotine With Membrane Depolarization By 50 mM KCl (Table 2-4) 74

Figure 2-5: NCI-H69: Dose Response Studies With NNK (Table 2-5) 75

Figure 2-6: NCI-H69: Inhibition Of Response To 5 nM NNK by α-BTX (Table 2-6) 76

Figure 2-7: NCI-H69: Effect Of Chronic Exposure To 10% CO_2 On Dose Response To NNK (Table 2-7) 77

Figure 2-8: NCI-H69: Comparison Of Response To 30 nM NNK In An Environment Of 5% and 10% CO_2 (Table 2-8) 78

LIST OF FIGURES

FIGURE PAGE

Figure 2-9: NCI-H69: Inhibiting Effects of α-BTX On The 79
Response To 30nM NNK In An Environment Of 10% CO_2
(Table 2-9)

Figure 2-10: NCI-H69: Inhibiting Effects Of The N-type Calcium 80
Channel Blocker ω-Conotoxin (CTX) GVIA On The Response
To 30 nM NNK in 10% CO_2 (Table 2-10)

Figure 2-11: NCI-H69: Comparison Of The Inhibiting Effects Of 81
α-BTX Or The N-type Calcium Channel Blocker ω-Conotoxin
(CTX) GVIA On The Response To 30nM NNK In An Environment
Of 10% CO_2 And The Response To 30nM NNK In An Environment
Of 5% CO_2 (Tables 2-8, 2-9 and 2-10)

Figure 2-12: PNEC: Dose Response Studies With Nicotine 82
(Table 2-11)

Figure 2-13: PNEC: Dose Response Studies With Calcium in 83
Buffer At A Nicotine Concentration of 1 μM (Table 2-12)

Figure 2-14: PNEC: Inhibition Of Response To 1 μM Nicotine 84
by α-BTX (Table 2-13)

Figure 2-15: PNEC: Dose Response Studies With NNK 85
(Table 2-14)

Figure 2-16: PNEC: Dose Response Studies With Calcium in 86
Buffer At A NNK Concentration of 1 nM (Table 2-15)

Figure 2-17: PNEC: Inhibition Of Response To 1 nM NNK by 87
α-BTX (Table 2-16)

Figure 2-18: PNEC: Inhibiting Effects Of The Broad Spectrum 88
Blocker Of Neuronal nAChR, Hexamethonium, On The Response
To 1 nM NNK (Table 2-17)

LIST OF FIGURES

FIGURE PAGE

Figure 3-1: Reverse Transcriptase-Polymerase Chain Reaction 133
(RT-PCR) For "L, P And N" Type VOCC In Untreated NCI-H69
And PNEC Cells.

Figure 3-2: cDNA Sequence Homology Of NCI-H69 353bp "L" 135
Band With GenBank M76558

Figure 3-3: cDNA Sequence Homology Of PNEC 353bp "L" 136
Band With GenBank M76558

Figure 3-4: cDNA Sequence Homology Of NCI-H69 390bp "N" Band 137
With GenBank M94172

Figure 3-5: cDNA Sequence Homology Of NCI-H69 345bp "P" Band 138
With GenBank S76537

Figure 3-6: cDNA Sequence Homology Of PNEC 345bp "P" Band 139
With GenBank S76537

Figure 4-1: Relative Quantitative Reverse Transcriptase Polymerase 170
Chain Reaction (RQ RT-PCR): Comparison Of Expression Levels
of "L" Type VOCC by NCI-H69 And PNEC Treated With Nicotine,
NNK And Hypoxia Using "L" Type Primers And A 2:8 Ratio Of 18S
Primer/Competimer.

Figure 4-2: RQ RT-PCR: Comparison Of Expression Levels of 171
"N" Type VOCC by NCI-H69 And PNEC Treated With Nicotine,
NNK And Hypoxia Using "N" Type Primers And A 2:8 Ratio Of 18S
Primer/Competimer.

LIST OF FIGURES

FIGURE PAGE

Figure 4-3: RQ RT-PCR: Comparison Of Expression Levels of 172
"P" Type VOCC by NCI-H69 And PNEC Treated With Nicotine,
NNK And Hypoxia Using "P" Type Primers And A 2:8 Ratio Of 18S
Primer/Competimer.

Figure 4-4: RQ RT-PCR: Comparison Of "L, N and P" Type 173
Calcium Channel Expression In Untreated PNEC And Untreated
NCI-H69 Expressed Relative To Untreated NCI-H69.

Figure 4-5: RQ RT-PCR: Comparison Of "L" Type Calcium 174
Channel Expression In NCI-H69 And PNEC Treated With
Nicotine, NNK Or Hypoxia Expressed Relative To Untreated
NCI-H69.

Figure 4-6: RQ RT-PCR: Comparison Of "N" Type Calcium 175
Channel Expression In NCI-H69 And PNEC Treated With
Nicotine, NNK Or Hypoxia Expressed Relative To Untreated
NCI-H69.

Figure 4-7: RQ RT-PCR: Comparison Of "P" Type Calcium 176
Channel Expression In NCI-H69 And PNEC Treated With
Nicotine, NNK Or Hypoxia Expressed Relative To Untreated
NCI-H69.

Figure 4-8: RQ RT-PCR: Comparison Of "L, N and P" Type 177
Calcium Channel Expression In NCI-H69 Treated With Nicotine,
NNK Or Hypoxia Expressed Relative To Untreated NCI-H69.

Figure 4-9: RQ RT-PCR: Comparison Of "L, N and P" Type 178
Calcium Channel Expression In PNEC Treated With Nicotine
or NNK Expressed Relative To Untreated NCI-H69.

Figure 4-10: RQ RT-PCR: Comparison Of "P" Type Calcium 179
Channel Expression In PNEC Treated With Nicotine or NNK
Expressed Relative To Untreated NCI-H69.

LIST OF ABBREVIATIONS

α-BTX – alpha bungarotoxin

α_7-nACHR – nicotinic acetylcholine receptor comprised of alpha 7 subunits

BCA – bicinchoninic acid assay to determine protein concentration

BSA – bovine serum albumin

$CaCl_2$ – calcium chloride

CsCl – cesium chloride

CTX – conotoxin

dATP – deoxy- adenine triphosphate

dCTP – deoxy- cytosine triphosphate

dGTP – deoxy-guanosine triphosphate

DNA – deoxyribonucleic acid

dNTP – deoxy- nucleotide triphosphate

dTTP - deoxy- thymidine triphosphate

EDTA – ethylene diamine tetratacetic acid

GIT – guanidine isothiocyanate

Ki-*ras* – intracellular signaling factor

M-MLV – Maloney-Murine Leukemia Virus – source of reverse transcriptase enzyme in the reverse transcription reaction.

MAP – mitogen activated/associated protein

LIST OF ABBREVIATIONS

NNK – nicotine-derived carcinogenic nitrosamine 4-(methylnitrosamino)-1-(3-pyridyl)-1-butanone

NNN – nicotine-derived carcinogenic nitrosamine N'-nitrosonornicotine

ω-CTX GVIA – omega conotoxin GVIA

ω-CTX MVIIA – omega conotoxin MVIIA

PAC – pulmonary adenocarcinoma of Clara cell phenotype

PBS – phosphate buffered saline

PNEC – pulmonary neuroendocrine cell

Random decamers – first-strand primers used in the reverse transcriptase reaction to reverse transcribe all RNA.

RNA – ribonucleic acid

RNasin – placental RNase inhibitor

RQ – relative quantitative

RT-PCR – reverse transcriptase polymerase chain reaction

SCLC – small cell lung carcinoma

TBE – TBE buffer

Tris – tris buffer

NCI-H69 – Cell line derived from human SCLC

PART 1: GENERAL INTRODUCTION AND OVERVIEW

Chapter 1: Growth Promotion Of Human Small Cell Lung Cancer

I. Human Lung Cancer And Smoking

According to the American Cancer Society (1997), the incidence of human lung cancer continues to increase in all industrialized nations with smoking repeatedly identified as a key risk factor (Wagenaar and Tazelaar 1994). Human small cell lung cancer (SCLC), referred to as a "smoking-specific" cancer, occurs almost exclusively in smokers with a history of chronic lung disease (Weiss 1991). Representing 25% of all human lung cancer cases, SCLC is initially responsive to radiation and chemotherapy, however, the five year survival rate is below 5% (Hansen and Rorth 1997). The low survival rate is due to resumption of cancer growth associated with extensive metastatic spread (Cook et al. 1993).

II. Mechanisms Of Carcinogenesis

One frequently proposed hypothesis for this smoking-associated growth promotion was the possible genetic mutation of a factor, such as Ki-*ras*, known to have a key role in the signal transduction pathway utilized by many growth factors

(Segar and Krebs 1995). This phenomenon is well described in human pulmonary adenocarcinomas (PAC) derived from the bronchiolar Clara cells (Linnoila 1990). Exposure of laboratory rodents to the tobacco-specific carcinogenic nicotine-derived nitrosamine 4-(methylnitrosamino)-1-(3-pyridyl)-1-butanone (NNK) results in the formation of PAC of a Clara cell phenotype (Hecht and Hoffman 1988; Schuller et al. 1990). These PAC cells have a high incidence of Ki-*ras* gene mutation (Mitsudomi et al. 1991) which is most commonly a point mutation at codon 12 (Mitsudomi et al. 1991, Yesner 1993). Formation of this mutation was highly correlated with the metabolism of NNK to O^6-methylguanine (Belinsky et al. 1989) indicating that metabolism of NNK by the PAC cells preceded mutation of the Ki-*ras* gene. In contrast, SCLC cells are unable to metabolize NNK (Falzon et al. 1986a) due to a lack of the necessary enzyme profile (Falzon et al. 1986b), thereby making them unable to generate the NNK metabolite, O^6-methylguanine, associated with mutation of the Ki-*ras* gene. In light of the inability of SCLC cells to metabolize NNK, any growth promotion effect of NNK on SCLC must utilize a separate mechanism.

II. Pulmonary Neuroendocrine Cells And The Biogenic Amine Serotonin

Progress toward understanding the factors potentially driving the high relapse rate of SCLC has come largely from the realization that this histologic cancer demonstrates a neuroendocrine phenotype and, therefore, shares many morphologic and functional characteristics with normal pulmonary neuroendocrine cells (PNEC, Linnoila 1996). PNEC possess a cell membrane oxygen binding protein that responds to changes in the relative proportions of the intrapulmonary gases O_2 and CO_2 (Youngson et al. 1993). Under conditions of decreased lung oxygenation such as in the normal neonatal lung or the pathologic predicament of chronic lung diseases, PNEC exhibit a hyperplastic response and enhanced secretion of the biogenic amine serotonin (5-hydroxytryptamine, 5-HT, Youngson et al. 1993, Johnson and Georgieff 1989, Guyton and Hall 1996). The classic pulmonary physiological consequences of 5-HT release are constriction of bronchial smooth muscle and concentration dependent vasodilatation or vasoconstriction (Garrison 1990). Recent advances in the understanding of normal and neoplastic PNEC physiology has identified 5-HT as an autocrine growth factor for these cells (Cattaneo et al. 1993, Schuller and Hegedus 1989) although neuropeptides of the bombesin family were the first autocrine growth factors discovered to promote growth of normal and neoplastic PNECs (Bunn et al. 1994). In one study, almost

100% of SCLC were found to express the biogenic amine growth factor 5-HT whereas only a subset of cells expressed neuropeptides of the MB family and their receptors (Gazdar 1994). These findings collectively suggested that growth promotion occurring during the recurrence phase of human SCLC involves a combination of factors including 5-HT, nicotine-derived carcinogenic nitrosamines and chronic hypoxia associated with chronic lung disease. Research, described in detail below, examining this growth promotion phenomenon have collectively shown that cell lines derived from SCLC are regulated by a mitogenic autocrine serotonergic loop driven by stimulation of α-bungarotoxin (α-BTX)-sensitive neuronal α_7 nicotinic acetylcholine receptors (α_7-nAChR) by nicotine and nicotine-derived metabolites and by concurrent hypoxia (Figure 1-1)1.

IV. The Mitogenic Autocrine Serotonergic Loop

The mitogenic autocrine serotonergic loop in PNEC begins with activation of the neuronal α-BTX-sensitive α_7-nAChR expressed at the cell surface. The only successful in vivo experimental induction of a neuroendocrine lung cancer type was achieved in hamsters exposed simultaneously to carcinogenic nitrosamines and hyperoxic lung injury (Schuller et al. 1988, Schuller et al. 1990) or to nicotine and

1 All Figures can be found in the Appendix at the end of Part I.

hyperoxic lung injury (Schuller at al. 1995). A series of in vitro investigations using cell lines derived from SCLC and normal fetal hamster PNEC has attempted to elucidate the mechanisms of this phenomenon. Neuroendocrine cell lines derived from lung carcinoid tumors or SCLC (Schuller et al. 1994) proliferated when treated with nicotine or the structurally related NNK. This proliferation was potentiated by simultaneous exposure to elevated atmospheric CO_2 (Schuller 1989, Schuller and Hegedus 1989). Similar effects of nicotine, NNK and CO_2 were observed in cell lines derived from SCLC and the mitogenic response was blocked by 5-HT/MB receptor antagonists and protein kinase C inhibitors (Schuller 1994). Proliferation is also blocked in the presence of the α_7-nAChR antagonists α-BTX and hexamethonium, a broad spectrum blocker of all neuronal nicotinic receptors (Schuller 1989, Schuller and Hegedus 1989). A separate study demonstrated release of 5-HT by SCLC in response to nicotine (Cattaneo et al. 1993). Together these findings implicate an initial interaction of nicotine and/or NNK at the cell surface α_7-nAChRs of SCLC and the subsequent role of 5-HT in a mitogenic kinase signaling pathway.

V. The Role Of Hypoxia

The nicotine and NNK-induced cell proliferation occurred at 10% but not 5% atmospheric CO_2 in one dose exposure experiments (Maneckjee and Minna 1990,

Schuller 1994). This level of atmospheric CO_2 is important because the intrapulmonary concentration of CO_2 in the healthy adult lung is 5% whereas a CO_2 concentration of 10% simulates the intrapulmonary levels of this gas in a mildly diseased lung (Guyton and Hall 1996). Therefore, growth promotion in response to nicotine and NNK was most remarkable under the hypoxic conditions of a chronically diseased lung which is in agreement with the high incidence of SCLC in smokers with chronic lung disease.

VI. The Role Of NNK

The significance of the tobacco-specific carcinogenic nitrosamine NNK in the growth promotion of SCLC became disturbingly apparent when studies investigating the binding affinity of NNK for the α_7-nAChR of SCLC and fetal hamster PNEC were performed. They revealed that the affinity of NNK to the α_7 receptor was 1,300 times greater than that of nicotine and 3,500 times greater than that of the carcinogenic nicotine-derived nitrosamine N-nitrosonornicotine (NNN). Moreover, NNK-induced cell proliferation and DNA synthesis measured by incorporation of ^{3}H- thymidine was completely inhibited by α-BTX (Schuller and Orloff, 1998). NNN and NNK are formed from nicotine by nitrosation reactions during the processing of tobacco and also by endogenous nitrosation of nicotine within the body (Fischer et al. 1990, Hecht and Hoffmann 1988). Both NNK and

NNN cause lung tumors in laboratory rodents and are implicated in the high lung cancer burden observed in smokers, however, NNK is a much more potent carcinogen (Hecht and Hoffman 1988). The rich flavor of tobacco has long been associated with the tradition of curing or processing tobacco which is now known to generate the powerful tobacco-specific carcinogenic nitrosamine NNK. It is likely that this tradition has driven NNK-induced mitogenic serotonergic pathways in the SCLCs of tobacco users who have been sold products by an industry that has been made accountable only for the nicotine levels of their goods.

VII. Activation Of Downstream Signals

It is increasingly apparent that the release and re-uptake of the autocrine growth factors 5-HT and MB followed by the downstream activation of protein kinase C (PKC), raf kinases and c-*fos* are important events in the proliferative response to CO_2 , nicotine, and NNK (Fig 1-1). Activation of PKC by the addition of the PKC activator phorbol 12,13-dibutyrate mimicked the stimulating effect of 10% CO_2 when added to cells in an atmosphere of 5% CO_2 . In contrast, inhibition of PKC by the addition of the PKC inhibitors clomiphene and H7 reduced the mitogenic response to CO_2 in a dose-dependent manner (Schuller 1994). A 3-4 fold increase in the expression of c-*fos* RNA by Northern analysis was detected within 15 minutes following exposure of fetal hamster PNEC to 10% CO_2 (Miller et al.

1996). Nicotine stimulation of the GLC-8 SCLC line increased mitogen-activated protein (MAP) kinase activity in a concentration- and time-sependent manner (Cattaneo et al. 1997). Signaling pathways in many other cell types that involve PKC and c-*fos* activation are known to also include activation of one or more *raf* kinases. Investigations are currently underway that strongly suggest that activation of one or more *raf* kinases are involved in cell lines derived from SCLC and in fetal hamster PNEC (Jull and Schuller, unpublished). This serotonergic mitogenic response to elevated atmospheric CO_2 is unique to the neuroendocrine human lung cancer cell lines and PNEC as extensive examination of nonneuroendocrine human lung cancer cell lines (Merryman et al. 1997) has failed to detect a similar response in normal human bronchial and bronchiolar cells (Schuller, unpublished)

VIII. Searching For A Therapeutic Target

While the work thus far on the biology of this serotonergic mitogenic pathway in SCLC has made great strides, it does not yet provide a unique therapeutic target. Avoidance of nicotine and tobacco-derived carcinogenic nitrosamines could be achieved by behavioral modification, however, the hypoxia of chronic lung disease is unavoidable. While the α_7-nAChR is currently being explored as a potential target for diagnostic imaging of SCLC (Schuller and Kabalka, unpublished), this strategy may encounter some problems due to expression of this receptor in

selected areas of the hippocampus and adrenal medulla. The search for therapeutic targets is therefore additionally focusing on the role of Ca^{2+} movement prior to activation of the kinase cascade given the widespread role of Ca^{2+} as a second messenger. All nicotinic receptors are ligand-gated ion channels composed of 5 subunits that enclose a central aqueous pore through which the ions flow (Lindstrom et al. 1995). The α_7-nAChR ion channel is unique in that it demonstrates a selective permeability for Ca^{2+} ions, whereas the other neuronal nicotinic receptors ion channels do not display a preference for a single ion type (Gopalakrishnan et al. 1995 and 1996). The snake venom α-BTX binds with high affinity only to the small subset of neuronal nicotinic receptors (Gopalakrishnan et al. 1995 and 1996) having the α_7 and α_8 subunits which are expressed primarily in the brain and retina, respectively (Chini et al. 1994, Lindstrom et al. 1995). It is therefore apparent that the mitogenic autocrine serotonergic loop initiated by binding of nicotine or NNK at cell surface membrane α-BTX-sensitive α_7-nAChRs of SCLC begins with the influx of extracellular Ca^{2+} through the α_7-nAChR Ca^{2+} channel, however, this specific event has never been experimentally demonstrated. Membrane depolarization due to the Ca^{2+} influx leads to activation of voltage operated Ca^{2+} channels (VOCC). Chronic nicotinic stimulation with upregulation of the α_7-nAChR Ca^{2+} channels of SCLC is likely to result in upregulation of specific VOCC subtypes which would be potential therapeutic targets.

Chapter 2: Voltage Operated Calcium Channels (VOCC)

I. Evolution Of Calcium Channel Classification

Decades of study have led to a continuously evolving classification and functional description of various types of Ca^{2+} channels based on properties including voltage- and time-dependent kinetics, pharmacology, cellular distribution, and, most recently, genetic sequence homology (Tsien et al. 1991, De Waard et al. 1996, Clapham 1995, Cassola and Afeche 1996, Ertel and Ertel 1996 , McClesky 1994, Wickman and Clapham 1995, Stea et al. 1993, Uchitel 1997). Information from these sources is summarized in Figures 1-2 to 1-5. Early division of VOCC types into families based on kinetics, pharmacology and distribution has been largely confirmed and extensively refined by the analysis of cDNA sequence homology.

II. Pharmacological Classification Of Calcium Channels

High degrees of sequence homology suggest that the multiple classes of VOCC have evolved from a common ancestor (Tsien et al. 1991) but have diverged into at least two main subfamilies distinguished pharmacologically by their sensitivity to

dihydropyridines (DHP) (Figure 1-2). VOCC subtypes defined by their well-established responses to specific agonists and antagonists are designated as "L" which are DHP-sensitive, and "N, P, Q and T" which are DHP-insensitive (McCleskey 1994). Early kinetic work detected a distinct division of the channels into "low voltage activated" (LVA) and "high voltage activated" (HVA) classes. LVA channels, which include only the "T" subtype, are activated by low voltage depolarization to allow the brief passage of ions as would be needed for initiation of an action potential. HVA channels, which include the " L, N, P, Q," and new less well-defined "R" subtypes, require a much greater degree of membrane depolarization to be activated but allow ion passage for a more extended period of time. SCLC, as noncontractile cells, are more likely to express and use HVA. "L" channels are sensitive to widely used therapeutic "calcium channel blockers" including DHPs (nicardipine, nifedipine and nimodipine), phenylalkylamines (verapamil), and benzodiazepines (diltiazem) (Murad 1990), in addition to calciseptine from mamba snake venom, nitrendipine (DHP antagonist) and ω-agatoxin (ω-Agt) IIIA. Calciseptine is found in the venom of the mamba snake and agatoxins are polypeptides found in funnel-web spider venoms . Toxins affecting neuronal VOCC (Figure 1-3, Uchitel 1997, Cassola and Afeche 1996) include conotoxins (CTX) which marine snails use to paralyze their fish prey, funnel-web spider venoms (polyamines, polypeptides and grammotoxin), and mamba snake venoms (fasciculin, calciseptine, FS2 and calcicludine). Among the DHP-

insensitive VOCC subtypes, sensitivity differences are most effective in descriminating "N" from the "P" and "Q" subtypes.

III. Physical Structure Of Calcium Channels

Ion channels for different ion types all have a similar physical structure (McCleskey 1994, De Waard et al. 1996, Tsien et al. 1991). The channels are heteroligomeric complexes composed of a central ion pore designated as the α_1 subunit and additional adjacent subunits (α_2/δ, β, and γ) which modulate the action of the pore. For VOCC, the γ subunit has been defined in muscle but has not been found to be expressed in neuronal tissue. The α_1 subunit is composed of four homologous repeats referred to as domains I-IV each of which contains six transmembrane α-helical subunits referred to as S 1-6 interconnected by variably sized loops. Subunit 4 , which opens the channel in response to membrane depolarization, has repeated motifs of positively charged amino acids at every third or fourth position followed by hydrophobic amino acids. The actual ion pore is formed by the transmembrane α-helices S4, S5, S6 and the loop connecting S5 to S6. The "alpha-1 interaction domain" (AID, De Waard et al. 1996) which interacts with the β subunit is the cytoplasmic loop separating the first and second hydrophobic repeats (I-II) that contain 18 amino acids of which nine are conserved. The AID epitope is QQ-E----L-GY---WI---E. Interactions of the channels with

some proteins such as syntaxin involve the cytoplasmic loop between domains II and III. Slight variations in the amino acid sequences of the α_1 subunit transmembrane α-helices and intervening loops are responsible for the antagonist/agonist sensitivites of each pharmacologically-defined VOCC family. Amino acid conservation of each α_1 subunit is higher (85%) between species than between different α_1 subunits within a single species (30-70%) which is similar to evolutionary conservation observed for other highly conserved proteins.

IV. Calcium Channel Genes

Any discussion of variations in amino acid sequence inevitably leads to the pursuit of the genes encoding the sequences and questions about posttranslational processing differences that might yield splice variants. That is exactly what happened with VOCCs. Genes coding the α_1 subunits are summarized in Figure 1-4 (Stea et al. 1993). GenBank cDNA sequences detected for the subunit genes in neuronal or neuroendocrine tissues for α_1 and ancillary subunits are summarized in Figure 1-5 (Barry et al. 1995, Dubel et al. 1992, Fujita et al. 1993, Hui et al. 1991, Kamphuis and Henriksen 1998, Ma et al. 1992, Mikami et al. 1989, Mori et al. 1991, Niidome et al. 1992, Seino et al. 1992, Snutch et al. 1990, Snutch et al. 1991, Soong et al. 1993, Starr et al. 1991, Williams et al. 1992a & b, Williams et al. 1994,).

V. The α_1 Subunit

The α_1 subunit is coded by 5 genes designated A-E (Snutch et al. 1990, Soong et al. 1993) for which the gene names agreed upon by most researchers are now indicated as CACNA1A-E referring to calcium channel alpha-1 subunit gene A-E. The genetic examination of neuronal VOCC has largely preserved the original pharmacological distinctions but has added the possibility that several different genes can code for pharmacologically similar VOCCs. This occurs for "L" type VOCC which are now further divided into "skeletal", "cardiac", and "neuroendocrine" subtypes coded by the S, C, and D genes (Tanabe et al. 1990, Williams et al. 1992a). Expression of the S gene has not been detected in neural tissues, and the C gene-encoded "L" channels have subsequently been detected in neural tissue despite having been named for their original cardiac site of discovery. Pharmacological "N" VOCCs are coded by the B gene (Williams et al. 1992b, Fujita et al. 1993, Stea et al. 1993) and the pharmacologically similar "P" and "Q" types are both coded by the A gene (Mori et al. 1991). An additional unique LVA type channel designated as "R" is coded by the E gene (Ellinor et al. 1993). Of all the ancillary subunits, it is currently believed that the β subunit is the most important modulator of α_1 subunit function (Mori et al. 1991, Ellinor et al. 1993, Stea et al. 1993, Hullin et al. 1992). The β subunit modulates the efficiency of

coupling between voltage sensing and pore opening but does not affect voltage sensing itself. α_1 subunits are variably functional in the absense of the beta subunit. The "beta interaction domain" (BID, De Waard et al. 1994), which modulates α_1 subunit function by interacting with AID, is comprised of 30 amino acids at the N-terminus of the second most conserved domain of β subunits. BID has 2 consensus sites for PKC thereby making it a potential regulatory target for PKC. The β subunit is encoded by four genes (Birnbaumer et al. 1994, De Waard et al. 1996) which yield four subdomains of which subdomains I and II are highly conserved. The genes are conveniently referred to as B1-4. The α_2 and δ subunits are encoded by the same gene which is well-conserved. Both subunits are encoded in the same primary transcript and are generated by posttranslational cleavage in muscle cells. Separate α_2 and δ polypeptides have not been identified from neuronal VOCCs. Transcripts of the γ subunit have not been detected in neural tissue. GenBank contains many cDNA sequences for the VOCC subunits that have been identified in cells of neuronal origin. Sequence homology for similar subunits coded for by specific genes for the α_1 subunit (CACNA1A-E) is often very high between species indicating that these are highly conserved genes. In some cases such as the "N" type CACNA1B (Williams et al. 1992a & b), two distinct sequences representing posttranslational splice variants are detected using the same set of primers in a reverse transcription-polymerase chain reaction (RT-PCR).

VI. Gene Target Verification

The structural similarity of all ion channel types and the high level of sequence homology within the VOCC make the choice of RT-PCR primers that will be specific for the targeted VOCC subunit subtype difficult as primers that generate a specific VOCC GenBank cDNA sequence in one species or one cell type may not generate that same cDNA band under different conditions. This necessitates the sequencing of cDNA bands generated by RT-PCR in order to verify that the target sequence has been successfully amplified and to screen for previously unidentified cDNA sequences with high homology to concensus motifs likely to represent VOCCs. The α_1 subunit is followed in importance by the β subunit which is an important modulator of the α_1 subunit pore function (De Waard et al. 1996). The β subunit BID's potential as a regulatory target for PKC may allow activated PKC generated by the autocrine serotonergic mitogenic pathway in SCLC to modulate β subunit expression or function which would in turn influence VOCC expression and function.

Chapter 3: Project Overview – Hypotheses And Objectives

I. The Central Hypothesis

Nicotine and the nicotine-derived carcinogenic nitrosamine NNK act at the α_7-nAChR of normal and neoplastic PNEC to stimulate growth by a mechanism that moves Ca^{2+}.

II. The Specific Hypotheses And Objectives

1. Stimulation of normal and neoplastic PNEC by nicotine and the nicotine-derived carcinogenic nitrosamine NNK results in the influx of extracellular Ca^{2+} through the α_7-nAChR Ca^{2+} channel. This process will be examined by flow cytometry. The objective is to demonstrate movement of Ca^{2+} into cells in response to nicotine or NNK and to document the inhibition of this response by selective Ca^{2+} channel antagonists. This objective will be achieved by measuring alterations in intracellular Ca^{2+} levels as indicated by changes in the fluorescence intensity ratios of the Ca^{2+} indicator dyes fluo-3 and Fura Red (Novak and Rabinovitch 1994).

2. VOCC subtype expression is upregulated in neoplastic PNEC derived from SCLC of chronic smokers relative to normal fetal PNEC.

i. This process will be examined by quantifying pharmacological subtype expression using radio-ligand receptor binding studies on intact cells and by identifying specific cDNA sequence expression for genetic subtypes using nonquantitative reverse transcription- polymerase chain reaction (RT-PCR) with sequencing of bands to verify targeted sequences. The objective is to demonstrate variable expression of specific pharmacologic and genetic subtypes by the two populations. The aim is to show different pharmacological receptor-binding saturation characteristics and different RT-PCR band expression for the two populations.

ii. This process will be examined by quantifying differences in the expression of specific cDNA sequences for VOCC subsets in the two cell populations in response to nicotine, NNK and hypoxia using relative quantitative (RQ) RT-PCR. The objective is to demonstrate that there is a difference in the expression pattern of specific genetic VOCC subtypes in the two cell populations and that the level of expression is altered by treatment with nicotine, NNK and hypoxia. This will be demonstrated by documenting quantitative differences in the respective band intensities.

APPENDIX

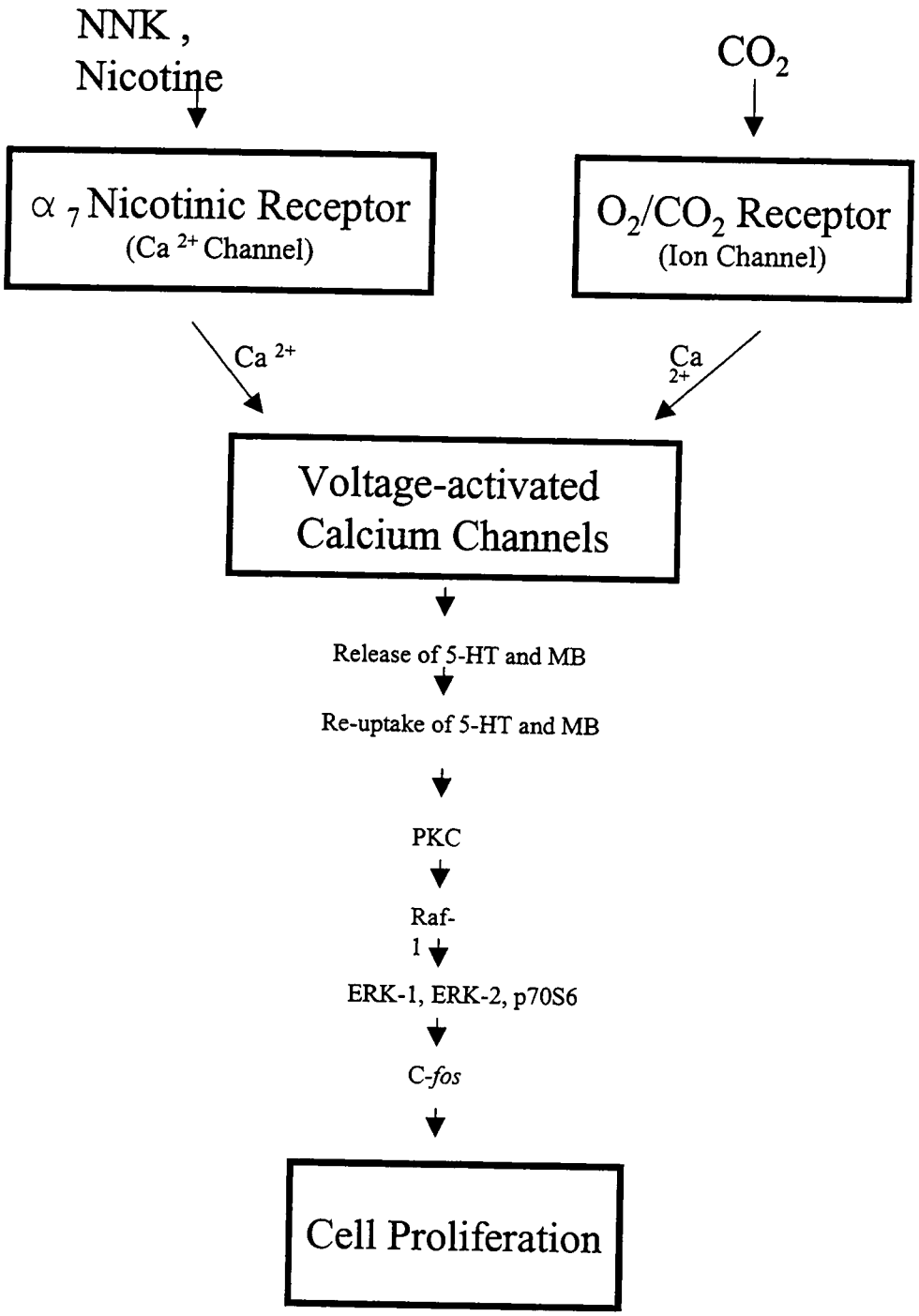


Figure 1-1: Serotonergic Mitogenic Pathway In

Pulmonary Neuroendocrine Cells

Classification based on affinity of ligands to the alpha-1 subunit which is the pore through which Ca^{2+} flows. Other subunits (β and $\alpha_2\delta$) have regulatory functions. (McCleskey 1994, Murad 1990, Tsien et al. 1991)

LVA (transient, low voltage activated)

T
- funnel web toxin
- octanol
- amiloride
- tetrandrine
- low nickel concentration

HVA (long lasting, high voltage activated)

L
- 1,4 dihydropyridines (DHP)
- phenylalkylamines
- ω-ATX IIIA
- calciseptine
- nitrendipine acts as DHP antagonist
- benzodiazepines

N
- ω-conotoxin (CTX) especially ω-CTX GVIA
- DHP resistant
- G-protein linked (Go/beta gamma inhibits: Gs stimulates)

P
- funnel web toxin
- ω-CTX MVIIC
- ω-ATX IVA
- DHP and ω-CTX GVIA resistant

Q
- similar resistance/sensitivity as P type

R
- DHP, conotoxin, agatoxin unresponsive

Figure 1-2: Voltage-Gated Calcium Channels

Conotoxins (Uchitel 1997, Cassola and Afeche 1996)

Omega-conotoxins (CTX) – voltage activated calcium channel subsets
- ω-CTX GVIA - irreversibly N-type inhibition
- ω-CTX MVIIA – reversible N type inhibition
- ω-CTX MVIIC - P-type inhibition
- ω-CTX MVIID – non-N type inhibition preferentially

Micro-conotoxins – skeletal muscle sodium channels

Gamma-conotoxins – sodium channels

Alpha-conotoxins – nicotinic Ach receptors

Funnel-web Spider Venoms

Polyamines:
- funnel web toxin (FTX) – Ca^{2+} channel blocker (P, possibly T)
- alpha-agatoxins (ATX, acylpolyamines)

Polypeptides:
- omega-ATX – voltage activated Ca channel antagonists. N, P.
- w-ATX IVA – potent P/Q type blocker. No effect on T,L,N.

micro-ATX – neuronal NA channel agonist

Omega Grammotoxin SIA (ω-GTX SIA) – blocks P, possibly Q, not L

Mamba Snake Venoms

fasciculin I – inhibits acetylcholinesterase
calciseptine – L (not N or T), P/Q uncertain
FS2 – similar to Calciseptine. L.
calcicludine – blocks HVA type L and N (not T)

Figure 1-3: Neuronal Calcium Channel Toxins

Calcium channels are heteroligomeric complexes of at least 4 subunits (α_1, $\alpha_{2/\delta}$, β) in neuronal tissues. A fifth subunit (γ) defined in muscle has not been found to be expressed in neuronal tissue. (McCleskey 1994, De Waard et al. 1996, Tsien et al. 1991, Stea et al. 1995)

Alpha-1 Subunit

5 genes –A,B,C,D,E in brain (S not expressed in neuronal tissues to date)

Related gene groups based on high % of amino acid identity:

L-type channels – S, C, D ("skeletal, cardiac, and neuroendocrine") genes

P/Q type channels – A gene

N-type channels – B gene

Amino acid conservation between species (85%) is greater than between different alpha-1 subunits within the same species (30-70%) -> this level is similar to evolutionary conservation of other highly conserved proteins. Alpha-1 subunits are composed of 4 large repeated domains (I, II, III, IV) each of which contains 6 alpha-helical transmembrane subunits (S1-S6) interconnected by variably sized loops. Subunit 4 forms the pore and has repeated motifs of positively charged amino acids at every 3rd or 4th position followed by hydrophobic amino acids. The pore is also formed by the loop connecting S5 & S6, and by alpha-helical segments of S5 and S6. The "alpha-1 interaction domain" (AID) which interacts with the beta subunit is the cytoplasmic loop separating the first and second hydrophobic repeats (I-II) having 18aa of which 9 are conserved. The AIDx epitope is QQ-E—L-GY—WI---E.

Figure 1-4: Genetic Basis of Voltage-ActivatedCalcium Channels in Neural/Neuronally derived Tissues

Specific Gene Name	Chromosomal Site	Subunit	Channel type
A gene: CACNA1A	19p13	α_{1A}	P/Q

Comments: variable sensitivity to ω-CTX, FTX & ATX,

B gene: CACNA1B	9q34	α_{1B}	N

Comments: ω-CTX sensitive, Efficient expression in HEK cells requires co-expression of α_2- and B-subunits (Williams et al.1992b). RbB-I subunit by itself forms functional channels but properties are modulated by co-expression of the B-subunit (Stea et al. 1993)

C gene: CACNA1C	12p13.3	α_{1C}	L

Comments: DHP sensitive. Original isolation from rabbit heart (PCARD3), later found in brain (Mikamie et al 1989)

D gene:CACNA1D	3p14.3	α_{1D}	L

Comments: DHP sensitive. Homology α_{1C}(60-70%), α_{1S} (65%). In neural and insulin-producing tissues. Variable size proteins (1610-2180aa) due to alternative splicing (Hui et al. 1991).

E gene:CACNA1E	1q25-q31	α_{1E}	R

Comments: In neurons and neuroendocrine cells including pancreatic islets.

Figure 1-4: (continued)

GenBank#	Name	Source	Reference
Alpha-1A			
S76537	SCLC-P	human SCLC NCI-H146	Barry et al. 1995
Alpha-1B			
M94172	α_{1B-1}	human neuroblastoma	Williams et al. 1992a
M94173	α_{1B-2}	human neuroblastoma	Williams et al. 1992a
Alpha-1D			
M76558	α_{1D}	human neuroblastoma	Williams et al. 1992b

Figure 1-5: CDNA Sequenced from Alpha-1 Subunits of Voltage-Activated Calcium Channels

PART II: CALCIUM MOVEMENT

Chapter 1: Abstract

Nicotine stimulation of the cell surface α_7-nAChR, which is a functional Ca^{2+} channel, of human SCLC and fetal hamster PNEC causes these cells to release the autocrine growth factors 5-HT and mammalian bombesin. The release and reuptake of these factors leads to cell proliferation. Thus, nicotine acting at the cell surface α_7-nAChR initiates a mitogenic autocrine loop with growing evidence of downstream activation of intracellular kinase-driven signaling cascades involving the *raf* kinases. The present study utilized flow cytometry to demonstrate the influx of extracellular Ca^{2+} into NCI-H69 cells and PNEC in response nicotine and its' derivative the carcinogenic nitrosamine NNK. Ca^{2+} influx was demonstrated in both of these cell types in response to nicotine and NNK. The modest response of PNEC to nicotine and NNK compared to NCI-H69 supported the hypothesis that PNEC have fewer or less responsive nAChRs and possibly lacked or had reduced numbers of nAChRs with additional α subunit subtypes. The tremendous responsiveness of the NCI-H69 was hypothesized to reflect the smoking-induced massive upregulation of cell surface α_7-nAChR in the SCLC cell lines all of which are derived from patients who were chronic smokers. NNK consistently demonstrated a greater affinity for the α_7-nAChR Ca^{2+}

channels than did nicotine as evidenced by the much lower concentration of NNK (100 pM) compared to nicotine (1 μM) required to maximize the Ca^{2+} response.

The demonstration of Ca^{2+} movement in both of these cell types in response to nicotine and NNK strongly implicated a central role for Ca^{2+} as a second messenger in the serotonergic mitogenic kinase-driven signaling pathway. Ca^{2+} movement required the binding of ligands to α_7-nAChR Ca^{2+} channels and proper functioning of voltage-activated Ca^{2+} channels (VOCC). Characterization of VOCC subtypes with the largest role in growth promotion is the next logical step and may provide possible therapeutic targets near the initiation of the signaling pathway.

Chapter 2: Introduction

SCLC, referred to as a "smoking-specific" cancer, occurs almost exclusively in smokers with a history of chronic lung disease (Weiss 1991). Representing 25% of all human lung cancer cases, SCLC is initially responsive to radiation and chemotherapy, however, the five year survival rate is below 5% (Hansen and Rorth, 1997). The low survival rate is due to resumption of cancer growth associated with extensive metastatic spread (Cook et al. 1993).

Progress toward understanding the factors potentially driving this resumption of growth has come largely from the realization that SCLC cells are of neuroendocrine origin and, therefore, share many morphologic and functional characteristics with normal PNEC (Linnoila 1996). Under conditions of decreased lung oxygenation such as in the normal neonatal lung or the pathologic predicament of chronic lung diseases, PNEC exhibit a hyperplastic response and enhanced secretion of the biogenic amine 5-HT (Youngson et al. 1993, Johnson and Georgieff 1989, Guyton and Hall 1996). Recent advances in the understanding of normal and neoplastic PNEC physiology has identified 5-HT as an autocrine growth factor for these cells (Cattaneo et al. 1993, Schuller and Hegedus 1989). Neuropeptides of the bombesin family were the first autocrine growth factors discovered to promote growth of

normal and neoplastic PNEC (Bunn et al. 1994). These findings collectively suggested that growth promotion occurring during the recurrence phase of human SCLC involves a combination of factors including 5-HT, nicotine or nicotine-derived products such as the tobacco-specific carcinogenic NNK and chronic hypoxia associated with chronic lung disease. Research examining this growth promotion phenomenon have collectively shown that cell lines derived from SCLC are regulated by a mitogenic autocrine serotonergic loop driven by stimulation of the α-BTX-sensitive α_7-nAChR by nicotine and nicotine-derived nitrosamines and by concurrent hypoxia.

The mitogenic autocrine serotonergic loop in PNEC begins with activation of cell surface membrane α-BTX-sensitive α_7-nAChR. Neuroendocrine cell lines derived from lung carcinoid tumors or SCLC proliferate when treated with nicotine or the structurally related NNK. This proliferation is potentiated by simultaneous exposure to elevated atmospheric CO_2 (Schuller 1989, Schuller and Hegedus 1989) and blocked by 5-HT/MB receptor antagonists and protein kinase C inhibitors (Schuller 1994). Proliferation is also blocked in the presence of the α_7-nAChR antagonists α-BTX and hexamethonium, a broad spectrum blocker of all neuronal nicotinic receptors (Schuller 1989, Schuller and Hegedus 1989). A separate study demonstrated release of 5-HT by SCLC in response to nicotine (Cattaneo et al. 1993). Together these findings implicate an initial interaction of nicotine and/or

NNK at the α_7-nAChR of SCLC and the subsequent role of 5-HT in a kinase-driven mitogenic signaling pathway.

Given the widespread role of Ca^{2+} as a second messenger, it is hypothesized that Ca^{2+} movement precedes activation of the kinase cascade. All nicotinic receptors are ligand-gated ion channels composed of 5 subunits that enclose a central aqueous pore through which the ions flow (Lindstrom et al. 1995). The α_7-nAChR ion channel is unique in that it demonstrates a selective permeability to Ca^{2+} ions. This is in contrast to the other neuronal nicotinic receptor ion channels all of which do not display a preference for a single ion type (Gopalakrishnan et al. 1995 and 1996). The snake venom α-BTX binds with high affinity only to the small subset of neuronal nicotinic receptors (Gopalakrishnan et al. 1995 and 1996) having the α_7 and α_8 subunits which are expressed primarily in the brain and retina, respectively (Chini et al. 1993, Lindstrom et al. 1995). It is therefore apparent that the mitogenic autocrine serotonergic loop initiated by binding of nicotine or NNK at the cell surface membrane α-BTX-sensitive α_7-nAChR of SCLC begins with the influx of extracellular Ca^{2+} through the α_7-nAChR Ca^{2+} channel, however, this specific event has never been experimentally demonstrated.

The central hypothesis of the present study is that nicotine and the nicotine-derived carcinogenic nitrosamine NNK act at the α_7-nAChR of

normal and neoplastic PNEC to stimulate growth by a mechanism that moves Ca^{2+}. The specific hypothesis is that the stimulation of normal and neoplastic PNEC by nicotine and the nicotine-derived carcinogenic nitrosamine NNK will result in the influx of extracellular Ca^{2+} through the α_7-nAChR Ca^{2+} channel. This process will be examined by flow cytometry.

The objective is to demonstrate movement of Ca^{2+} into cells in response to nicotine or NNK and to document the inhibition of this response by selective Ca^{2+} channel antagonists. This objective will be achieved by measuring alterations in intracellular Ca^{2+} levels as indicated by changes in the fluorescence intensity ratios of the Ca^{2+} indicator dyes fluo-3 and Fura Red (Novak and Rabinovitch 1994).

The SCLC cell line designated as NCI-H69 is going to be used because it is a classic SCLC cell line based on its origin from a white male that was a chronic smoker (Phelps et al. 1996).

Chapter 3: Materials and Methods

NCI- H69 Cell Line: NCI-H69 cells from a human SCLC were purchased from the American Cell Type Culture Collection (Rockville, Maryland). Cells were grown at 37° in an atmosphere of 5% CO_2 and RPMI media supplemented with fetal bovine serum (10%, v/v), L-glutamine (2mM), penicillin (100U/ml) and streptomycin (100μg).

Fetal Hamster PNEC: Cultures of fetal hamster PNEC were established from fetal hamster lung periphery harvested on day 15 of gestation and maintained in an atmosphere of 10% CO_2, a condition which selectively promotes the growth of PNEC (Schuller 1994). The cells were routinely maintained in RPMI medium supplemented with fetal bovine serum (10%, v/v), L-glutamine (2mM), and gentamycin sulfate (50mg/ml).

Flow Cytometry: NCI-H69 cells or fetal hamster PNEC were washed with PBS without Ca^{2+} and Mg^{2+}, placed into assay tubes at $1x10^7$cells per ml, and exposed to a final concentration of 5M and 10M of the cell permeable ester forms of the Ca^{2+}-indicator dyes fluo-3 and Fura Red (Molecular Probes, Eugene, OR), respectively, for

30 minutes at 37°C in the dark in an atmosphere of 5% CO_2. The cells were centrifuged (3 min at 70xg), rinsed (1X PBS without Ca^2 and Mg^{2+}), and resuspended in 1ml of buffer (150mM NaCl, 5mM KCl, 1.2M Kh_2PO_4, 1.2mM $MgSO_4$, 30mM $CaCl_2$, 6mM glucose, 25mM Hepes, pH 7.4). The samples were filtered (40 μm nylon strainers, Falcon, Franklin Lakes, NJ), incubated (37°C, no light, 5% CO_2.), and treated with agonists and antagonists in varying concentrations as warranted for the specific experiment The wavelength emissions were measured every four seconds for 180 seconds with 3 pretreatment baseline readings using a flow cytometer (FACSCAN, Becton Dickinson, Franklin Lakes, NJ) equipped with a 488 nm argon-ion laser. The amount of fluorescence of fluo-3 increases with increasing intracellular Ca^{2+} whereas the Fura Red fluorescence decreases, therefore, changes in the ratio of fluo-3/Fura Red fluorescence provided a qualitative measure of changes in the amount of intracellular Ca^{2+} (Novak and Rabinovitch 1994). The baseline ratio for each treatment tube was standardized to a value of 1.0 and all subsequent changes in the ratio were expressed relative to the standardized baseline ratio. Data were summarized in table and figure form.

Experimental Treatment Groups:

NCI-H69: Dose Response Studies With Nicotine - Cells were treated with 30 nM, 100 nM or 1 μM of +/- nicotine immediately prior to reading in a buffer

containing 50 mM Ca^{2+}.

NCI-H69: Dose Response Studies With Calcium In Buffer At A Nicotine Concentration of 1 μM – Cells were treated with 1μM nicotine immediately prior to reading in buffer containing 5, 10, 25, 50 or 75 mM Ca^{2+}.

NCI-H69: Inhibition Of Response To 1 μM Nicotine By α-BTX- Cells were pretreated with 10 μM α-BTX (20 minutes, 37°, 5% CO_2) and exposed to 1μM nicotine immediately prior to reading.

NCI-H69: Comparison Of Response To 1 μM Nicotine With Membrane Depolarization By 50 mM KCl – Cells were treated with either 1μM nicotine or 50 mM KCl immediately prior to reading.

NCI-H69: Dose Response Studies With NNK – Cells were treated with 100 pM, 500 pM, 1 nM, 5 nM, 10 nM or 30 nM NNK immediately prior to reading.

NCI-H69: Inhibition Of Response To 5 nM NNK By α-BTX - Cells were pretreated with 10 μM α-BTX (20 minutes, 37°, 5% CO_2) and treated with 5nM NNK immediately prior to reading.

NCI-H69: Effect Of Chronic Exposure To 10% CO_2 On Dose Response To NNK - Cells that had been cultured for one week at 10% CO_2 were treated with 100 pM, 500 pM, 1 nM, 5 nM, 10 nM or 30 nM NNK immediately prior to reading.

NCI-H69: Comparison Of Response To 30 nM NNK In An Environment Of 5% And 10% CO_2 – Cells that had been cultured for one week at 5 or 10% CO_2 were treated with 30 nM NNK immediately prior to reading.

NCI-H69: Inhibiting Effects Of α-BTX On The Response To 30nM NNK In An Environment Of 10% CO_2 - Cells that had been cultured for one week at 10% CO_2 were pretreated with 10 μM α-BTX (20 minutes, 37°, 5% CO_2) or given no pretreatment. All cells were treated with 30 nM NNK immediately prior to reading.

NCI-H69: Inhibiting Effects Of The N-type Calcium Channel Blocker ω-Conotoxin (CTX) GVIA On The Response To 30 nM NNK In 10% CO_2 - Cells that had been cultured for one week at 10% CO_2 were pretreated with 40 pM ω-CTX GVIA(20 minutes, 37°, 5% CO_2) or given no pretreatment. All cells were treated with 30 nM NNK immediately prior to reading.

PNEC: Dose Response Studies With Nicotine - Cells were treated with 100 pM, 500 pM, 1 nM, 20 nM, 30 nM or 1 μM of +/- nicotine immediately prior to reading

in a buffer containing 50mM Ca^{2+}.

PNEC: Dose Response Studies With Calcium in Buffer At A Nicotine Concentration Of 1 μM – Cells were treated with 1μM nicotine immediately prior to reading in buffer containing 50 mM Ca^{2+} or lacking Ca^{2+} (PBS without Ca^{2+}).

PNEC: Inhibition Of Response To 1 μM Nicotine By α-BTX - Cells were pretreated with 10 μM α-BTX (20 minutes, 37°, 5% CO_2) and treated with 1μM nicotine immediately prior to reading.

PNEC: Dose Response Studies With NNK - Cells were treated with 100 pM, 500 pM, 1 nM, 20 nM, 30 nM or 1μM NNK immediately prior to reading.

PNEC: Dose Response Studies With Calcium In Buffer At A NNK Concentration Of 1 nM - Cells were treated with 1nM NNK immediately prior to reading in buffer containing 50 mM Ca^{2+} or lacking Ca^{2+} (PBS without Ca^{2+}).

PNEC: Inhibition Of Response To 1 nM NNK By α-BTX - Cells were pretreated with 10 μM α-BTX (20 minutes, 37°, 5% CO_2) and treated with 1nM NNK immediately prior to reading.

PNEC: Inhibiting Effects Of The Broad Spectrum Blocker Of Neuronal nAChR, Hexamethonium, On The Response To 1 nM NNK - Cells were pretreated with 1uM hexamethonium (20 minutes, 37°, 5% CO_2) and treated with 1nM NNK immediately prior to reading.

Chapter 4: Results

The flow cytometry results for each experimental treatment set are presented in Tables 2-1 to 2-17 containing a standardized ratio prior to treatment of 1.0 at time zero followed by standardized ratios every four seconds to 180 seconds. The ratios for selected treatment groups are graphed over time in Figures 2-1 to 2-18.

Experimental Treatment Groups: 1

NCI-H69: Dose Response Studies With Nicotine (Table 2-1, Fig 2-1)- There was a nearly 5x increase in the ratio following treatment with 1μM nicotine. The ratio was not altered by treatment with 30 nM and 100 nM nicotine.

NCI-H69: Dose Response Studies With Calcium In Buffer At A Nicotine Concentration of 1 μM (Table 2-2, Fig 2-2) – The largest ratio increase, which was greater than 3x, occurred in cells treated with 1μM nicotine in the presence of 50 mM Ca^2. Buffer with only 25 mM and 10 mM Ca^{2+} was associated with a less than 2x increase and no ratio change, respectively.

---

1 All Tables and Figures can be found within the Appendix of part II.

NCI-H69: Inhibition Of Response To 1 μM Nicotine By α-BTX (Table 2-3, Fig 2-3)- Pretreatment with 10 μM α-BTX reduced the ratio increase in response to 1μM nicotine from nearly 5x to 1.5x.

NCI-H69: Comparison Of Response To 1 μM Nicotine With Membrane Depolarization By 50 mM KCl (Table 2-4, Fig 2-4)– There was a 2x ratio increase following depolarization of the membrane by 50 mM KCl and a nearly 5x increase with 1μM nicotine.

NCI-H69: Dose Response Studies With NNK (Table 2-5, Fig 2-5) – There was a similar 1.4 to 1.6x ratio increase for NNK concentrations ranging from 100 pM to 30 nM .

NCI-H69: Inhibition Of Response To 5 nM NNK By α-BTX (Table 2-6, Fig 2-6) – There was a nearly 1.1x increase following treatment with 5nM NNK that was reduced to no ratio change for cells pretreated with 10 μM α-BTX.

NCI-H69: Effect Of Chronic Exposure To 10% CO_2 On Dose Response To NNK (Table 2-7, Fig 2-7) – For cells chronically treated 10% CO_2, there was a slightly larger ratio increase of 1.25x at 30 nM than the 1.1x increase for 100 pM NNK. Both ratio increases are less than the 1.4 to 1.6x ratio increase without

chronic 10% CO_2 treatment.

NCI-H69: Comparison Of Response To 30 nM NNK In An Environment Of 5% And 10% CO_2 (Table 2-8, Fig 2-8) – The 1.5x ratio increase in response to 30 nM NNK was reduced slightly to 1.3x for cells chronically treated 10% CO_2.

NCI-H69: Inhibiting Effects Of α-BTX On The Response To 30nM NNK In An Environment Of 10% CO_2 (Table 2-9, Fig 2-9) – The 1.3x ratio increase following 30 nM NNK treatment of cells chronically treated 10% CO_2 was reduced to no ratio change when cells chronically treated 10% CO_2 were pretreated with 10 μM α-BTX.

NCI-H69: Inhibiting Effects Of The N-type Calcium Channel Blocker ω-Conotoxin (CTX) GVIA On The Response To 30 nM NNK In 10% CO_2 (Table 2-10, Fig 2-10) - The 1.3x ratio increase following 30 nM NNK treatment of cells chronically treated 10% CO_2 was reduced to no ratio change when cells chronically treated 10% CO_2 were pretreated with 40 pM ω-CTX GVIA. Summarized in Fig 2-11 is a comparison of NCI-H69 response to 30 nM NNK in 5% CO2 compared to the response in 10% CO2 with and without antagonism by CTX or BTX

PNEC: Dose Response Studies With Nicotine (Table 2-11, Fig 2-12) - There

was a 1.25x ratio increase following treatment with 30 nM and 1 μM nicotine, however, the ratio was unchanged by the 100 pM treatment.

PNEC: Dose Response Studies With Calcium In Buffer At A Nicotine Concentration Of 1 μM (Table 2-12, Fig 2-13) – There was a 1.2x ratio increase in cells treated with 1μM nicotine immediately prior to reading in buffer containing 50 mM Ca^{2+}, however, the ratio was unchanged for cells in buffer lacking calcium (PBS without Ca^{2+}).

PNEC: Inhibition Of Response To 1 μM Nicotine By α-BTX (Table 2-13, Fig 2-14) - There was a similar 1.2x to 1.25x ratio increase for cells treated with 1μM nicotine immediately prior to reading regardless of whether they had also received pretreatment with 10 μM α-BTX.

PNEC: Dose Response Studies With NNK (Table 2-14, Fig 2-15) – There was a ratio increase of 1.2x and 1.1x for cells treated with 1 nM and 100 pM NNK, respectively. No ratio change occurred with 1 μM NNK.

PNEC: Dose Response Studies With Calcium In Buffer At A NNK Concentration Of 1 nM (Table 2-15, Fig 2-16)– There was a ratio increase of 1.25x for cells treated with 1nM NNK immediately prior to reading in buffer

containing 50 mM Ca^{2+}, however, there was no ratio change for cells in buffer lacking calcium (PBS without Ca^{2+}).

PNEC: Inhibition Of Response To 1 nM NNK By α-BTX (Table 2-16, Fig 2-17) - There was a nearly 1.25x increase following treatment with 1nM NNK that was reduced to no ratio change for cells pretreated with 10 μM α-BTX.

PNEC: Inhibiting Effects Of The Broad Spectrum Blocker Of Neuronal nAChR, Hexamethonium, On The Response To 1 nM NNK (Table 2-17, Fig 2-18) - There was a nearly 1.25x increase following treatment with 1nM NNK that was reduced to no ratio change for cells pretreated with 1uM hexamethonium.

Chapter 5: Discussion

The flow cytometry results support the project's specific hypothesis that the stimulation of normal and neoplastic PNEC by nicotine and the nicotine-derived carcinogenic nitrosamine NNK would result in the influx of extracellular Ca^{2+} through the α_7-nAChR Ca^{2+} channel. NCI-H69 cells demonstrated a large 5x ratio increase when treated with nicotine, however, this response occurred only at the comparatively high dose of 1μM and not at lower doses. The source of Ca^{2+} was clearly extracellular rather than representing release from intracellular stores because the response was quenched in the absence of extracellular buffer Ca^{2+}. The external application of a KCl solution is a standard method for depolarizing cellular membranes to allow the influx of Ca^{2+} (Stea et al. 1995, DeWaard et al. 1996) . The amount of Ca^{2+} influx exceeded that which occurred with exposure to KCl thereby indicating that the influx phenomenon was utilizing a unique channel for Ca^{2+} entry in addition to potential activation of VOCCs. Substantial but not complete blockage of the response to 1 μM nicotine by pretreatment with α-BTX identifies one unique channel through which most of the Ca^{2+} enters as the α_7-nAChR Ca^{2+} channel based on the known specificity of α-BTX. The snake venom α-BTX binds with high affinity only to the small subset of neuronal nicotinic receptors (Gopalakrishnan et al. 1995 and 1996) having the α_7 and α_8 subunits

which are expressed primarily in the brain and retina, respectively (Chini et al. 1993, Lindstrom et al. 1995). While most of the Ca^{2+} entered via stimulated α_7-nAChR Ca^{2+} channels, nicotine must also stimulate Ca^{2+} movement through additional channels which could include neuronal nicotinic receptors having α subunits other than α_7. Indeed, NCI-H69 have recently been shown to also express nAChRs with the α_3 and α_5 subunits (Schuller unpublished).

Treatment of NCI-H69 cells with NNK resulted in a much smaller ratio increase of 1.4 to 1.6x compared to the 5x ratio increase observed for 1μM nicotine. However, this ratio response was reproducible across a wide range of NNK doses including the very small dose of 100 pM which is 10,000x smaller than the 1μM nicotine dose required for the nicotine-induced 5x ratio increase. Unlike the response to nicotine, the NNK response was completely blocked by pretreatment with α-BTX. Together these findings indicate that NNK stimulates the influx of Ca^{2+} exclusively via the α_7-nAChR Ca^{2+} channel and that NNK is a much more potent activator of this channel than is nicotine. This increased sensitivity to NNK is supported by recent binding studies. The affinity of NNK to the α_7 receptor was shown to be 1,300 times greater than that of nicotine and 3,500 times greater than that of the carcinogenic nicotine metabolite N-nitrosonornicotine (NNN), and that NNK-induced cell proliferation and DNA synthesis measured by incorporation of ^{3}H-thymidine was completely inhibited by α-BTX (Schuller and Orloff, 1998). It

has also been shown that cell lines derived from SCLC cannot metabolize NNK (Falzon et al. 1986a,b) and, therefore, cannot generate the metabolites which are believed to cause the ki-*ras* mutations that are a common finding in non-small cell carcinomas. Ki-*ras*, which plays a key role in the signal transduction pathway utilized by many growth factors (Segar and Krebs 1995), is frequently mutated in PAC derived from the bronchiolar Clara cells (Linnoila 1990). Exposure of laboratory rodents to the tobacco-specific carcinogenic nitrosamine NNK results in the formation of PAC of a Clara cell phenotype (Hecht and Hoffman 1988; Schuller et al. 1990). These PAC cells have a high incidence of Ki-*ras* gene mutation (Mitsudomi et al. 1991) which is most commonly a point mutation at codon 12 (Mitsudomi et al. 1991, Yesner 1993). Formation of this mutation was highly correlated with the metabolism of NNK to O^6-methylguanine (Belinsky et al. 1989) indicating that metabolism of NNK by the PAC cells preceded mutation of the Ki-*ras* gene. In contrast, SCLC cells are unable to metabolize NNK (Falzon et al. 1986a) due to a lack of the necessary enzyme profile (Falzon et al. 1986b), thereby making them unable to generate the NNK metabolite, O^6-methylguanine, associated with mutation of the Ki-*ras* gene. In light of the inability of SCLC cells to metabolize NNK, any growth promotion effect of NNK on SCLC must utilize a separate mechanism. This mechanism is most likely direct stimulation of the α_7-nAChR Ca^{2+} channel as supported by the flow cytometry findings.

Culturing NCI-H69 cells for one week in a hypoxic environment at 10% atmospheric CO_2 resulted in a small reduction in the responsiveness of the cells to NNK. The largest ratio increase achieved with NNK after subchronic 10% atmospheric CO_2 was 1.25x which was approximately 50% less than the largest non-hypoxic ratio increases of 1.4x to 1.6x. These ratio increases were all significantly lower than the 5x increase measured with nicotine which was effective at 1μM but not at lower doses. Somewhat larger NNK doses were required to reach the maximal ratio increase under the hypoxic conditions as evidenced by the slightly larger ratio increase with 30 nM than with 100 pM NNK suggesting that there may have been a mild decrease in sensitivity to NNK. However, these doses are still significantly less than the 1μM dose needed for nicotine indicating that the cells are still much more sensitive to NNK stimulation.

The proliferation of neuroendocrine cell lines derived from lung carcinoid tumors or SCLC (Schuller 1994) treated with nicotine or the structurally related NNK is potentiated by simultaneous exposure to elevated atmospheric CO_2 (Schuller 1989, Schuller 1994, Schuller and Hegedus 1989) and blocked by 5-HT/MB receptor antagonists and protein kinase C inhibitors. With single dose exposures to nicotine or NNK, cell proliferation occurred at 10% but not 5% atmospheric CO_2 (Maneckjee and Minna 1990, Schuller 1994). This is important because the intrapulmonary concentration of CO_2 in the healthy adult lung is 5%

whereas a CO_2 concentration of 10% simulates the intrapulmonary levels of this gas in a mildly diseased lung (Guyton and Hall 1996). Therefore, growth promotion in response to nicotine and NNK was most remarkable under the hypoxic conditions of a chronically diseased lung which is in agreement with the high incidence of SCLC in smokers with chronic lung disease. At the flow cytometry level, the present results suggested that hypoxic growth potentiation of SCLC mediated by a cell membrane oxygen binding receptor may be accompanied by a slightly reduced sensitivity to single-dose NNK treatments.

Complete blockage of the response of subchronically hypoxic NCI-H69 with α-BTX pretreatment again indicated that NNK was interacting with the α_7-nAChR to initiate movement of Ca^{2+}. This was consistent with previous findings that NNK-induced SCLC cell line proliferation was blocked in the presence of the α_7-nAChR antagonists α-BTx and hexamethonium, a broad spectrum blocker of all neuronal nicotinic receptors (Schuller 1989, Schuller and Hegedus 1989). Complete blockage also occurred following pretreatment with ω-CTX GVIA, a VOCC blocker, which indicated that the NNK-induced movement of Ca^{2+} required the function of VOCCs. NNK appears to stimulate initial Ca^{2+} entry by ligating the α_7-nAChR resulting in membrane depolarization and subsequent influx of most of the Ca^{2+} through activated VOCCs. It would be helpful to identify which VOCC subtypes are most involved in this movement of Ca^{2+} as they might provide a

suitable therapeutic target for circumvention of the serotonergic mitogenic pathway. CTXs, Ca^{2+} channel blockers that marine snails use to paralyze their fish prey, have varying selectivity for the pharmacological VOCC subtypes. The primary target of ω-CTX GVIA is the N-type VOCC which it irreversibly inhibits (Cassola and Afeche 1996, Clapham 1995, De Waard et al. 1996, Ertel and Ertel 1996, Fujita et al. 1993, McCleskey 1994, Stea et al. 1995, Tsien et al. 1991, Uchitel 1997, Wickman and Clapham 1995). The potential for overlapping sensitivities of the VOCC subtypes particularly in neoplastic cells makes it impossible to exclude the possible functional significance of the other VOCC subtypes in the NNK-induced Ca^{2+} influx. Collectively these flow cytometry findings elucidate a pattern of NNK-induced Ca^{2+} influx that begins with ligation of the α_7-nAChR and is propagated by subsequent activation of VOCC.

PNEC responded similarly to both the typical 1 μM and the lower 30 nM dose of nicotine but achieved only a 1.25x ratio increase which was far less than the 5x ratio increase observed for NCI-H69 treated with 1 μM nicotine. The response of PNEC to NNK was similarly reduced with a ratio increase of only 1.2x to 1.1x compared to the NCI-H69 response of 1.4x to 1.6x. Nicotine and NNK both induced the influx of extracellular Ca^{2+} as evidence by the lack of response in a buffer that lacked Ca^{2+}. Although PNEC displayed a modest ratio increase in response to nicotine and NNK, the NNK response was completely blocked by α-

BTX pretreatment as it had been for the NCI-H69 while the small nicotine ratio increase was unchanged by α-BTX pretreatment. The PNEC response to NNK was also completely blocked by the broad spectrum neuronal nAChR blocker hexamethonium. This suggested that the PNEC response to NNK was completely mediated by the α_7-nAChR in a fashion similar to that described above for NCI-H69 but that PNEC had fewer or far less responsive α_7-nAChRs. The modest response of PNEC to nicotine compared to NCI-H69 supports the idea that PNEC had fewer or less responsive nAChRs and possibly lacked or had reduced numbers of nAChRs with additional α subunit subtypes. In support of this, recent investigations have shown that fetal hamster PNEC did not express the additional nAChRs subtypes having the α_3 and α_5 subunits which are found on cell lines derived from human SCLC (Schuller unpublished). The relative unresponsiveness to both nicotine and NNK of the PNEC α_7-nAChR compared to NCI-H69 is hypothesized to reflect the smoking-induced massive upregulation of these receptors in the SCLC cell lines all of which are derived from patients who were chronic smokers.

The demonstration of Ca^{2+} movement in both of these cell types in response to nicotine and NNK strongly implicates a central role for Ca^{2+} as a second messenger in the serotonergic mitogenic kinase-driven signaling pathway. Ca^{2+} movement has now been definitively shown to require ligand binding to α_7-nAChR

Ca^{2+} channels and proper functioning of VOCC. Characterization of VOCC subtypes with the largest role in growth promotion is the next logical step and may provide possible therapeutic targets near the initiation of the signaling pathway.

APPENDIX

Table 2-1: NCI-H69: Dose Response Studies With Nicotine (Figure 2-1)

	X Values	A	B	C
	Time (sec)	30nM Nic	100nM Nic	1uM Nic
	X	Y	Y	Y
1	0	1.000	1.000	1.000
2	4	1.009	0.994	2.989
3	8	0.973	0.984	4.141
4	12	1.028	0.999	4.824
5	16	1.022	1.026	4.549
6	20	1.046	1.023	4.607
7	24	1.047	1.000	4.614
8	28	1.036	1.011	4.658
9	32	1.010	1.023	4.396
10	36	0.972	0.988	4.760
11	40	0.947	1.036	4.321
12	44	1.027	1.023	4.822
13	60	0.877	1.011	4.558
14	75	1.105	1.013	4.865
15	90	1.067	1.011	4.601
16	105	0.971	0.997	4.765
17	120	1.026	1.017	4.597
18	135	1.088	1.018	4.397
19	150	1.005	1.019	4.663
20	165	1.011	1.018	4.757
21	180	1.044	0.999	4.967

Table 2-2: NCI-H69: Dose Response Studies With Calcium In Buffer At A Nicotine Concentration of 1 μM (Figure 2-2)

	X Values	A	B	C	D
	Time (sec)	10mM Ca	25mM Ca	50mM Ca	75mM Ca
	X	Y	Y	Y	Y
1	0	1.000	1.000	1.000	1.000
2	4	1.000	1.375	2.085	2.017
3	8	1.055	1.432	3.271	2.624
4	12	0.987	1.432	3.293	2.787
5	16	1.030	1.477	3.240	2.708
6	20	1.043	1.375	3.237	2.774
7	24	1.061	1.587	3.127	2.728
8	28	1.003	1.587	3.056	2.683
9	32	1.076	1.528	3.359	2.743
10	36	1.021	1.704	3.209	2.886
11	40	1.094	1.469	3.364	2.815
12	44	1.078	1.587	3.341	2.655
13	60	1.050	1.655	3.162	2.597
14	75	1.098	1.592	3.281	2.872
15	90	1.065	1.667	2.899	2.626
16	105	1.097	1.592	3.173	2.563
17	120	1.093	1.736	3.504	2.874
18	135	1.127	1.667	3.253	2.758
19	150	1.146	1.736	3.172	3.003
20	165	1.224	1.736	3.215	3.002
21	180	1.148	2.037	3.160	3.056

Table 2-3: NCI-H69: Inhibition Of Response To 1 μM Nicotine By α-BTX (Figure 2-3)

	X Values	A	B
	Time (sec)	BTX	1uM Nic
	X	Y	Y
1	0	1.000	1.000
2	4	1.508	2.989
3	8	1.461	4.141
4	12	1.493	4.824
5	16	1.479	4.549
6	20	1.460	4.607
7	24	1.426	4.614
8	28	1.490	4.658
9	32	1.476	4.396
10	36	1.363	4.760
11	40	1.330	4.321
12	44	1.207	4.822
13	60	1.168	4.558
14	75	1.322	4.865
15	90	1.492	4.601
16	105	1.503	4.765
17	120	1.492	4.597
18	135	1.521	4.397
19	150	1.436	4.663
20	165	1.501	4.757
21	180	1.530	4.967

Table 2-4: NCI-H69: Comparison Of Response To 1 μM Nicotine With Membrane Depolarization By 50 mM KCl (Figure 2-4)

	X Values	A	B
	Time (sec)	KCL	1uM Nic
	X	Y	Y
1	0	1.000	1.000
2	4	1.910	2.989
3	8	2.005	4.141
4	12	2.195	4.824
5	16	1.955	4.549
6	20	2.198	4.607
7	24	2.042	4.614
8	28	2.158	4.658
9	32	2.115	4.396
10	36	2.251	4.760
11	40	2.037	4.321
12	44	2.175	4.822
13	60	2.156	4.558
14	75	2.057	4.865
15	90	1.900	4.601
16	105	2.030	4.765
17	120	2.141	4.597
18	135	2.024	4.397
19	150	1.985	4.663
20	165	2.172	4.757
21	180	2.113	4.967

Table 2-5: NCI-H69: Dose Response Studies With NNK (Figure 2-5)

	X Values	A	B	C
	Time (sec)	30nM NNK	1nM NNK	100pM NNK
	X	Y	Y	Y
1	0	1.000	1.000	1.000
2	4	1.463	1.658	1.481
3	8	1.570	1.603	1.485
4	12	1.307	1.654	1.479
5	16	1.497	1.611	1.473
6	20	1.273	1.616	1.531
7	24	1.380	1.577	1.492
8	28	1.389	1.607	1.467
9	32	1.396	1.622	1.452
10	36	1.461	1.635	1.502
11	40	1.322	1.595	1.483
12	44	1.396	1.548	1.444
13	60	1.492	1.556	1.477
14	75	1.446	1.593	1.508
15	90	1.339	1.615	1.509
16	105	1.320	1.550	1.447
17	120	1.452	1.530	1.516
18	135	1.442	1.546	1.501
19	150	1.489	1.528	1.451
20	165	1.574	1.543	1.543
21	180	1.302	1.552	1.448

Table 2-6: NCI-H69: Inhibition Of Response To 5 nM NNK By α-BTX (Figure 2-6)

	X Values	A	B
	Time (sec)	5nM NNK	BTX & NNK
	X	Y	Y
1	0	1.000	1.000
2	4	1.045	0.974
3	8	1.080	0.996
4	12	1.016	0.982
5	16	1.082	0.974
6	20	1.085	0.990
7	24	1.089	0.989
8	28	1.067	0.986
9	32	1.105	0.995
10	36	1.050	0.970
11	40	1.038	0.970
12	44	1.051	0.957
13	60	1.047	0.957
14	75	1.072	0.951
15	90	1.099	0.970
16	105	1.075	0.960
17	120	1.133	0.950
18	135	1.055	0.995
19	150	1.099	0.972
20	165	1.062	0.933
21	180	1.063	1.004

Table 2-7: NCI-H69: Effect Of Chronic Exposure To 10% CO_2 On Dose Response To NNK (Figure 2-7)

	X Values	A	B	C	D	E	F
	Time (sec)	30nM NNK	10nM NNK	5nM NNK	1nM NNK	500pM NNK	100pMNNK
	X	Y	Y	Y	Y	Y	Y
1	0	1.000	1.000	1.000	1.000	1.000	1.000
2	4	1.264	1.248	0.968	1.407	1.264	0.976
3	8	1.113	1.358	1.017	1.348	1.249	1.133
4	12	1.257	1.349	0.931	1.281	1.288	1.024
5	16	1.225	1.255	0.993	1.283	1.233	1.042
6	20	1.238	1.323	1.015	1.334	1.284	1.095
7	24	1.335	1.316	0.984	1.345	1.216	0.961
8	28	1.179	1.230	0.899	1.242	1.297	1.112
9	32	1.131	1.342	1.001	1.360	1.291	1.091
10	36	1.268	1.286	0.994	1.282	1.336	1.153
11	40	1.120	1.369	1.005	1.264	1.219	1.058
12	44	1.188	1.263	1.039	1.276	1.273	1.076
13	60	1.204	1.336	0.953	1.347	1.166	1.048
14	75	1.203	1.313	0.962	1.374	1.226	1.076
15	90	1.103	1.324	0.986	1.283	1.222	1.118
16	105	1.246	1.376	1.020	1.270	1.237	1.066
17	120	1.298	1.274	1.016	1.383	1.176	1.030
18	135	1.298	1.322	0.928	1.257	1.252	1.015
19	150	1.177	1.263	1.033	1.284	1.289	1.109
20	165	1.229	1.188	0.916	1.258	1.270	1.172
21	180	1.214	1.276	1.051	1.353	1.227	1.069

Table 2-8: NCI-H69: Comparison Of Response To 30 nM NNK In An Environment Of 5% And 10% CO_2 (Figures 2-8 and 2-11)

	X Values	A	B
	Time (sec)	10%	5%
	X	Y	Y
1	0	1.000	1.000
2	4	1.327	1.403
3	8	1.168	1.504
4	12	1.320	1.253
5	16	1.286	1.435
6	20	1.300	1.221
7	24	1.402	1.323
8	28	1.238	1.332
9	32	1.187	1.338
10	36	1.331	1.401
11	40	1.176	1.267
12	44	1.248	1.338
13	60	1.264	1.430
14	75	1.263	1.386
15	90	1.158	1.284
16	105	1.308	1.265
17	120	1.363	1.392
18	135	1.362	1.383
19	150	1.236	1.427
20	165	1.290	1.509
21	180	1.275	1.249
22		1.275	1.249

Table 2-9: NCI-H69: Inhibiting Effects Of α-BTX On The Response To 30nM NNK In An Environment Of 10% CO_2 (Figures 2-9 and 2-11)

	X Values	A	B
	Time (sec)	10% CO2	BTX & NNK
	X	Y	Y
1	0	1.000	1.000
2	4	1.327	1.032
3	8	1.168	0.916
4	12	1.320	0.983
5	16	1.286	0.995
6	20	1.300	1.011
7	24	1.402	1.030
8	28	1.238	0.995
9	32	1.187	0.994
10	36	1.331	0.984
11	40	1.176	1.023
12	44	1.248	1.013
13	60	1.264	1.036
14	75	1.263	1.161
15	90	1.158	1.047
16	105	1.308	1.045
17	120	1.363	1.047
18	135	1.362	1.067
19	150	1.236	1.020
20	165	1.290	1.031
21	180	1.275	1.015

Table 2-10: NCI-H69: Inhibiting Effects Of The N-type Calcium Channel Blocker ω-Conotoxin (CTX) GVIA On The Response To 30 nM NNK In 10% CO_2 (Figures 2-10 and 2-11)

	X Values	A	B
	Time (sec)	10% CO2	CTX & NNK
	X	Y	Y
1	0	1.000	1.000
2	4	1.327	1.027
3	8	1.168	0.999
4	12	1.320	0.993
5	16	1.286	1.012
6	20	1.300	0.989
7	24	1.402	1.010
8	28	1.238	1.004
9	32	1.187	0.970
10	36	1.331	0.994
11	40	1.176	0.974
12	44	1.248	0.996
13	60	1.264	0.992
14	75	1.263	0.993
15	90	1.158	1.001
16	105	1.308	0.997
17	120	1.363	0.974
18	135	1.362	1.001
19	150	1.236	1.029
20	165	1.290	0.995
21	180	1.275	1.022

Table 2-11: PNEC: Dose Response Studies With Nicotine (Figure 2-12)

	X Values	A	B	C	D
	Time (sec)	1uM Nic	30nM Nic	500pM Nic	100pM Nic
	X	Y	Y	Y	Y
1	0	1.000	*1.000*	*1.000*	1.000
2	4	1.208	*1.232*	*1.335*	1.055
3	8	1.176	*1.249*	*1.289*	1.007
4	12	1.152	*1.214*	*1.271*	1.008
5	16	1.201	*1.223*	*1.292*	0.935
6	20	1.170	*1.204*	*1.290*	1.006
7	24	1.187	*1.193*	*1.267*	0.995
8	28	1.190	*1.226*	*1.260*	1.007
9	32	1.169	*1.206*	*1.285*	1.010
10	36	1.163	*1.237*	*1.237*	0.994
11	40	1.180	*1.218*	*1.277*	1.003
12	44	1.214	*1.196*	*1.252*	0.991
13	60	1.194	*1.222*	*1.255*	1.000
14	75	1.228	*1.217*	*1.249*	0.991
15	90	1.181	*1.199*	*1.242*	1.000
16	105	1.198	*1.223*	*1.244*	0.982
17	120	1.175	*1.212*	*1.262*	0.990
18	135	1.176	*1.203*	*1.227*	0.961
19	150	1.167	*1.213*	*1.252*	0.947
20	165	1.155	*1.211*	*1.241*	0.940
21	180	1.166	*1.196*	*1.293*	0.941

Table 2-12: PNEC: Dose Response Studies With Calcium in Buffer At A Nicotine Concentration Of 1 μM (Figure 2-13)

	X Values	A	B
	Time (sec)	1uM Nic	PBS & Nic
	X	Y	Y
1	0	1.000	1.000
2	4	1.208	0.984
3	8	1.176	0.960
4	12	1.152	1.007
5	16	1.201	1.002
6	20	1.170	0.988
7	24	1.187	0.991
8	28	1.190	0.989
9	32	1.169	0.977
10	36	1.163	1.003
11	40	1.180	1.033
12	44	1.214	0.981
13	60	1.194	1.061
14	75	1.228	1.015
15	90	1.181	0.949
16	105	1.198	0.848
17	120	1.175	0.873
18	135	1.176	0.823
19	150	1.167	0.845
20	165	1.155	0.959
21	180	1.166	0.983

Table 2-13: PNEC: Inhibition Of Response To 1 μM Nicotine By α-BTX (Figure 2-14)

	X Values	A	B
	Time (sec)	1uM Nic	BTX & Nic
	X	Y	Y
1	0	1.000	1.000
2	4	1.208	1.236
3	8	1.176	1.238
4	12	1.152	1.253
5	16	1.201	1.236
6	20	1.170	1.152
7	24	1.187	1.243
8	28	1.190	1.176
9	32	1.169	1.154
10	36	1.163	1.206
11	40	1.180	1.205
12	44	1.214	1.168
13	60	1.194	1.199
14	75	1.228	1.179
15	90	1.181	1.191
16	105	1.198	1.235
17	120	1.175	1.179
18	135	1.176	1.202
19	150	1.167	1.201
20	165	1.155	1.176
21	180	1.166	1.190

Table 2-14: PNEC: Dose Response Studies With NNK (Figure 2-15)

	X Values	A	B	C
	Time (sec)	1uM NNK	1nM NNK	100pM NNK
	X	Y	Y	Y
1	0	1.000	1.000	1.000
2	4	1.001	1.224	1.096
3	8	0.998	1.228	1.125
4	12	0.998	1.218	1.123
5	16	0.975	1.201	1.138
6	20	0.974	1.179	1.131
7	24	0.958	1.234	1.116
8	28	0.961	1.176	1.089
9	32	0.986	1.218	1.088
10	36	0.960	1.218	1.113
11	40	1.018	1.218	1.136
12	44	0.946	1.197	1.139
13	60	0.984	1.211	1.104
14	75	0.985	1.101	1.063
15	90	0.935	1.190	1.112
16	105	0.982	1.183	1.096
17	120	0.971	1.132	1.127
18	135	0.987	1.076	1.076
19	150	1.009	1.228	1.090
20	165	0.948	1.165	1.089
21	180	0.947	1.165	1.106

Table 2-15: PNEC: Dose Response Studies With Calcium In Buffer At A NNK Concentration Of 1 nM (Figure 2-16)

	X Values	A	B
	Time (sec)	1nM NNK	PBS & NNK
	X	Y	Y
1	0	1.000	1.000
2	4	1.224	1.020
3	8	1.228	0.990
4	12	1.218	0.995
5	16	1.201	0.936
6	20	1.179	0.970
7	24	1.234	0.989
8	28	1.176	1.002
9	32	1.218	0.995
10	36	1.218	0.976
11	40	1.218	0.978
12	44	1.197	0.997
13	60	1.211	1.011
14	75	1.101	0.981
15	90	1.190	0.939
16	105	1.183	0.950
17	120	1.132	0.964
18	135	1.076	0.986
19	150	1.228	0.949
20	165	1.165	0.998
21	180	1.165	0.949

Table 2-16: PNEC: Inhibition Of Response To 1 nM NNK By α-BTX (Figure 2-17)

	X Values	A	B
	Time (sec)	1nM NNK	BTX & NNK
	X	Y	Y
1	0	1.000	1.000
2	4	1.224	0.933
3	8	1.228	0.964
4	12	1.218	0.968
5	16	1.201	1.059
6	20	1.179	1.001
7	24	1.234	1.003
8	28	1.176	0.945
9	32	1.218	0.941
10	36	1.218	0.962
11	40	1.218	0.998
12	44	1.197	1.063
13	60	1.211	0.963
14	75	1.101	0.971
15	90	1.190	1.048
16	105	1.183	0.938
17	120	1.132	0.991
18	135	1.076	0.978
19	150	1.228	0.990
20	165	1.165	1.045
21	180	1.165	1.027

Table 2-17: PNEC: Inhibiting Effects Of The Broad Spectrum Blocker Of Neuronal nAChR, Hexamethonium, On The Response To 1 nM (Figure 2-18)

	X Values	A	B
	Time (sec)	1nM NNK	Hex & NNK
	X	Y	Y
1	0	1.000	1.000
2	4	1.224	0.967
3	8	1.228	1.001
4	12	1.218	0.906
5	16	1.201	1.013
6	20	1.179	0.985
7	24	1.234	0.961
8	28	1.176	0.938
9	32	1.218	0.968
10	36	1.218	0.928
11	40	1.218	0.946
12	44	1.197	0.996
13	60	1.211	0.935
14	75	1.101	0.988
15	90	1.190	0.940
16	105	1.183	0.941
17	120	1.132	0.892
18	135	1.076	1.013
19	150	1.228	0.905
20	165	1.165	0.976
21	180	1.165	0.937

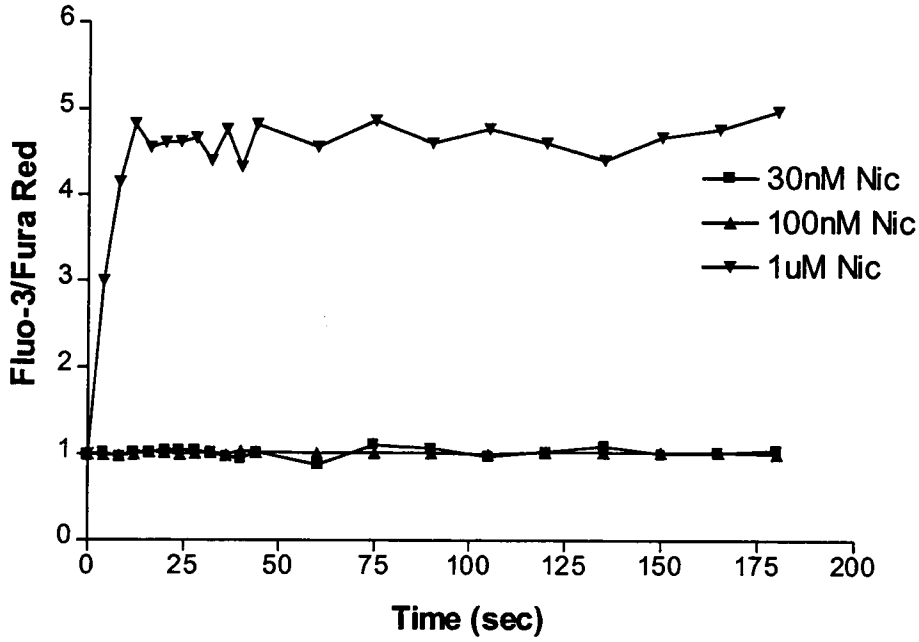


Figure 2-1: NCI-H69: Dose Response Studies With Nicotine (Table 2-1)

There was a nearly 5x increase in the ratio following treatment with 1μM nicotine.

The ratio was not altered by treatment with 30 nM and 100 nM nicotine.

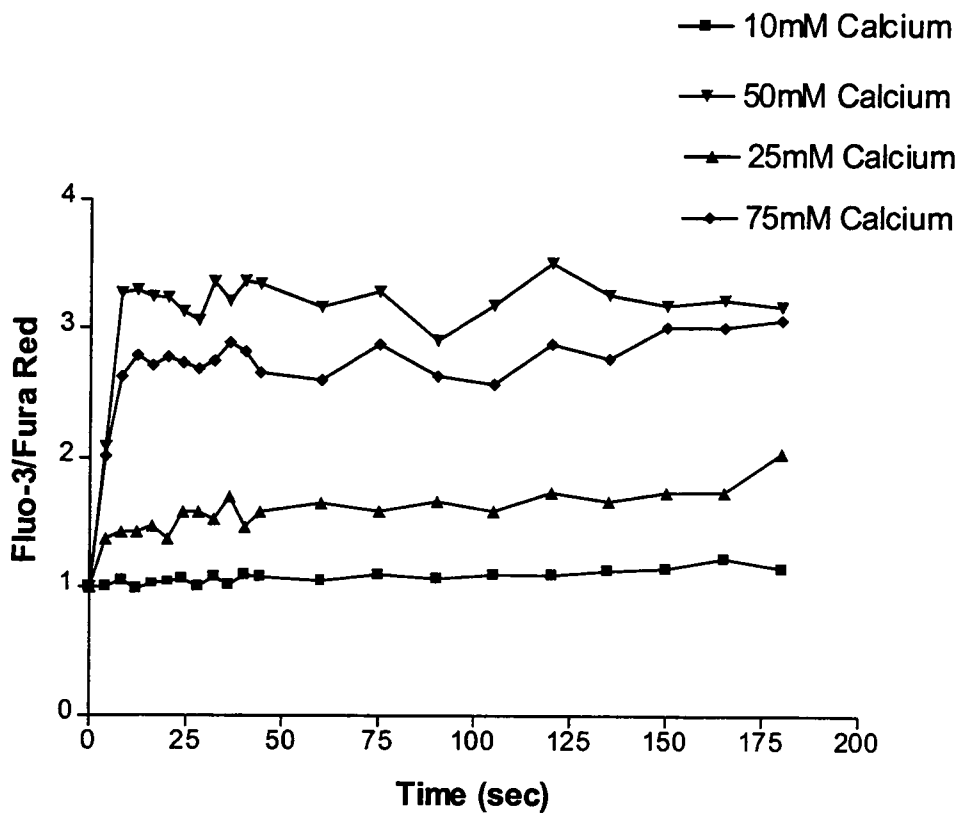


Figure 2-2: NCI-H69: Dose Response Studies With Calcium in Buffer At A Nicotine Concentration of 1 μM (Table 2-2)

The largest ratio increase, which was greater than 3x, occurred in cells treated with 1μM nicotine in the presence of 50 mM Ca^2. Buffer with only 25 mM and 10 mM Ca^{2+} was associated with a less than 2x increase and no ratio change, respectively.

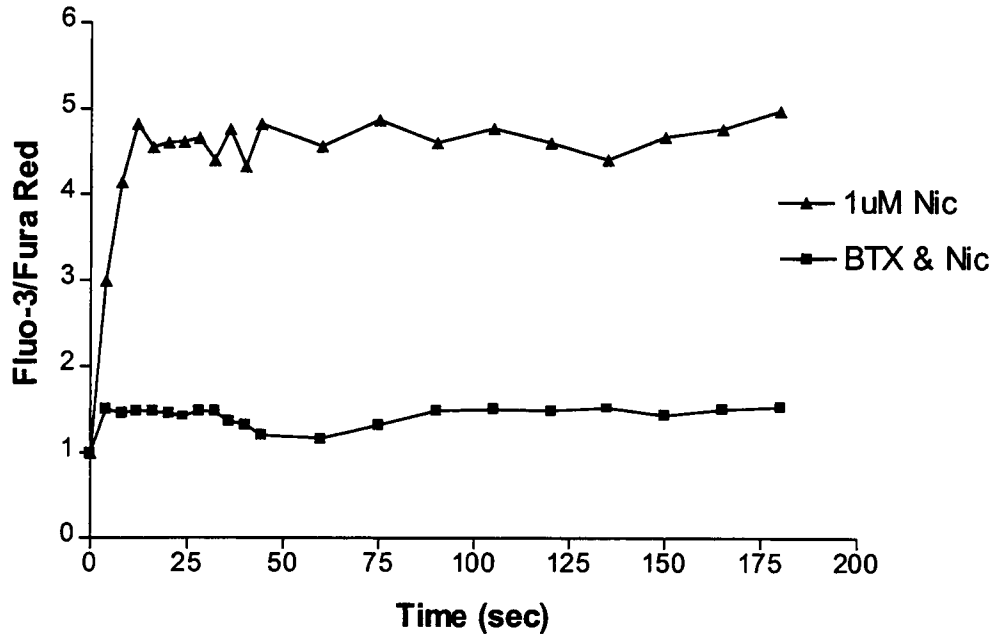


Figure 2-3: NCI-H69: Inhibition Of Response To 1 μM Nicotine by α-BTX (Table 2-3)

Pretreatment with 10 μM α-BTX reduced the ratio increase in response to 1μM nicotine from nearly 5x to 1.5x.

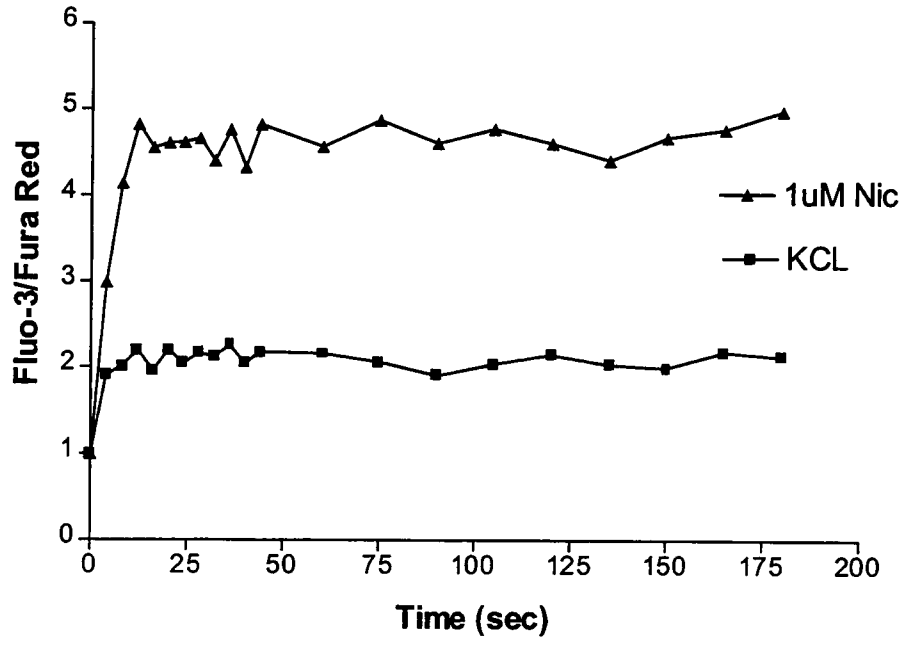


Figure 2-4: NCI-H69: Comparison Of Response To 1 μM Nicotine With Membrane Depolarization By 50 mM KCl (Table 2-4)

There was a 2x ratio increase following depolarization of the membrane by 50 mM KCl and a nearly 5x increase with 1μM nicotine.

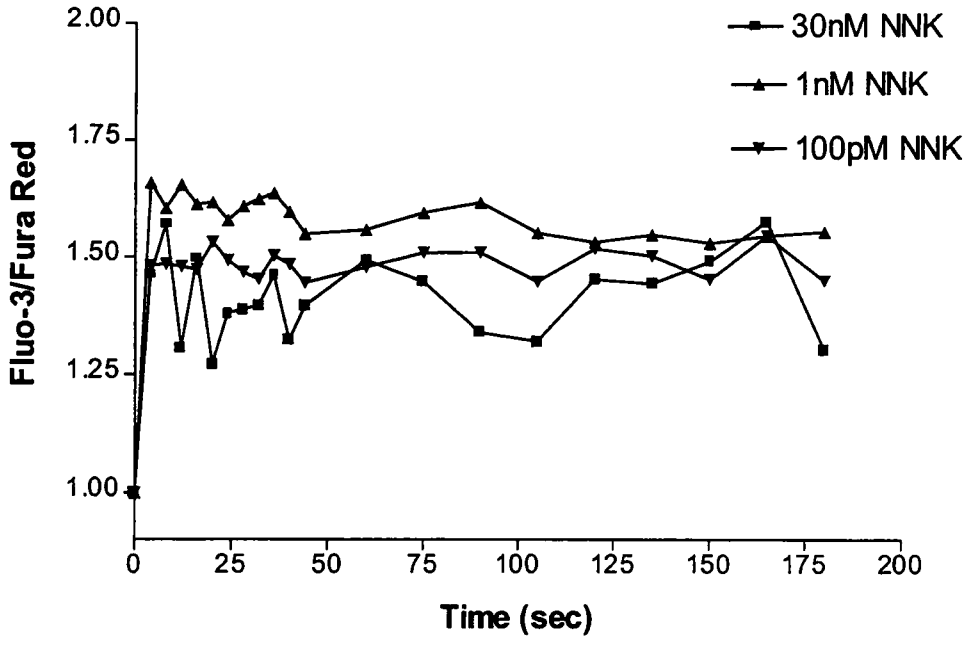


Figure 2-5: NCI-H69: Dose Response Studies With NNK (Table 2-5)

There was a similar 1.4 to 1.6x ratio increase for NNK concentrations ranging from 100 pM to 30 nM .

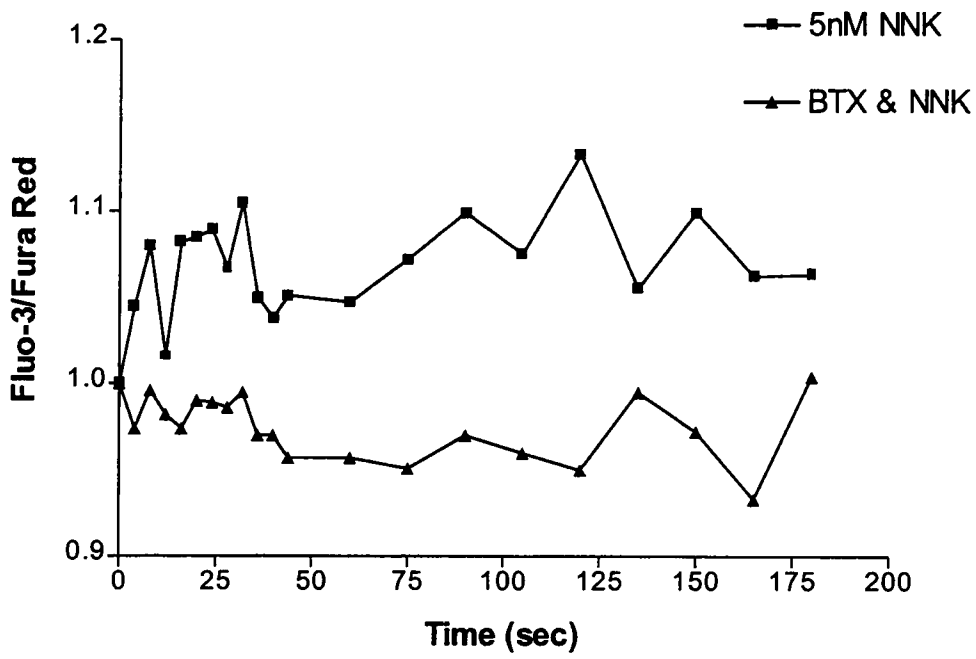


Figure 2-6: NCI-H69: Inhibition Of Response To 5 nM NNK By α-BTX (Table 2-6)

There was a nearly 1.1x increase following treatment with 5nM NNK that was reduced to no ratio change for cells pretreated with 10 μM α-BTX.

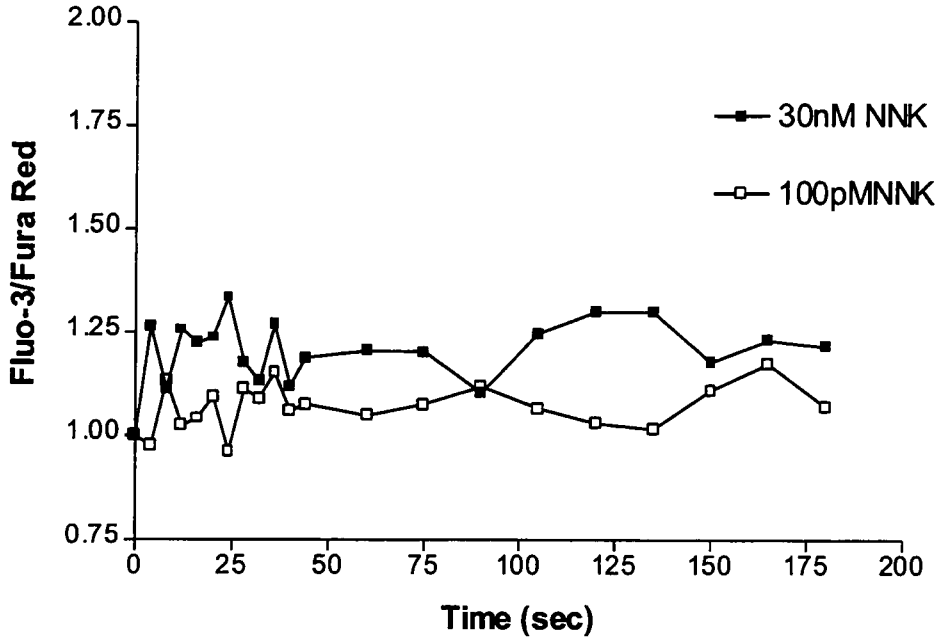


Figure 2-7: NCI-H69: Effect Of Chronic Exposure To 10% CO_2 On Dose Response To NNK (Table 2-7)

For cells subchronically treated 10% CO_2, there was a slightly larger ratio increase of 1.25x at 30 nM than the 1.1x increase for 100 pM NNK. Both ratio increases are less than the 1.4 to 1.6x ratio increase without subchronic 10% CO_2 treatment.

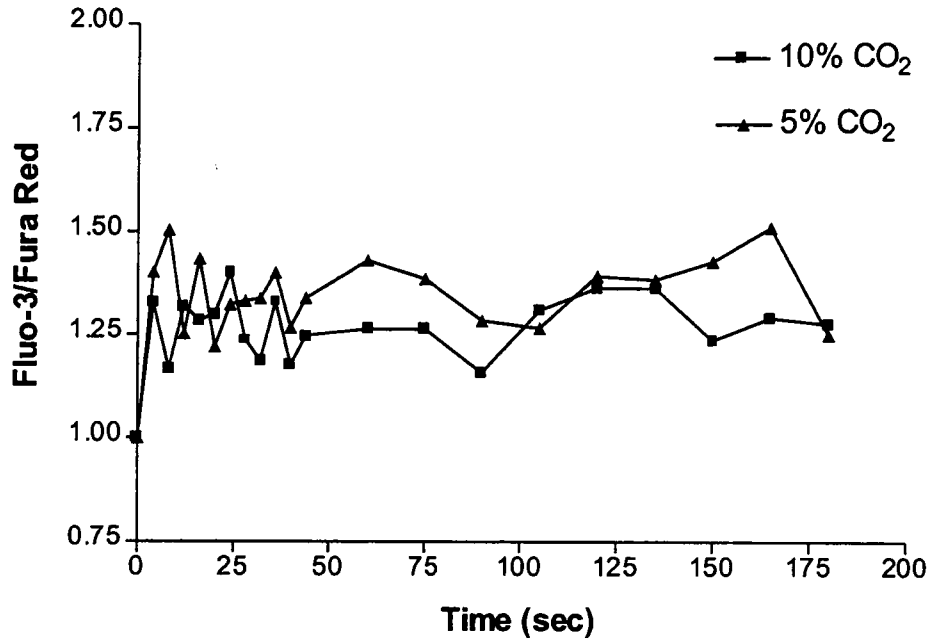


Figure 2-8: NCI-H69: Comparison Of Response To 30 nM NNK In An Environment Of 5% And 10% CO_2 (Table 2-8)

The 1.5x ratio increase in response to 30 nM NNK was reduced slightly to 1.3x for cells subchronically treated 10% CO_2.

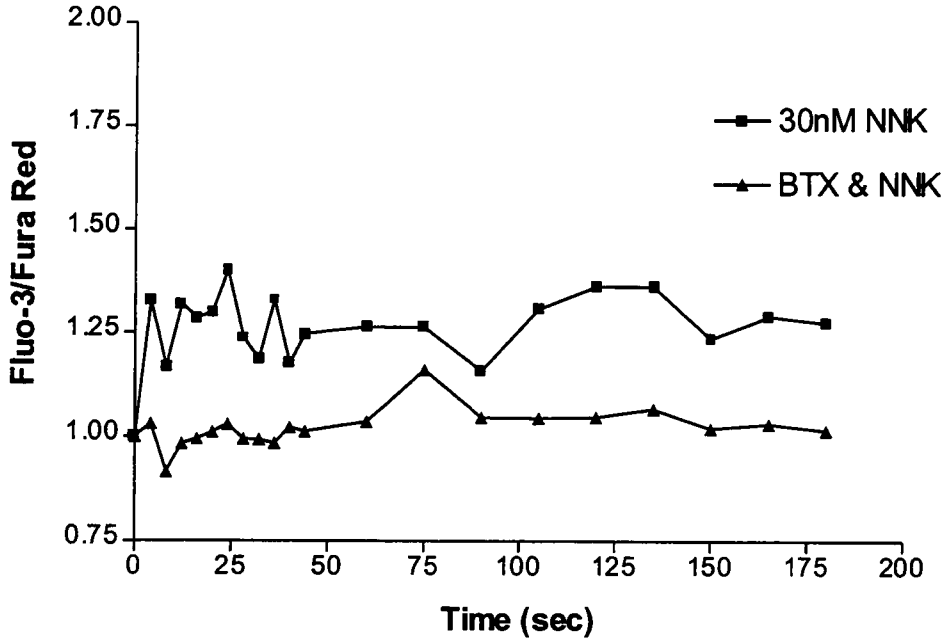


Figure 2-9: NCI-H69: Inhibiting Effects of α-BTX On The Response To 30nM NNK In An Environment Of 10% CO_2 (Table 2-9)

The 1.3x ratio increase following 30 nM NNK treatment of cells subchronically treated 10% CO_2 was reduced to no ratio change when cells subchronically treated 10% CO_2 were pretreated with 10 μM α-BTX.

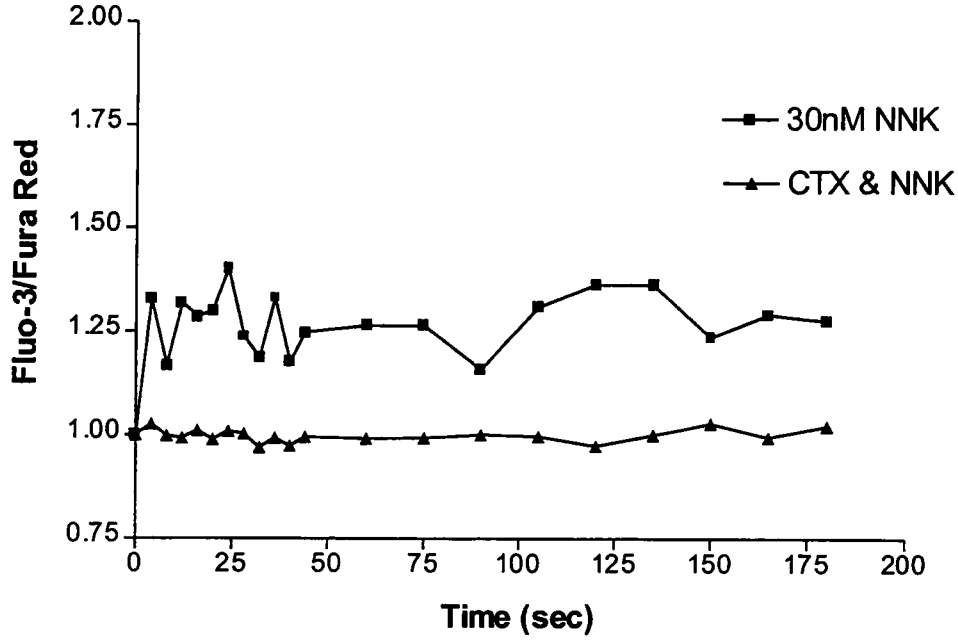


Figure 2-10: NCI-H69: Inhibiting Effects Of The N-type Calcium Channel Blocker ω-Conotoxin (CTX) GVIA On The Response To 30 nM NNK In 10% CO_2 (Table 2-10)

The 1.3x ratio increase following 30 nM NNK treatment of cells subchronically treated 10% CO_2 was reduced to no ratio change when cells subchronically treated 10% CO_2 were pretreated with 40 pM ω-CTX GVIA.

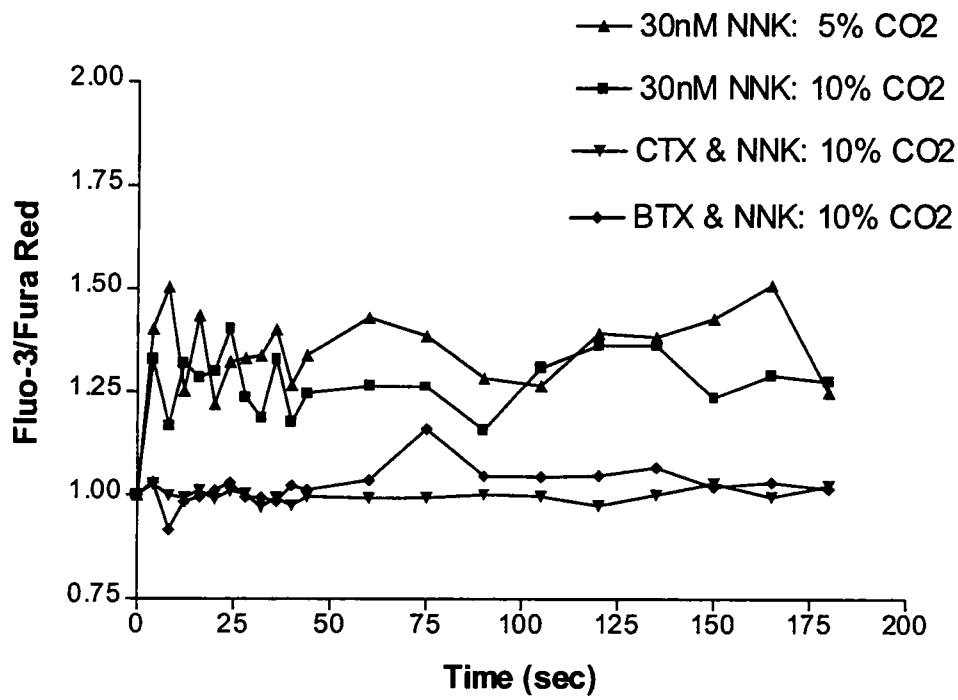


Figure 2-11: NCI-H69: Comparison Of The Inhibiting Effects Of α-BTX Or The N-type Calcium Channel Blocker ω-Conotoxin (CTX) GVIA On The Response To 30nM NNK In An Environment Of 10% CO_2 And The Response To 30nM NNK In An Environment Of 5% CO_2 (Tables 2-8, 2-9 and 2-10)

The 1.5x ratio increase in response to 30 nM NNK was reduced slightly to 1.3x for cells subchronically treated 10% CO_2. The response was completely blocked by α-BTX or ω-CTX GVIA in cells subchronically exposed to 10% CO_2.

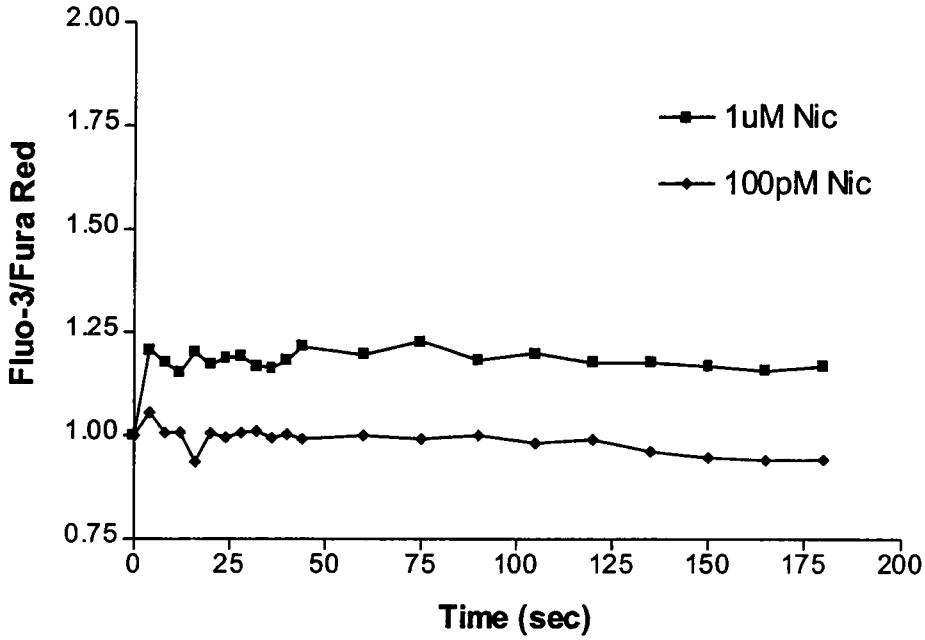


Figure 2-12: PNEC: Dose Response Studies With Nicotine (Table 2-11)

There was a 1.25x ratio increase following treatment with 30 nM and 1 μM nicotine, however, the ratio was unchanged by the 100 pM treatment.

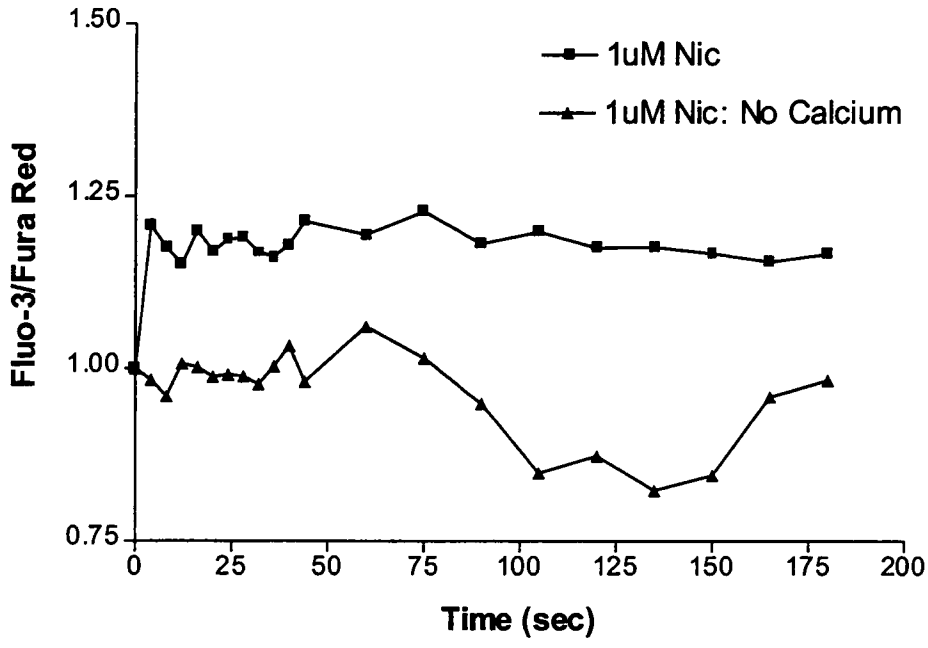


Figure 2-13: PNEC: Dose Response Studies With Calcium In Buffer At A Nicotine Concentration of 1 μM (Table 2-12)

There was a 1.2x ratio increase in cells treated with 1μM nicotine immediately prior to reading in buffer containing 50 mM Ca^{2+}, however, the ratio was unchanged for cells in buffer lacking Ca^{2+} (PBS without Ca^{2+}).

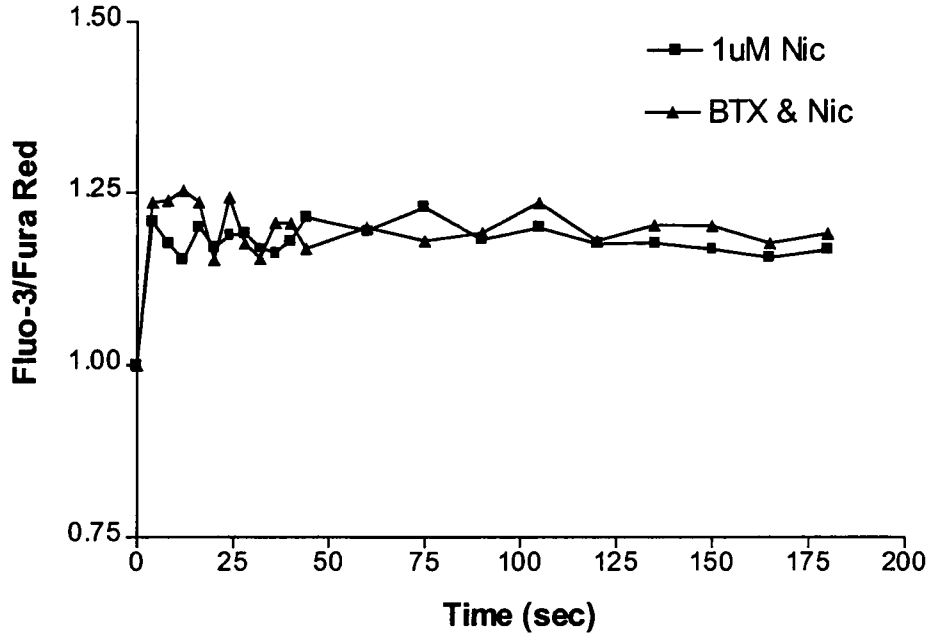


Figure 2-14: PNEC: Inhibition Of Response To 1 μM Nicotine By α-BTX (Table 2-13)

There was a similar 1.2x to 1.25x ratio increase for cells treated with 1μM nicotine immediately prior to reading regardless of whether they had also received pretreatment with 10 μM α-BTX.

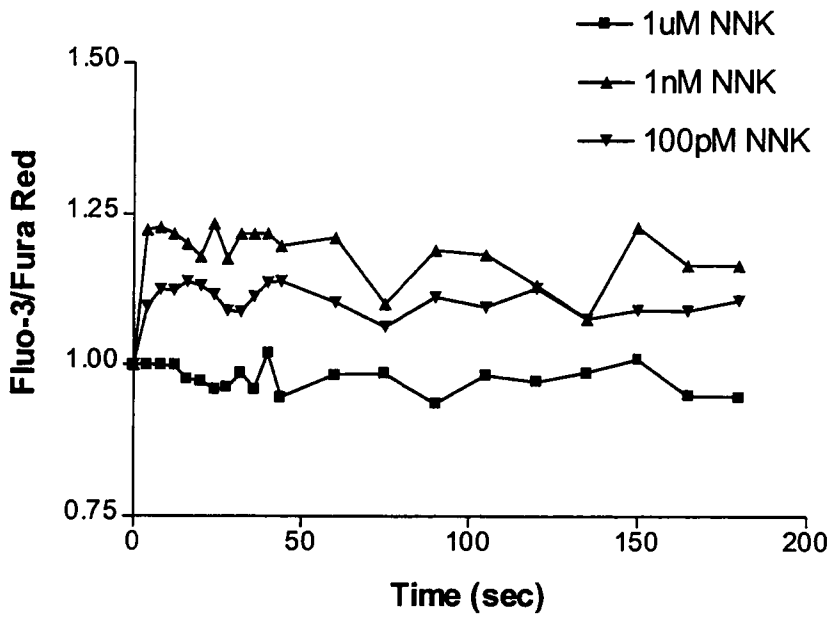


Figure 2-15: PNEC: Dose Response Studies With NNK (Table 2-14)

There was a ratio increase of 1.2x and 1.1x for cells treated with 1 nM and 100 pM NNK, respectively. No ratio change occurred with 1 μM NNK.

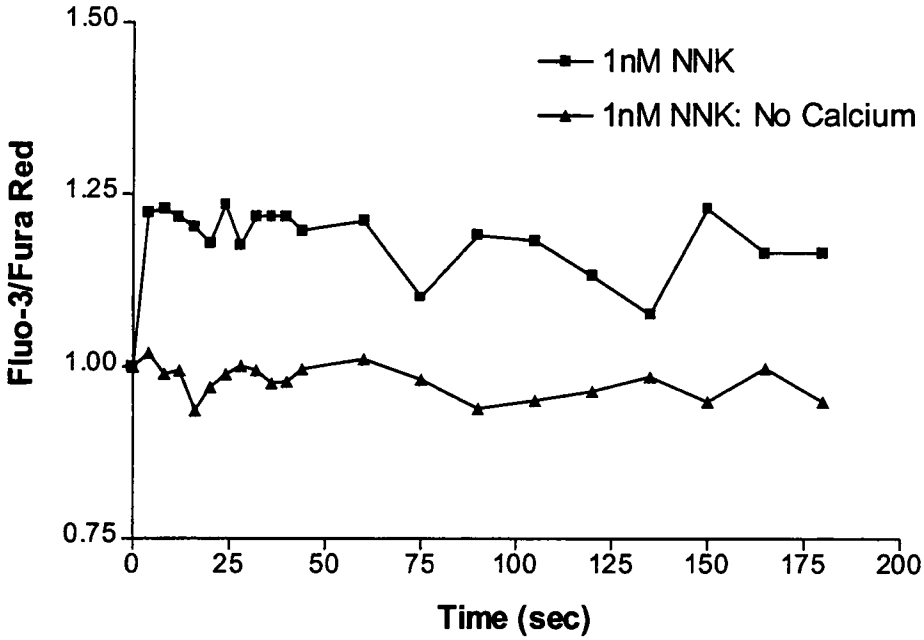


Figure 2-16: PNEC: Dose Response Studies With Calcium In Buffer At A NNK Concentration of 1 nM (Table 2-15)

There was a ratio increase of 1.25x for cells treated with 1nM NNK immediately prior to reading in buffer containing 50 mM Ca^{2+}, however, there was no ratio change for cells in buffer lacking Ca^{2+} (PBS without Ca^{2+}).

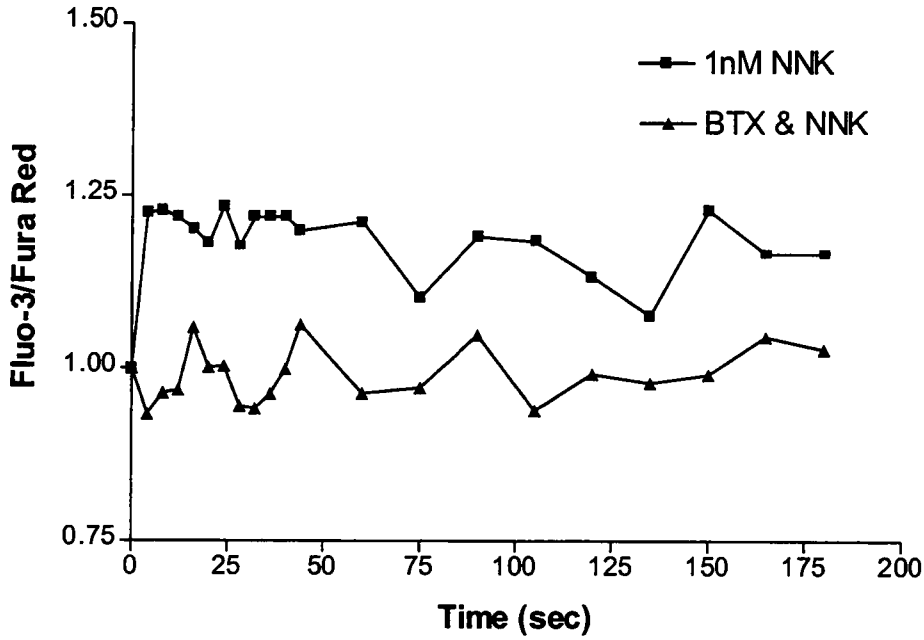


Figure 2-17: PNEC: Inhibition Of Response To 1 nM NNK By α-BTX (Table 2-16)

There was a nearly 1.25x increase following treatment with 1nM NNK that was reduced to no ratio change for cells pretreated with 10 μM α-BTX.

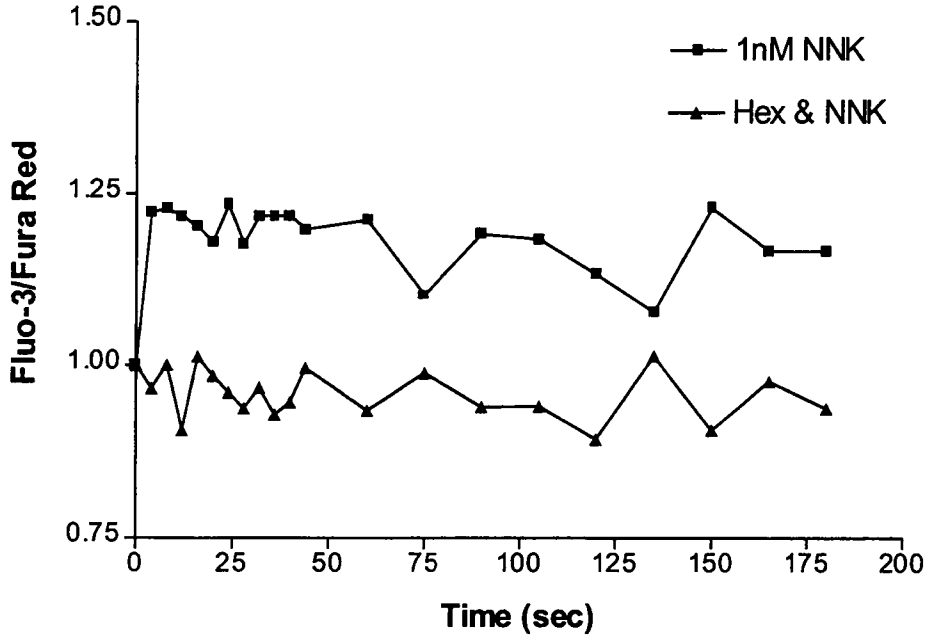


Figure 2-18: PNEC: Inhibiting Effects Of The Broad Spectrum Blocker Of Neuronal nAChR, Hexamethonium, On The Response To 1 nM NNK (Table 2-17)

There was a nearly 1.25x increase following treatment with 1nM NNK that was reduced to no ratio change for cells pretreated with 1uM hexamethonium.

PART III: CHARACTERIZATION OF VOLTAGE OPERATED CALCIUM CHANNELS

Chapter 1: Abstract

Ligand binding of nicotine or NNK to the cell surface α_7-nAChR of SCLC and PNEC stimulates release of the autocrine growth factor 5-HT. The release and reuptake of 5-HT leads to cell proliferation. Thus, tobacco-specific nicotinic agonists acting at the cell surface α_7-nAChR initiate a mitogenic autocrine loop with growing evidence of downstream activation of intracellular kinase-driven signaling cascades involving the *raf* kinases . The initiation of this growth promotion by ligand binding to the α_7-nAChR Ca^{2+} channel and the central role of Ca^{2+} as a second messenger in kinase-driven signaling pathways strongly suggests that cellular tools for controlling Ca^{2+} movement, such as VOCC, are upregulated in SCLC cells derived from chronic smokers. It was previously shown using flow cytometry that nicotine treatment of NCI-H69 cells caused influx of extracellular Ca^{2+} through the α_7-nAChR followed by Ca^{2+} movement through VOCC.

In the present study, characterization of VOCC subtypes on NCI-H69 and PNEC using classical radioligand binding studies did not produce informative saturation or competition curves possibly due to the delicate character of the neoplastic cells or lack of complete specificity of the ligands. Examination of VOCC subtype mRNA expression using RT-PCR was very successful. NCI-H69 demonstrated high expression levels of all three "L, N, and P" VOCC subtype cDNA targets. In

contrast, PNEC demonstrated a complete lack of the "N" type VOCC band and significantly less of the "L and P" subtypes. These results supported the hypothesis that the neoplastic cells have more VOCC subtypes and express them at greater levels than do the PNEC. The greater expression of VOCC subtypes by the NCI-H69 has probably resulted from chronic stimulation of the α_7-nAChR by nicotine and nicotine derived carcinogenic nitrosamines.

Chapter 2: Introduction

The "smoking specific" human SCLC, which occurs almost exclusively in smokers with a history of chronic lung disease (Weiss 1991), has a post-therapy five year survival rate below 5% (Cook et al. 1993) due to resumption of cancer growth associated with extensive metastatic spread (Hansen and Rorth 1997). The mechanism by which smoking and the hypoxia of chronic lung disease promote the growth of this aggressive cancer type is under investigation.

Due to their neuroendocrine phenotype, SCLC cells share many morphologic and functional characteristics with normal PNEC (Linnoila 1996) including a cell membrane oxygen binding protein that responds to changes in the relative proportions of the intrapulmonary gases O_2 and CO_2 (Youngson et al. 1993). Changes in oxygenation leads to PNEC hyperplasia and enhanced secretion of the biogenic amine 5-HT (Youngson et al. 1993, Johnson and Georgieff 1989, Guyton and Hall 1996) which causes bronchoconstriction (Garrison 1990).

Recent advances in the understanding of normal and neoplastic PNEC physiology has identified 5-HT as an autocrine growth factor for cells with the

PNEC phenotype (Cattaneo et al. 1993, Schuller and Hegedus 1989) and demonstrated that almost 100% of SCLC secrete 5-HT (Gazdar 1994). These findings collectively suggested that growth promotion occurring during the recurrence phase of human SCLC involves a combination of factors including 5-HT, nicotine or nicotine-derived nitrosamines, and chronic hypoxia associated with chronic lung disease.

The experimental growth promotion of SCLC in hamsters was driven by a mitogenic autocrine serotonergic loop that began with the activation of α-BTX-sensitive α_7-nAChRs on the cell surface by simultaneous exposure to carcinogenic nitrosamines and hyperoxic lung injury (Schuller et al. 1988, Schuller et al. 1990). This growth promotion also occurred with exposure to nicotine and hyperoxic lung injury (Schuller at al. 1995). In vitro growth promotion of cell lines derived from human SCLC in response to nicotine or the structurally related NNK was further potentiated by simultaneous exposure to elevated atmospheric CO_2 (Schuller 1989, Schuller and Hegedus 1989) and blocked by 5-HT receptor antagonists and PKC inhibitors (Schuller 1994). Proliferation was also blocked in the presence of the α_7-nAChR antagonists α-BTX and hexamethonium, a broad spectrum blocker of all neuronal nicotinic receptors (Schuller 1989, Schuller and Hegedus 1989). A separate study demonstrated release of 5-HT by SCLC in response to nicotine (Cattaneo et al. 1993). Together these findings implicate an initial interaction of

nicotine and/or NNK at the cell surface α_7-nAChRs of SCLC and the subsequent role of 5-HT in a kinase driven mitogenic signaling pathway.

It was shown in Part II of this dissertation using flow cytometry that the stimulation of normal and neoplastic PNEC by nicotine and the nicotine-derived carcinogenic nitrosamine NNK resulted in the influx of extracellular Ca^{2+}. While most of the Ca^{2+} entered SCLC via stimulated α_7-nAChR Ca^{2+} channels, nicotine must have also stimulated Ca^{2+} movement through additional channels which could include neuronal nicotinic receptors having α subunits other than α_7 that would not have been blocked by α-BTX. Indeed, NCI-H69 cells have recently been shown to express nAChRs with the α_3 and α_5 subunits (Schuller unpublished). NNK stimulated the influx of Ca^{2+} in NCI-H69 exclusively via the α_7-nAChR Ca^{2+} channel and was a much more potent activator of this channel than was nicotine. This increased sensitivity to NNK was supported by recent binding studies. The affinity of NNK to the α_7 receptor was shown to be 1,300 times greater than that of nicotine and 3,500 times greater than that of the carcinogenic nicotine metabolite N-nitrosonornicotine (NNN). NNK-induced cell proliferation and DNA synthesis measured by incorporation of ^{3}H-thymidine has been experimentally completely inhibited by α-BTX (Schuller and Orloff, 1998). Culturing NCI-H69 cells for one week in a hypoxic condition with 10% atmospheric CO_2 resulted in a small reduction in the responsiveness of the cells to NNK. At the flow cytometry level,

the present results suggested that subchronic hypoxic growth potentiation of SCLC mediated by a cell membrane oxygen binding receptor may be accompanied by a slightly reduced sensitivity to single-dose NNK treatments.

Complete blockage of the response to NNK was observed for subchronically hypoxic NCI-H69 pretreated with α-BTX or with ω-CTX GVIA, a VOCC blocker. NNK, therefore, appears to stimulate initial Ca^{2+} entry by binding to the α_7-nAChR resulting in membrane depolarization followed by subsequent influx of most of the Ca^{2+} through activated VOCCs. The response of PNEC to NNK appeared to be completely mediated by α_7-nAChRs in a fashion similar to that described for NCI-H69 but PNEC had fewer or far less responsive α_7-nAChRs. The modest response of PNEC to nicotine compared to NCI-H69 cells supported the hypothesis that PNEC have fewer or less responsive nAChRs and possibly lack or have reduced numbers of nAChRs with additional α subunit subtypes. In support of this, recent investigations have shown that fetal hamster PNEC do not express the additional nAChR subtypes having the α_3 and α_5 subunits which are found on cell lines derived from SCLC (Schuller unpublished). The relative unresponsiveness to both nicotine and NNK of the PNEC α_7-nAChR compared to NCI-H69 is hypothesized to reflect the smoking-induced massive upregulation of these receptors in the SCLC cell lines all of which are derived from patients who were chronic smokers.

The demonstration of Ca^{2+} movement in both of these cell types in response to nicotine and NNK strongly implicates a central role for Ca^{2+} as a second messenger in the serotonergic mitogenic kinase-driven signaling pathway. Ca^{2+} movement required ligand binding to α_7-nAChR Ca^{2+} channels and proper functioning of voltage-activated Ca^{2+} channels (VOCC). The increased Ca^{2+} responsiveness of the NCI-H69 to nicotine and NNK compared to the PNEC is probably representative of a generalized upregulation of the entire serotonergic mitogenic pathway. This could include increased expression of VOCC subtypes potentially presenting as increases in the expression level, sensitivity, and range of subtypes present. Upregulation of VOCC expression by the tumor cells could provide a novel target to be used for diagnostic imaging and radiopharmaceutical therapies.

Characterization of VOCC subtypes can utilize both the pharmacological and the genetic subtype classification systems. Decades of study have led to a continuously evolving classification and functional description of various types of Ca^{2+} channels based on properties including voltage- and time-dependent kinetics, pharmacology, cellular distribution, and, most recently, genetic sequence homology (Cassola and Afeche 1996, Clapham 1995, De Waard et al. 1996, Ertel and Ertel 1996 , McClesky 1994, Stea et al. 1995, Tsien et al. 1991, Uchitel 1997, Wickman and Clapham 1995). Early division of VOCC types into families based

on kinetics, pharmacology and distribution has been largely confirmed and extensively refined by the analysis of cDNA sequence homology. VOCC subtypes defined by their well-established responses to specific agonists and antagonists are designated as "L" which are dihydropyridine (DHP)-sensitive, and "N, P, Q and T" which are DHP-insensitive (McCleskey 1994). SCLC, as noncontractile cells, are more likely to express and use High Voltage Activated (HVA) channels which require a much greater degree of membrane depolarization to be activated but allow ion passage for a more extended period of time. "L" channels are sensitive to widely used therapeutic "calcium channel blockers" including DHPs (nicardipine, nifedipine and nimodipine), phenylalkylamines (verapamil), and benzodiazepines (diltiazem) (Murad 1990), in addition to calciseptine from mamba snake venom, nitrendipine (DHP antagonist) and ω-agatoxin (ω-ATX) IIIA. Calciseptine is found in the venom of the mamba snake and agatoxins are polypeptides found in funnel-web spider venoms. Toxins affecting neuronal VOCC (Uchitel 1997, Cassola and Afeche 1996) include conotoxins (CTX) which marine snails use to paralyze their fish prey, funnel-web spider venoms (polyamines, polypeptides and grammotoxin), and mamba snake venoms (fasciculin, calciseptine, FS2 and calcicludine). Among the DHP-insensitive VOCC subtypes, sensitivity differences are most effective in descriminating "N" from the "P" and "Q" subtypes.

Ion channels for different ion types all have a similar physical structure (De Waard et al. 1996, McCleskey 1994, Tsien et al. 1991). The channels are heteroligomeric complexes composed of a central ion pore designated as the α_1 subunit and additional adjacent subunits (α_2/δ, β, and γ) which modulate the action of the pore. The α_1 subunit is composed of four homologous repeats referred to as domains I-IV each of which contains six transmembrane α-helical subunits referred to as S 1-6 interconnected by variably sized loops (Tsien et al. 1991). Subunit 4 , which opens the channel in response to membrane depolarization, has repeated motifs of positively charged amino acids at every third or fourth position followed by hydrophobic amino acids. The actual ion pore is formed by the transmembrane α-helices S4, S5, S6 and the loop connecting S5 to S6. Slight variations in the amino acid sequences of the α_1 subunit transmembrane α-helices and intervening loops are responsible for the antagonist/agonist sensitivites of each pharmacologically-defined VOCC family.

Characterization of VOCC expression from a genetic subtype classification examines mRNA expression levels for the α_1 subunit genes (Barry et al. 1995, Dubel et al. 1992, Fujita et al. 1993, Hui et al. 1991, Kamphuis and Henriksen 1998, Ma et al. 1992, Mikami et al. 1989, Mori et al. 1991, Niidome et al. 1992, Seino et al. 1992, Snutch et al. 1991, Soong et al. 1993, Starr et al. 1991, Williams et al. 1992a & b, Williams et al. 1994,). The α_1 subunit is coded by 5 genes

designated A-E for which the gene names agreed upon by most researchers are now indicated as CACNA1A-E referring to calcium channel alpha-1 subunit gene A-E (Snutch et al. 1990, Soong et al. 1993). The genetic examination of neuronal VOCC has largely preserved the original pharmacological distinctions but has added the possibility that several different genes can code for pharmacologically similar VOCCs (Stea et al. 1995). Pharmacological "N" and "L" VOCCs are coded by the B (Williams et al. 1992b, Fujita et al. 1993, Stea et al. 1993) and the C/D genes (Tanabe et al. 1990, Williams et al. 1992a), and the pharmacologically similar "P" and "Q" types are both coded by the A gene (Mori et al. 1991). GenBank contains many cDNA sequences for the VOCC subunits that have been identified in cells of neuronal origin. Sequence homology for similar subunits coded for by specific genes for the α_1 subunit (CACNA1A-E) is often very high between species indicating that these are highly conserved genes. In some cases such as the "N" type CACNA1B, two distinct sequences representing posttranslational splice variants are detected using the same set of primers for RT-PCR (Williams et al. 1992a). The structural similarity of all ion channel types and the high level of sequence homology within the VOCC make the choice of RT-PCR primers that will be specific for the targeted VOCC subunit subtype difficult as primers that generate a specific VOCC GenBank cDNA sequence in one species or one cell type may not generate that same cDNA band under different conditions. This necessitates the sequencing of cDNA bands generated by RT-PCR in order to

verify that the target sequence has been successfully amplified and to screen for previously unidentified cDNA sequences with high homology to concensus motifs likely to represent VOCCs.

The specific hypothesis to be tested in Part III is that VOCC subtype expression is upregulated in SCLC of chronic smokers relative to normal fetal PNEC. The first part of testing this hypothesis is to characterize VOCC subtypes in untreated NCI-H69 and fetal hamster PNEC. This will be examined by quantifying pharmacological subtype expression using radio-ligand receptor binding studies on intact cells and by identifying specific cDNA α_1 subunit mRNA expression for genetic subtypes using nonquantitative RT-PCR with sequencing of bands to verify targeted sequences. Pharmacological targeting of "L" subtypes utilized verapamil and nifedipine, while, "N" subtypes will be examined using ω-CTX GVIA and ω-CTX MVIIA. RT-PCR will use primer pairs which target GenBank α_1 subunit cDNA sequences isolated from human SCLC or brain tissue. Sequences previously documented in tissues of neural or neuroendocrine origin have the highest probability of being expressed by SCLC and fetal hamster PNEC, both of which have a neuroendocrine phenotype. The target sequences are GenBank #S76537 (Barry et al. 1995) , M94172 & M94173 (Williams et al. 1992a) and M76558 (Williams et al. 1992b) corresponding to alpha-1a (P/Q), alpha-1b (N), and alpha-1d (L) subtypes, respectively. The objective is to demonstrate a difference in

expression of specific pharmacological and genetic subtypes by the two populations.

Chapter 3: Materials and Methods

NCI- H69 Cell Line: NCI-H69 cells from a human SCLC were purchased from the American Cell Type Culture Collection (Rockville, Maryland). Cells were grown at 37° in an atmosphere of 5% CO_2 and RPMI media supplemented with fetal bovine serum (10%, v/v), L-glutamine (2mM), penicillin (100U/ml) and streptomycin (100μg).

Fetal Hamster PNEC: Cultures of fetal hamster PNEC were established from fetal hamster lung periphery harvested on day 15 of gestation and maintained in an atmosphere of 10% CO_2, a condition which selectively promotes the growth of PNEC (Schuller 1994). The cells were routinely maintained in RPMI medium supplemented with fetal bovine serum (10%, v/v), L-glutamine (2mM), and gentamycin sulfate (50mg/ml).

RADIO-LIGAND RECEPTOR BINDING

Classic radioligand binding studies were performed with 5 x 10^6 NCI-H69 cells or PNEC, prewashed with PBS, per tube using ligands with preferential affinity for

the targeted channel subtypes. A total protein concentration per tube was determined using the Bicinchoninic Acid Assay (BCA, Pierce, Rockford, IL) method. "N" type channel studies used ^{125} I-ω- CTX GVIA, ω- CTX GVIA, and ω-CTX MVIIA (Tsien et al. 1991, Uchitel 1997, Cassola and Afeche 1996). "L" type channel studies used ^{3}H-desmethoxyverapamil and nifedipine (Tsien et al. 1991, Uchitel 1997, Cassola and Afeche 1996). The total reaction volume was 250µl which included 25 µl cold ligand or water, 25µl radioligand and 250µl intact cell suspension in buffer (75 mM Tris, 5 mM $CaCl_2$, 2 mM EDTA, 1 mg/ml BSA, pH 7.4). Following preincubation with cold ligand (30 min, room temp), the reaction was incubated (60 min, room temp) and terminated by the addition of 100 µl cold buffer. Samples were washed with buffer, centrifuged (23,000 X g for 5 min) three times and counted on the Tri-Carb 2300TR Liquid Scintillation Analyzer (Packard, Meriden, CT).

Specific Binding Experiments:

NCI-H69: Saturation Studies Targeting "L" type VOCC –

I. 50pM nifedipine with ^{3}H-desmethoxyverapamil (1.9pM, 12.1pM, 19.9pM, 46.1pM, 77.6pM, 86.4pM, 383pM, 450.9pM, 1.17nM and 111.37nM)

II. 50pM nifedipine with ^{3}H-desmethoxyverapamil (12.1pM, 19.9pM,

48.3pM, 95.9pM, 191.5pM, 465.3pM, 1.06nM and 11.2nM)

III. 50pM nifedipine with ^{3}H-desmethoxyverapamil (38.6pM, 102.3pM, 219.3pM, 320.2pM, 366.7pM, 943.9pM, 1.83nM, 3.59nM and 15.95nM).

IV. 50pM nifedipine with ^{3}H-desmethoxyverapamil (406pM, 593pM, 1.01nM, 1.27nM, 1.43nM, 1.86nM and 2.02nM)

V. 2nM nifedipine with ^{3}H-desmethoxyverapamil (406pM, 593pM, 1.01nM, 1.27nM, 1.43nM, 1.86nM and 2.02nM)

VI. 2nM nifedipine with ^{3}H-desmethoxyverapamil (406pM, 593pM, 1.01nM, 1.27nM, 1.43nM, 1.86nM and 2.02nM) using cells kept in 10% CO_2 for 7 days.

VII. 500nM nifedipine with ^{3}H-desmethoxyverapamil (12pM, 251pM, 2.02nM, 5.7nM, 11.3nM, 23.8nM, 37.2nM, 57nM, 76.3nM and 100.2nM)

VIII. 1μM nifedipine with ^{3}H-desmethoxyverapamil (8.23pM, 18.6pM, 24pM, 37.9pM, 57.8pM and 89.1pM)

IX. 1μM nifedipine with ^{3}H-desmethoxyverapamil (18.6pM, 24pM, 37.9pM, 57.8pM and 89.1pM)

NCI-H69: Competition Studies Targeting "L" type VOCC –

I. 46pM ^{3}H-desmethoxyverapamil vs nifedipine (50pM, 500pM, 5nM, 50nM, 500nM and 1μM)

II. 7nM ^{3}H-desmethoxyverapamil vs nifedipine (0, 500pM, 5nM, 50nM, 100nM, 500nM and 1μM)

III. 21pM ^{3}H-desmethoxyverapamil vs nifedipine (0, 50pM, 500pM, 5nM, 50nM and 500nM)

IV. 26pM ^{3}H-desmethoxyverapamil vs nifedipine (0, 10pMand 20pM)

NCI-H69: Saturation Studies Targeting "N" type VOCC –

I. 1μM ω-CTX GVIA with ^{125}I-ω-CTX GVIA (5pM, 7pM, 17pM, 28pM, 63pM, 100pM, 130pM, 145pM, 241pM and 228pM)

II. 1μM ω- CTX GVIA with ^{125}I-ω- CTX GVIA (2.7pM, 6.7pM, 11.4pM, 17.6pM, 22.4pM, 41.1pM, 56.1pM, 107pM, 156pM and 217pM)

III. 1μM ω- CTX GVIA with ^{125}I-ω- CTX GVIA (19.3pM, 25.1pM, 64.9pM, 97pM, 133pM, 172pM, 495pM and 1.2nM)

NCI-H69: Competition Studies Targeting "N" type VOCC –

I. 37pM ^{125}I-ω- CTX GVIA vs ω- CTX GVIA (0 and 1μM)

II. 46pM ^{125}I-ω- CTX GVIA vs ω- CTX GVIA (0 and 1μM)

III. 37pM ^{125}I-ω- CTX GVIA vs ω- CTX MVIIA (0 and 1μM)

IV. 46pM ^{125}I-ω- CTX GVIA vs ω- CTX MVIIA (0, 1μM and 10μM)

V. 43pM ^{125}I-ω- CTX GVIA vs ω- CTX MVIIA (0, 100nM and 500nM)

VI. 44pM ^{125}I-ω- CTX GVIA vs ω- CTX MVIIA (0, 100nM, 500nM and 1μM)

VII. 21pM ^{125}I-ω- CTX GVIA vs ω- CTX MVIIA (0, 100nM, 500nM and 1μM)

PNEC: Saturation Studies Targeting "L" type VOCC –

I. 2nM nifedipine with ^{3}H-desmethoxyverapamil (406pM, 593pM, 1.0nM, 1.3nM, 1.4nM, 1.9nM and 2nM)

RT-PCR AND BAND SEQUENCING

RNA Isolation : RNA was isolated from NCI-H69 and PNEC using the guanidine isothiocyanate (GIT)/cesium chloride (CsCl) overnight ultracentrifugation method (MacDonald et al. 1987). The floating NCI-H69 and adherent PNEC cells were removed from their culture flasks by pouring and scraping, respectively, and placed in a 50 ml conical tube. The cells were centrifuged (1900x, 3 min) and the media

from above the cell pellet was discarded. The cells were resuspended in 25 ml of PBS, centrifuged (1900x, 3 min), and PBS from above the cell pellet was discarded. A GIT buffer solution was prepared by adding 47.2 g (4M final) GIT and 1mL 3M sodium acetate pH 7 to a final volume of 100ml of sterile water. The GIT buffer solution was sterile filtered (1mm filter) and 1ml 2-mercaptoethanol was added under a fume hood. The cell pellet was dissolved in 8 ml GIT buffer . The cell pellet was passed through a 20 gauge needle on a 30ml syringe three times in order to shear the DNA. A CsCl buffer solution was prepared by adding 95.97 g (5.7M final) CsCl, 1ml 3M sodium acetate pH 7 and 2ml 0.5M EDTA pH 8.0 to a final volume of 100ml sterile water. The CsCl buffer solution was sterile filtered (0.8 μm filter). For each cell sample, a Seton tube (Seton Scientific, Los Gatos, CA) was partially filled with 4 ml of the CsCl buffer solution. The sheared DNA solution was carefully placed in the seton tube on top of the CsCl buffer solution by expelling the DNA solution from the syringe along the inner wall of the seton tube above the level of the CsCl buffer solution. The total fluid level reached completely to the top of tube in order to avoid potential collapsing of the tube during the overnight centrifugation. The seton tubes were placed in a swinging bucket rotor in a balanced arrangement and centrifuged overnight (32,000 RPM, 19°). Following centrifugation, each seton tube was carefully removed from the rotor under a RNA-PCR hood. For each tube, the supernatant was removed using an autoclaved RNA pipette until the remaining supernatant was within 0.5 cm of tube base. The cup-

like tube base containing the RNA pellet was separated from the remainder of the seton tube by cutting the tube with a sterile razor blade 5mm above the level of the remaining supernatant. All remaining supernatant was removed from the free cup-like seton tube base using a P-1000 pipette and care was taken not to disturb the small translucent RNA pellet. The RNA pellet was resuspended in 400µl sodium acetate by flushing and scraping at the pellet with the solution and pipette tip. The RNA solution was transferred to a 1ml Eppendorf tube and the tube was placed on ice. The RNA was precipitated by adding 1ml of 100% ethanol to the tube followed by freezing (80°, 15 min). The tube containing the frozen precipitated RNA was centrifuged (14,000 RPM, 4°, 10 min) and the supernatant was discarded. The RNA pellet was washed by adding 100µl of 80% ethanol and then centrifuged (14,000 RPM, 4°, 5 min). The RNA pellet was dissolved by adding 50µl nuclease free water. The RNA concentration of this final RNA solution was determined by measuring the optical density of 3µl of sample in 297µl water at 260 and 280 nm using a UV-160 UV-Visible Recording Spectrophotometer (Shimadzu Corp. Kyoto, Japan).

DNase I/ Reverse Transcription (RT) :. RNA was purified of any potential contamination by genomic DNA by using DNase I according to the technique described by Ambion (Austin, TX, Bauer et al. 1997, Dixon et al. 1998). Each reaction began with 2ug RNA obtained by the GIT/CsCl method. The RNA, 1µl of

DNase I 10x buffer and1μl DNase I were added to a 10ul total of nuclease free water. The mixture was incubated at room temperature (15 min). The reaction was stopped by adding 1μl of 25mM EDTA to the tube followed by a 65 ° incubation for 10 minutes.

Purified RNA was reverse transcribed into cDNA using the RETROscript™ kit (Ambion) according to the technique described by Ambion (Farrell 1997, Farrell 1993, Innis et al. 1990). Each reverse transcription (RT) reaction began with 2ug of DNase I-treated RNA which was in a 10μl volume following the DNase I treatment. 2ul (50mM) of random decamer primers (Ambion) were added to the 10μl RNA solution. The solution was heated to 82C for 3 minutes and then placed on ice. To the iced mixture was added 1μl (0.5mM) each of dGTP, dATP, dCTP and dTTP, 2μl DTT, 2μl of 10x buffer (100mMTris-HCl pH 8.3, 500mM Kcl, 15mM MgCl2), 1μl (40U) RNasin ribonuclease inhibitor (Promega, Madison, WI) and 1μl (200U) M-MLV reverse transcriptase (Gibco, Gaithersburg, MD) yielding a final volume of 20ul. Tubes to be used as the negative control RT reactions in which cDNA copies would not be made from RNA contained 1μl water substituted for the 1μl M-MLV, thereby creating a reaction lacking the reverse transcriptase enzyme. The total mixture was incubated (1hour, 37°) and then heated (10 min, 92°). The final product was used immediately for PCR or frozen at -20° for later use.

Polymerase Chain Reaction (PCR): The amplification of cDNA was performed using the QuantumRNA™ kit (Ambion) according to the technique described by Ambion (Farrell 1997, Farrell 1993, Innis et al. 1990). Each PCR reaction began with 5ul of the cDNA product from the DNase I/RT procedure. The cDNA was added to 4µl (0.2mM) dNTPs, 5ul 10x PCR buffer (100mM Tris-HCl pH 8.3, 500 mM KCl, 15mM $MgCl_2$), and 2.5µl DMSO. Each reaction tube received either 5 µl of a 10µM gene specific primer mixture or 1µl of the cyclophilin primer mixture provided by Ambion as an internal control for amplification of a moderately expressed "housekeeping" message (Finnegan et al. 1993). All tubes were supplemented with 0.25µl (1.25U) SuperTaq polymerase (Ambion). Nuclease free water was added to bring the final volume of each reaction to 50ul. Gene specific primers used were as follows:S76537 "P/Q" type from human SCLC forward GCT TAT GTC TGT CTG CTG ATC G and reverse GAC AAA GAG ATT CAG CAT CAG (Barry et al. 1995) ; M94172 and M94173 "N" type splice variants from human neuroblastoma forward GTC GCC AAC AGC TGG CCA GGA GC and reverse CGA AAG TGA GCG TGT CCT CAG GC (Williams et al. 1992a) ; and M76558 "L" type from human neuroblastoma forward GTG CCC TGC ACA CAG TAG TCG C and reverse GGC GCG GGC AGG TCG GCT GTT GG (Williams et al. 1992b). Anticipated cDNA band sizes for each primer pair based on the number of bases separating the primers in the GenBank sequences were 345 bp ("P" type,

Barry et al. 1995), 200 and 392 bp ("N" type splice variants, Williams et al. 1992a), and 354 bp ("L" type, Williams et al. 1992a). The cyclophilin primers provided by Ambion were designed to amplify a 216 bp DNA product (QuantumRNA™ Instruction Manual, Ambion). Due to the difference in melting temperatures for the gene specific primers, annealing temperatures utilized for the L, N and P primers were 60°, 51°, and 56°, respectively, for 90 seconds. A common annealing temperature of 60° was used separately for all the gene specific primers and cyclophilin. The PCR program consisted of preheating (94°, 120 sec), melting (94°, 60 sec), annealing and extension (72°, 90 sec). The melting, annealing and extension cycle was repeated 32 additional times. There was a final extension (72°, 5 minutes) after which the product was chilled at 4° until removal from the DNA Machine PTC-200 Peltier Thermal Cycler (MJ Research, Watertown, MA).

Aliquots of the RT/PCR products were visualized using agarose gel electrophoresis. A 2% agarose gel was prepared by adding 2g regular agarose to 100ml 1X TBE and microwaving the mixture for 3 minutes until boiling. The agarose gel solution was supplemented with 1µl of ethidium bromide per 10µl gel to be used. Gel lanes were loaded with a mixture consisting of 22µl of PCR product and 2µl loading buffer (5Prime→3Prime, Inc., Boulder, CO). A marker lane was loaded with a mixture consisting of 2.5µl of a 100bp DNA ladder (Gibco), 2µl loading buffer and 7µl water. Gel electrophoresis was performed at 80 volts for 2

hours. The bands were visualized with ultraviolet light using a UVP GDS 7500 (Upland, CA). Bands to be sequenced were cut from the gel with a razor blade and the DNA was purified using the Gene Clean kit (BIO101, Vista, CA).

DNA sequencing was performed with the ABI Prism Dye Terminator Cycle Sequencing reaction kit (Perkin -Elmer Inc., Foster City, CA) on an ABI 373 DNA sequencer Initial (Perkin-Elmer Inc.). Sequence data text files were edited following comparison with the same data displayed in four-color electropherograms (Sequencing by Dr. Neil Quigley, UTK Molecular Biology Resource Facility). Sequences were generated with both the forward and reverse primers with subsequent comparison to attain a complete sequence and to verify that any bases differing from the target sequence were detected by both the forward and reverse primers. Data sequences were compared to published GenBank sequences using the DNASIS program to determine homology.

Chapter 4: Results

Specific Binding Experiments:

The results of the different sets of binding studies are summarized in Tables 3-1 to 3-51. For competition tables, the column headings "Total", "NS" and "S" indicate the total, nonspecific and specific binding, respectively, where the specific binding is derived numerically from the difference between the total and nonspecific binding. For saturation tables, the column heading "cpm" indicates the 10^3 radioactive counts per minute per mg protein. All concentrations are expressed in pM.

NCI-H69: Saturation Studies Targeting "L" type VOCC (Table 3-1) – Despite investigating wide concentration ranges for both the radioligand and cold ligand, saturation did not occur. The radioligand concentration needed to be at least 1nM in order to get reliable total counts and to generate increases in both the specific and nonspecific counts. Increasing the cold ligand was associated with a marked increase in nonspecific binding. For cold ligand concentrations of 50pM, the specific binding was larger than the nonspecific binding when the radioligand exceeded 1nM. For cold ligand concentrations greater than 1nM, the nonspecific

1 All Tables and Figures can be found in the Appendix located at the end of Part III.

binding was significantly larger than the specific binding. For cold ligand concentrations of 1μM, the nonspecific binding exceeded the total binding.

NCI-H69: Competition Studies Targeting "L" type VOCC (Table 3-2) –

Despite investigating wide concentration ranges for the radioligand and cold ligand, a competition event in which progressively larger concentrations of cold ligand beyond a threshold value compete with the radioligand thereby leading to a reduction in the cpm did not occur. The cpm pattern did not demonstrate a stable noncompetition baseline at lower cold ligand concentrations. The cpm frequently increased at intermediate concentrations of cold ligand.

NCI-H69: Saturation Studies Targeting "N" Type VOCC (Table 3-3) –

Despite investigating wide concentration ranges for the radioligand, saturation did not occur. At radioligand concentrations of 25pM or greater, the total counts began to consistently increase. A cold ligand concentration of 1μM in combination with radioligand concentrations greater than 25pM resulted in such high levels of nonspecific binding that they exceeded total binding thereby resulting in a negative value for specific binding.

NCI-H69: Competition Studies Targeting "N" type VOCC (Table 3-4) –

Despite utilizing two different cold ligands and a variety of concentrations of both the radioligand and cold ligands, a competition event in which progressively larger concentrations of cold ligand beyond a threshold value compete with the radioligand thereby leading to a reduction in the cpm did not occur. The cpm pattern did not demonstrate a stable noncompetition baseline at lower cold ligand concentrations. The cpm frequently increased with increasing concentrations of cold ligand.

PNEC: Saturation Studies Targeting "L" type VOCC (Table 3-5) – Despite utilizing a wide range of radioligand concentrations, a saturation phenomenon was not observed. Increases in the total binding as increasing concentrations of radioligand were used were predominantly due to rapidly increasing nonspecific binding which exceeded the specific binding.

RT-PCR

The three gene specific primers each produced a unique banding pattern in the two cell populations. Increasing the annealing temperature to 60° decreased the number of nonVOCC bands as demonstrated by band sequencing. Target VOCC bands identified by sequencing at 354bp, 392bp and 345bp for the L, N, and P

primers, respectively, are demonstrated in Figure 3-1a. CDNA control samples (Fig 3-1b) yielded a band for cyclophilin only when the RT reaction occurred in the presence of the M-MLV reverse transcriptase, thereby demonstrating that the DNase I treatment had successfully removed any contamination by genomic DNA. Any bands generated by RT-PCR, therefore, represent amplification of cDNA derived from total RNA rather than remnants of genomic DNA.

Both the NCI-H69 and PNEC generated a 354bp "L" band, however, the level of expression was much higher for the NCI-H69 cells. Sequencing studies revealed 100% sequence homology between the NCI-H69 354bp "L" band and the target GenBank #83566 (Fig 3-2) and 97% homology between the PNEC 354bp "L" band and the GenBank target (Fig 3-3).

The 392bp "N" band was expressed only by the NCI-H69 cells. There was 100% sequence homology between the NCI-H69 392bp "N" band and the target GenBank #M94172 (Fig 3-4). The 200bp "N" splice variant band was not expressed by either cell population. Fetal hamster PNEC generated bands at approximately 300 and 500bp with high levels of sequence homology to GenBank # AB002360 and Y15065 both of which were cloned from a human brain cDNA library. PNEC additionally generated a bright 350bp band that was highly homologous to a cDNA sequence encoded by a human hepatocellular carcinoma.

NCI-H69 cells consistently generated a bright 210-220bp band that was similar to a human nuclear matrix protein but had no homology to the targeted 200bp "N" splice variant.

The 345bp "P" band was expressed by both the NCI-H69 and PNEC with levels of expression somewhat higher for the NCI-H69 cells. There was 100% sequence homology between the NCI-H69 345bp "P" band and the GenBank target S76537 (Fig 3-5), and 87% homology between the PNEC 345bp "P" band and the GenBank target (Fig 3-6).

Chapter 5: Discussion

The specific hypothesis to be tested in Part III was that VOCC subtype expression is upregulated in SCLC of chronic smokers relative to normal fetal PNEC. It was successfully demonstrated that untreated NCI-H69 and fetal hamster PNEC differ in their patterns of expression of the different VOCC subtypes. This characterization was best performed using the cDNA specific gene expression technique of RT-PCR rather than the pharmacological approach of radioligand receptor binding studies.

Examination of VOCC subtype mRNA expression using RT-PCR was very successful. NCI-H69 cells consistently demonstrated bright bands representing expression of all three "L, N, and P" VOCC subtype cDNA targets. In contrast, fetal hamster PNEC demonstrated a complete lack of the "N" type VOCC band. Although the PNEC generated bands for the "L" and "P" type VOCC, the bands were not as bright as those generated by the NCI-H69 cells particularly for the "L" band. The brightness of individual bands could not be used to make precise comparisons about the levels of expression between VOCC subtypes but could be used to make general comparisons about the expression level of a single VOCC subtype between the two cell populations. This general comparison was possible

because the gene specific primer pair for a single VOCC subtype is likely to amplify cDNA with similar efficiency regardless of the cell type from which the mRNA was harvested. However, each of the different gene specific primer pairs for the different VOCC subtypes amplified the target cDNA sequence with its own unique efficiency, thus making it impossible to make expression level comparisons between the different VOCC subtypes except in the total absence of a band. Such a total absence of a band occurred for the "N" VOCC subtype target in the PNEC. In addition, reverse transcription of the three different mRNA targets may have occurred at different efficiencies but reverse transcription of a single mRNA target would have occurred at a similar efficiency regardless of the cell type. In consideration of the limitations of the RT-PCR technique, it was still possible to make general statements comparing the expression level of specific VOCC subtypes between the NCI-H69 and PNEC. The NCI-H69 cells demonstrated a much greater expression level of specific mRNA corresponding to the "L, N and P" VOCC subtypes. These results support the hypothesis that the neoplastic cells expressed more types and greater quantities of VOCC than did the fetal hamster PNEC.

The pharmacological approach for characterization of VOCC subtype expression using classic radioligand binding studies did not produce informative saturation or competition curves. The delicate character of the neoplastic cells may

have made them susceptible to physical damage during experimental manipulation of the cells or resulted in toxicity at higher ligand concentrations. This would have exposed additional surface proteins which contributed to the high levels of nonspecific binding. The ligands, although demonstrating a predilection for certain channel subtypes, may have been less specific than desired when used with the neoplastic cells.

Characterization of VOCC subtypes can utilize both the pharmacological and the genetic subtype classification systems. Decades of study have led to a continuously evolving classification and functional description of various types of Ca^{2+} channels based on properties including voltage- and time-dependent kinetics, pharmacology, cellular distribution, and, most recently, genetic sequence homology (Cassola and Afeche 1996, Clapham 1995, De Waard et al. 1996, Ertel and Ertel 1996 , McClesky 1994, Stea et al. 1995, Tsien et al. 1991, Uchitel 1997 and Wickman and Clapham 1995). Early division of VOCC types into families based on kinetics, pharmacology and distribution has been largely confirmed and extensively refined by the analysis of cDNA sequence homology. VOCC subtypes defined by their well-established responses to specific agonists and antagonists are designated as "L" which are dihydropyridine (DHP)-sensitive, and "N, P, Q and T" which are DHP-insensitive (McCleskey 1994). "L" channels are sensitive to widely used therapeutic "calcium channel blockers" including DHPs (nicardipine,

nifedipine and nimodipine), phenylalkylamines (verapamil), and benzodiazepines (diltiazem) (Murad 1990). Toxins affecting neuronal VOCC (Uchitel 1997, Cassola and Afeche 1996) include conotoxins (CTX) which marine snails use to paralyze their fish prey, funnel-web spider venoms (polyamines, polypeptides and grammotoxin), and mamba snake venoms (fasciculin, calciseptine, FS2 and calcicludine). Among the DHP-insensitive VOCC subtypes, sensitivity differences are most effective in descriminating "N" from the "P" and "Q" subtypes. The predilection of these antagonists and agonists to target a specific VOCC subtype is based on small differences in the physical structure of the VOCCs and does not disallow binding to other VOCC subtypes or other types of ion channels.

Ion channels for different ion types all have a similar physical structure (McCleskey 1994, De Waard et al. 1996, Tsien et al. 1991). The channels are heteroligomeric complexes composed of a central ion pore designated as the α_1 subunit and additional adjacent subunits (α_2/δ, β, and γ) which modulate the action of the pore. The α_1 subunit is composed of four homologous repeats referred to as domains I-IV each of which contains six transmembrane α-helical subunits referred to as S 1-6 interconnected by variably sized loops (Tsien et al. 1991). Slight variations in the amino acid sequences of the α_1 subunit transmembrane α-helices and intervening loops are responsible for the antagonist/agonist sensitivites of each pharmacologically-defined VOCC family.

The α_1 subunit is also very important in the characterization of VOCC expression using the genetic subtype classification which examines mRNA expression levels for the α_1 subunit genes (Barry et al. 1995, Dubel et al. 1992, Fujita et al. 1993, Hui et al. 1991, Kamphuis and Henriksen 1998, Ma et al. 1992, Mikami et al. 1989, Mori et al. 1991, Niidome et al. 1992,Seino et al. 1992, Snutch et al. 1991, Soong et al. 1993, Starr et al. 1991, Williams et al. 1992a & b, Williams et al. 1994, ,). The α_1 subunit is coded by 5 genes designated A-E for which the gene names are now indicated as CACNA1A-E referring to calcium channel alpha-1 subunit gene A-E (Snutch et al. 1990, Soong et al. 1993). The genetic examination of neuronal VOCC has largely preserved the original pharmacological distinctions but has added the possibility that several different genes can code for pharmacologically similar VOCCs (Stea et al. 1995). Pharmacological "N" and "L" VOCCs are coded by the B (Williams et al. 1992b, Fujita et al. 1993, Stea et al. 1993) and the C/D genes (Tanabe et al. 1990, Williams et al. 1992a), and the pharmacologically similar "P" and "Q" types are both coded by the A gene (Mori et al. 1991). GenBank contains many cDNA sequences for the VOCC subunits that have been identified in cells of neuronal origin. Sequence homology for similar subunits coded for by specific genes for the α_1 subunit (CACNA1A-E) is often very high between species indicating that these are highly conserved genes. In some cases such as the "N" type CACNA1B, two distinct

sequences representing posttranslational splice variants are detected using the same set of primers for RT-PCR (Williams et al. 1992a).

Due to the structural similarity of all ion channel types and the high level of sequence homology within the VOCC, agonists and antagonists display a predilection for a VOCC subtype but are unlikely to exclusively interact with only one specific ion channel subtype. The similarities among the channels also makes the choice of RT-PCR primers that will be specific for the targeted VOCC subunit subtype difficult as primers that generate a specific VOCC GenBank cDNA sequence in one species or one cell type may not generate that same cDNA band under different conditions. This necessitates the sequencing of cDNA bands generated by RT-PCR in order to verify that the target sequence has been successfully amplified and to screen for previously unidentified cDNA sequences with high homology to concensus motifs likely to represent VOCCs. Performance of this sequencing in the present study has served well as a quality control, particularly in the case of the 210-220 bp cDNA band generated with the "N" primer pair in the NCI-H69 which could have been mistaken for the 200 bp "N" splice variant.

The greater expression of VOCC subtypes by NCI-H69 has probably resulted from chronic stimulation of the α_7-nAChR by nicotine and tobacco-derived

carcinogenic nitrosamines such as NNK. The interaction of nicotine and/or NNK at the cell surface α_7-nAChRs of SCLC would upregulate the serotonergic mitogenic pathway which is likely to utilize Ca^{2+} as a second messenger for the subsequent stimulation of downstream kinases. We have shown in Part II of this dissertation using flow cytometry that the stimulation of normal and neoplastic PNEC by nicotine and the nicotine-derived carcinogenic nitrosamine NNK results in the influx of extracellular Ca^{2+}. Most of the Ca^{2+} entered SCLC via stimulated α_7-nAChR Ca^{2+} channels, nicotine must have also stimulated Ca^{2+} movement through additional channels which could include neuronal nicotinic receptors having α subunits other than α_7 that would not have been blocked by α-BTX. NNK stimulated the influx of Ca^{2+} in NCI-H69 exclusively via the α_7-nAChR Ca^{2+} channel and was a much more potent activator of this channel than was nicotine. Complete blockage of the response to NNK was observed for subchronically hypoxic NCI-H69 cells pretreated with α-BTX or with ω-CTX GVIA, a VOCC blocker. NNK, therefore, appears to stimulate initial Ca^{2+} entry by binding to the α_7-nAChR resulting in membrane depolarization followed by subsequent influx of most of the Ca^{2+} through activated VOCCs.

.

The demonstration of Ca^{2+} movement in both of these cell types in response to nicotine and NNK strongly implicates a central role for Ca^{2+} as a second messenger in the serotonergic mitogenic kinase-driven signaling pathway. Ca^{2+} movement

required ligand binding to α_7-nAChR Ca^{2+} channels and proper functioning of voltage-activated Ca^{2+} channels (VOCC). The increased Ca^{2+} responsiveness of the NCI-H69 cells to nicotine and NNK compared to the PNEC is probably representative of a generalized upregulation of the entire serotonergic mitogenic pathway. We have demonstrated using RT-PCR that NCI-H69 have increased expression of VOCC compared to the normal PNEC. Upregulation of VOCC expression by the tumor cells could provide a novel target to be used for diagnostic imaging and radiopharmaceutical therapies. Neoplastic cells with a PNEC phenotype such as the NCI-H69 may alter their VOCC subtype expression when exposed to nicotine, NNK and hypoxia which are believed to stimulate SCLC growth via the serotonergic mitogenic pathway. Future specific quantitative comparison of VOCC subtype expression levels by NCI-H69 and PNEC in response to nicotine, NNK and hypoxia will be performed using relative-quantitative RT-PCR.

APPENDIX

Table 3-1: NCI-H69: Saturation Binding With ^{3}H-desmethoxyverapamil And Nifedipine

	A	B	C	D	E	F	G	H
	I	Total	NS	S	II	Total	NS	S
	Y	Y	Y	Y	Y	Y	Y	Y
1	1.88	8.32	9.70	-1.37	12.14	5.73	3.42	2.31
2	12.14	8.59	7.39	1.20	19.91	3.38	4.30	-0.92
3	19.91	7.99	7.43	0.55	48.26	4.58	2.94	1.65
4	46.15	8.51	5.88	2.63	95.93	4.41	3.30	1.11
5	77.61	6.46	7.32	-0.86	191.48	4.92	3.78	1.14
6	86.42	6.18	7.53	-1.35	465.33	9.35	7.74	1.62
7	383.00	11.08	11.42	-0.34	1.06e+003	16.15	12.00	4.16
8	450.85	11.64	10.90	0.74	1.12e+004	158.58	93.85	64.73
9	1.17e+003	1.00e+003	482.29	519.12				
10	1.11e+005	2.21e+003	797.60	1.41e+003				

	A	B	C	D	E	F	G	H
	III	Total	NS	S	IV	Total	NS	S
	Y	Y	Y	Y	Y	Y	Y	Y
1	38.60	1.93	3.04	-1.11	406.00	7.43	5.15	2.28
2	102.30	3.16	3.02	-0.14	593.00	10.74	7.60	3.15
3	219.30	3.06	2.57	0.48	1.01e+003	17.59	11.00	6.59
4	320.20	5.20	3.52	1.68	1.27e+003	19.82	13.59	6.23
5	366.70	4.25	2.80	1.44	1.43e+003	25.57	13.20	12.36
6	943.90	6.76	4.71	2.04	1.86e+003	36.67	19.99	16.68
7	1.83e+003	13.26	7.53	5.73	2.02e+003	40.98	21.13	19.86
8	3.59e+003	33.58	15.77	17.82				
9	1.60e+004	189.69	81.72	107.98				

Table 3-1: (continued)

	A	B	C	D	E	F	G	H
	V	Total	NS	S	VI	Total	NS	S
	Y	Y	Y	Y	Y	Y	Y	Y
1	406.00	9.51	8.95	0.56	406.00	18.46	16.53	1.94
2	539.00	15.74	12.17	3.56	593.00	20.12	17.17	2.95
3	1.01e+003	15.89	13.92	1.97	1.01e+003	21.49	18.03	3.46
4	1.27e+003	18.79	11.31	7.48	1.27e+003	29.27	18.93	10.35
5	1.43e+003	25.32	14.52	10.79	1.43e+003	33.65	22.88	10.77
6	1.86e+003	38.64	30.10	8.54	1.86e+003	63.27	41.95	21.32
7						62.44	47.78	14.65

	A	B	C	D	E	F	G	H
	VII	Total	NS	S	VIII	Total	NS	S
	Y	Y	Y	Y	Y	Y	Y	Y
1	11.96	1.33	1.05	0.28	8.23	13.10	12.78	0.31
2	251.00	2.93	2.36	0.57	18.57	30.27	24.44	5.83
3	2.02e+003	16.23	13.83	2.40	24.00	78.69	54.56	24.14
4	5.71e+003	31.42	25.80	5.62	37.90	104.28	81.86	22.42
5	1.13e+004	93.48	33.23	6.02	57.80	78.13	93.61	-15.48
6	2.38e+004	165.25	197.64	-32.39	89.10	125.28	173.21	-47.93
7	3.72e+004	510.60	255.46	255.14				
8	5.70e+004	413.98	369.10	44.89				
9	7.63e+004	919.00	690.16	228.84				
10	1.00e+005	1.49e+003	820.27	668.58				

	A	B	C	D
	IX	Total	NS	S
	Y	Y	Y	Y
1	18.59	20.73	23.89	-3.16
2	24.00	63.57	63.44	0.13
3	37.90	108.28	98.58	9.70
4	57.80	146.35	146.35	-16.26
5	89.10	274.67	270.43	4.24

Table 3-2: NCI-H69: Competition Binding With ^{3}H-desmethoxyverapamil And Nifedipine

	A	B	C	D	E	F	G	H
	I	cpm	II	cpm	III	cpm	IV	cpm
	Y	Y	Y	Y	Y	Y	Y	Y
1	50.00	0.44	0.00	16.22	0.00	24.81	0.00	18.48
2	500.00	0.27	500.00	9.13	50.00	21.82	10.00	14.01
3	5.00e+003	0.23	5.00e+003	12.55	500.00	18.26	20.00	11.65
4	5.00e+004	0.34	5.00e+004	18.95	5.00e+003	14.99		
5	5.00e+005	0.31	1.00e+005	12.82	5.00e+004	12.84		
6	1.00e+006	0.28	5.00e+005	6.74	5.00e+005	11.78		
7			1.00e+006	6.79				

Table 3-3: NCI-H69: Saturation Binding With ^{125}I-ω-CTX GVIA and ω-CTX GVIA

	A	B	C	D	E	F	G	H
	I	Total	NS	S	II	Total	NS	S
	Y	Y	Y	Y	Y	Y	Y	Y
1	5.00	2.35	1.72	0.64	2.70	0.19	0.19	-3.14e-003
2	17.00	4.04	3.91	0.13	6.70	0.26	0.25	0.01
3	17.00	3.73	2.74	0.99	11.40	0.19	0.27	-0.08
4	28.00	6.74	6.39	0.35	17.60	0.67	0.74	-0.07
5	63.00	14.02	14.66	-0.64	22.40	0.79	0.57	0.22
6	100.00	19.85	20.20	-0.35	41.10	8.62	10.84	-2.21
7	130.00	26.51	26.93	-0.42	56.10	18.90	17.95	0.95
8	145.00	29.12	32.04	-2.91	107.00	29.75	33.17	-3.42
9	241.00	44.21	62.00	-17.80	156.00	47.19	70.56	-23.37
10	228.00	42.60	57.84	-15.24	217.00	57.79	53.90	3.90

	A	B	C	D
	III	Total	NS	S
	Y	Y	Y	Y
1	19.30	6.98	4.71	2.27
2	25.10	7.51	7.13	0.39
3	64.90	21.15	17.65	-3.50
4	97.00	33.45	33.05	0.40
5	133.00	41.37	43.92	-2.55
6	172.00	55.21	59.78	-4.56
7	495.00	172.57	184.86	-12.29
8	1.15e+003	344.91	423.65	-78.74

Table 3-4: NCI-H69: Competition Binding With ^{125}I-ω-CTX GVIA, ω-CTX GVIA and ω-CTX MVIIA

	A	B	C	D	E	F	G	H	I
	I	cpm	II	cpm	MVIIA:	III	cpm	IV	cpm
	Y	Y	Y	Y	Y	Y	Y	Y	Y
1	0.00	2.21	0.00	27.92		0.00	0.00	0.00	27.92
2	1.00e+006	3.26	1.00e+006	19.59		1.00e+006	2.28e+004	1.00e+006	22.46
3								1.00e+007	32.17

	A	B	C	D	E	F
	V	cpm	VI	cpm	VII	cpm
	Y	Y	Y	Y	Y	Y
1	0.00	20.57	0.00	37.81	0.00	4.18
2	1.00e+005	19.09	1.00e+005	25.91	1.00e+005	3.14
3	5.00e+005	16.29	5.00e+005	29.25	5.00e+005	3.22
4			1.00e+006	32.07	1.00e+006	3.95

Table 3-5: PNEC: Saturation Binding With ^{3}H-desmethoxyverapamil And Nifedipine

	A	B	C	D
	I	Total	NS	S
	Y	Y	Y	Y
1	406.0	18.5	12.0	6.5
2	593.0	16.9	13.3	3.6
3	1.0e+003	23.6	15.8	7.8
4	1.3e+003	24.2	16.2	8.0
5	1.4e+003	28.4	20.1	8.3
6	1.9e+003	53.1	33.8	19.3
7	2.0e+003	48.1	31.1	17.0

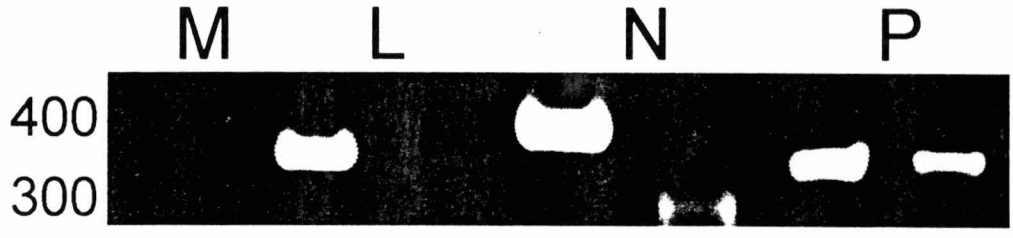


Figure 3-1: RT-PCR For L, P And N Type VOCC

In Untreated NCI-H69 And PNEC Cells.

Part a. Treatment lanes – **M**. 100bp DNA ladder marker lane, **1 and 2**. NCI-H69 and PNEC with L primer, respectively, **3 and 4**. H69 and PNEC with N primer, respectively, 4 and 5. H69 and PNEC with P primer, respectively. Lanes 1 and 2 have a 354 bp "L" band that is expressed more by the NCI-H69. Lane 3 has a 392 bp "N" band but lane 4 lacks the 392 bp "N" band. Lane 4 and 5 have a 345 bp "P" band that is expressed more by the NCI-H69.

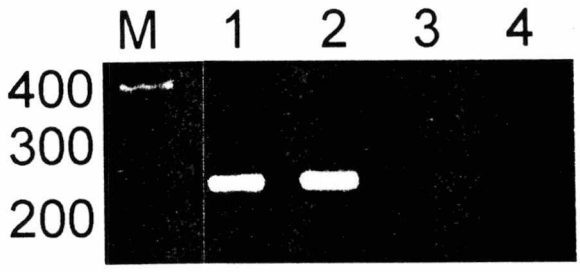


Figure 3-1: (continued)

Part b. Treatment lanes – **M**. 100bp DNA ladder marker lane, **1 and 2**. NCI-H69 and PNEC positive controls with cyclophilin primer, **3 and 4**. NCI-H69 and PNEC negative controls with cyclophilin primer. Lanes 1 and 2 both demonstrate expression of the 216 bp cyclophilin band verifying the presence of DNA in the samples. Lanes 3 and 4 do not express the cylophilin band, therefore, the samples were not contaminated by genomic DNA.

```
File1: L350H69
Mode: Normal                1 -     354
File2: M76558.HTM
Mode: Normal             4741 -    5094
Matching Percentage (Total Window: 100%, Alignment Window: 100%)
     1  GTGCCCTGCACACAGTAGTCGCTCAATAAATGTTCGTGGATGATGATGAT       50
        ||||||||||||||||||||||||||||||||||||||||||||||||||
  4741  GTGCCCTGCACACAGTAGTCGCTCAATAAATGTTCGTGGATGATGATGAT     4790

    51  GATGATGATGAAAAAAATGCAGCATCAACGGCAGCAGCAAGCGGACCACG      100
        ||||||||||||||||||||||||||||||||||||||||||||||||||
  4791  GATGATGATGAAAAAAATGCAGCATCAACGGCAGCAGCAAGCGGACCACG     4840

   101  CGAACGAGGCAAACTATGCAAGAGGCACCAGACTTCCTCTTTCTGGTGAA      150
        ||||||||||||||||||||||||||||||||||||||||||||||||||
  4841  CGAACGAGGCAAACTATGCAAGAGGCACCAGACTTCCTCTTTCTGGTGAA     4890

   151  GGACCAACTTCTCAGCCGAATAGCTCCAAGCAAACTGTCCTGTCTTGGCA      200
        ||||||||||||||||||||||||||||||||||||||||||||||||||
  4891  GGACCAACTTCTCAGCCGAATAGCTCCAAGCAAACTGTCCTGTCTTGGCA     4940

   201  AGCTGCAATCGATGCTGCTAGACAGGCCAAGGCTGCCCAAACTATGAGCA      250
        ||||||||||||||||||||||||||||||||||||||||||||||||||
  4941  AGCTGCAATCGATGCTGCTAGACAGGCCAAGGCTGCCCAAACTATGAGCA     4990

   251  CCTCTGCACCCCCACCTGTAGGATCTCTCTCCCAAAGAAAACGTCAGCAA      300
        ||||||||||||||||||||||||||||||||||||||||||||||||||
  4991  CCTCTGCACCCCCACCTGTAGGATCTCTCTCCCAAAGAAAACGTCAGCAA     5040

   301  TACGCCAAGAGCAAAAAACAGGGTAACTCGTCCAACAGCCGACCTGCCCG      350
        ||||||||||||||||||||||||||||||||||||||||||||||||||
  5041  TACGCCAAGAGCAAAAAACAGGGTAACTCGTCCAACAGCCGACCTGCCCG     5090

   351  CGCC.....                                               400
        ||||
  5091  CGCC.....                                              5140
```

Figure 3-2: cDNA Sequence Homology Of NCI-H69 354bp "L" Band With GenBank M76558

The NCI-H69 "L" band has 100% sequence homology with GenBank M76558.

```
File1: L350FE
Mode: Normal                1 -     354
File2: M76558.HTM
Mode: Normal             4740 -    5094
Matching Percentage (Total Window: 97%, Alignment Window: 97%)
     0  .GTGCCCTGCACACAGTAGTCGCTCAATAAATGTTCGTGGATGATGATGA       49
        ||||||||||||||||||||||||||||||||||||||||||||||||||
  4740  AGTGCCCTGCACACAGTAGTCGCTCAATAAATGTTCGTGGATGATGATGA     4789

    50  TGATGATGATGAAAAAAATGCAGCATCAACGGCAGCAGCAAGAGGACCAC       99
        |||||||||||||||||||||||||||||||||||||||| |||||||
  4790  TGATGATGATGAAAAAAATGCAGCATCAACGGCAGCAGCAAGCGGACCAC     4839

   100  GCGAACGAGGCAAACTATGCAAGAGGCACCAGACCCCCTATTTCTGGGGA      149
        |||||||||||||||||||||||||||||||||  ||| ||||||| ||
  4840  GCGAACGAGGCAAACTATGCAAGAGGCACCAGACTTCCTCTTTCTGGTGA     4889

   150  AGGACCAACTTCCCAGCCGAACAGCTCCAAGCAAACTGTCCTGTCTTGGC      199
        |||||||||||| |||||||| ||||||||||||||||||||||||||
  4890  AGGACCAACTTCTCAGCCGAATAGCTCCAAGCAAACTGTCCTGTCTTGGC     4939

   200  AAGCTGCAATCGATGCTGCTAGACAGGCCAAGGCTGCCCAAACCATGAGC      249
        |||||||||||||||||||||||||||||||||||||||||| ||||||
  4940  AAGCTGCAATCGATGCTGCTAGACAGGCCAAGGCTGCCCAAACTATGAGC     4989

   250  ACCTCCGCACCCCCACCTGTAGGATCTCTCTCCCAAAGAAAACGTCAGCA      299
        ||||| ||||||||||||||||||||||||||||||||||||||||||||
  4990  ACCTCTGCACCCCCACCTGTAGGATCTCTCTCCCAAAGAAAACGTCAGCA     5039

   300  ATACGCCAAGAGCAAAAAACAGGGTAACTCGTCCAACAGCCGACCTGCCC      349
        |||||||||||||||||||||||||||||||||||||||||||||||||||
  5040  ATACGCCAAGAGCAAAAAACAGGGTAACTCGTCCAACAGCCGACCTGCCC     5089

   350  GCGCC.....................................              399
        |||||
  5090  GCGCC.....................................             5139
```

Figure 3-3: cDNA Sequence Homology Of PNEC 354bp "L" Band With GenBank M76558

The PNEC "L" band has 97% sequence homology with GenBank M76558.

```
File1: N400H69
Mode: Normal                1 -     392
File2: M94172.HTM
Mode: Normal            10894 -   11285
Matching Percentage (Total Window: 100%, Alignment Window: 100%)
     1  GTCGCCAACAGCTGGCCAGGAGCCGGGACCCCACCCACAGGGCAGTGGTT       50
        ||||||||||||||||||||||||||||||||||||||||||||||||||
 10894  GTCGCCAACAGCTGGCCAGGAGCCGGGACCCCACCCACAGGGCAGTGGTT    10943

    51  CCGTGAATGGGAGCCCCTTGCTGTCAACATCTGGTGCTAGCACCCCCGGC      100
        ||||||||||||||||||||||||||||||||||||||||||||||||||
 10944  CCGTGAATGGGAGCCCCTTGCTGTCAACATCTGGTGCTAGCACCCCCGGC    10993

   101  CGCGGTGGGCGGAGGCAGCTCCCCCAGACGCCCCTGACTCCCCGCCCCAG      150
        ||||||||||||||||||||||||||||||||||||||||||||||||||
 10994  CGCGGTGGGCGGAGGCAGCTCCCCCAGACGCCCCTGACTCCCCGCCCCAG    11043

   151  CATCACCTACAAGACGGCCAACTCCTCACCCATCCACTTCGCCGGGGCTC      200
        ||||||||||||||||||||||||||||||||||||||||||||||||||
 11044  CATCACCTACAAGACGGCCAACTCCTCACCCATCCACTTCGCCGGGGCTC    11093

   201  AGACCAGCCTCCCTGCCTTCTCCCCAGGCCGGCTCAGCCGTGGGCTTTCC      250
        ||||||||||||||||||||||||||||||||||||||||||||||||||
 11094  AGACCAGCCTCCCTGCCTTCTCCCCAGGCCGGCTCAGCCGTGGGCTTTCC    11143

   251  GAACACAACGCCCTGCTGCAGAGAGACCCCCTCAGCCAGCCCCTGGCCCC      300
        ||||||||||||||||||||||||||||||||||||||||||||||||||
 11144  GAACACAACGCCCTGCTGCAGAGAGACCCCCTCAGCCAGCCCCTGGCCCC    11193

   301  TGGCTCTCGAATTGGCTCTGACCCTTACCTGGGGCAGCGTCTGGACAGTG      350
        ||||||||||||||||||||||||||||||||||||||||||||||||||
 11194  TGGCTCTCGAATTGGCTCTGACCCTTACCTGGGGCAGCGTCTGGACAGTG    11243

   351  AGGCCTCTGTCCACGCCCTGCCTGAGGACACGCTCACTTTCG.........      400
        |||||||||||||||||||||||||||||||||||||||||
 11244  AGGCCTCTGTCCACGCCCTGCCTGAGGACACGCTCACTTTCG.........    11293
```

Figure 3-4: cDNA Sequence Homology Of NCI-H69 392bp "N" Band With GenBank M94172

The NCI-H69 "N" band has 100% sequence homology with GenBank M94172.

```
File1: P345H69F
Mode: Normal                1 -     345
File2: S76537.HTM
Mode: Normal             2105 -    2450
Matching Percentage (Total Window: 99%, Alignment Window: 100%)
     1  GCTTATGTCTGTCTGCTGATCGCCATGCTCTTCTTCATCTATGCCATCAT       50
        ||||||||||||||||||||||||||||||||||||||||||||||||||
  2105  GCTTATGTCTGTCTGCTGATCGCCATGCTCTTCTTCATCTATGCCATCAT     2154

    51  TGGGATGCAGGTGTTTGGTAACATTGGCATCGACGTGGAGGACGAGGACA      100
        ||||||||||||||||||||||||||||||||||||||||||||||||||
  2155  TGGGATGCAGGTGTTTGGTAACATTGGCATCGACGTGGAGGACGAGGACA     2204

   101  GTGATGAAGATGAGTTCCAAATCACTGAGCACAATAACTTCCGGACCTTC      150
        ||||||||||||||||||||||||||||||||||||||||||||||||||
  2205  GTGATGAAGATGAGTTCCAAATCACTGAGCACAATAACTTCCGGACCTTC     2254

   151  TTCCAGGCCCTCATGCTTCTCTTCCGGAGTGCCACCGGGGAAGCTTGGCA      200
        ||||||||||||||||||||||||||||||||||||||||||||||||||
  2255  TTCCAGGCCCTCATGCTTCTCTTCCGGAGTGCCACCGGGGAAGCTTGGCA     2304

   201  CAACATCATGCTTTCCTGCCTCAGCGGGAAACCGTGTGATAAGAACTCTG      250
        ||||||||||||||||||||||||||||||||||||||||||||||||||
  2305  CAACATCATGCTTTCCTGCCTCAGCGGGAAACCGTGTGATAAGAACTCTG     2354

   251  GCATCCTGACTCGAGAGTGTGGCAATGAATTTGCTTATTTTTACTTTGTT      300
        ||||||||||||||||||||||||||||||||||||||||||||||||||
  2355  GCATCCTGACTCGAGAGTGTGGCAATGAATTTGCTTATTTTTACTTTGTT     2404

   301  TCCTTCATCTTCCTCTGCTCGTTTCTGATGCTGAATCTCTTTGTC.....      350
        ||||||||||||||||||||||||||||||||||||||||||
  2405  TCCTTCATCTTCCTCTGCTCGTTTCTGATGCTGAATCTCTTTGTC?....     2454
```

Figure 3-5: cDNA Sequence Homology Of NCI-H69 345bp "P" Band With GenBank S76537

The NCI-H69 "P" band has 100% sequence homology with GenBank S76537.

```
File1: P350FE
Mode: Normal                1 -     345
File2: S76537.HTM
Mode: Normal             2105 -    2451
Matching Percentage (Total Window: 87%, Alignment Window: 87%)

     1  GCTTATGTCTGTCTGCTGATCGCCATGCTCTTCTTCATCTACGCCATCAT       50
        |||||||||||||||||||||||||||||||||||||||| |||||||
  2105  GCTTATGTCTGTCTGCTGATCGCCATGCTCTTCTTCATCTATGCCATCAT     2154

    51  CGGGATGCAGGTGTTTGGCAACATCGGTATTGACG-GAGAAGATGAAGAC      100
         |||||||||||||||| ||||| || || |||| | || || || |||
  2155  TGGGATGCAGGTGTTTGGTAACATTGGCATCGACGTG-GAGGACGAGGAC     2204

   101  AGCGACGAGGACGAGTTCCAAATCACTGAGCACAATAACTTCCGGACCTT      150
        || || || || ||||||||||||||||||||||||||||||||||||||
  2205  AGTGATGAAGATGAGTTCCAAATCACTGAGCACAATAACTTCCGGACCTT     2254

   151  CTTCCAAGCACTCATGCTTCTCTTCCGGAGTGCCACGGGGGAAGCGTGGC      200
        |||||| || |||||||||||||||||||||||| |||||||| ||||
  2255  CTTCCAGGCCCTCATGCTTCTCTTCCGGAGTGCCACCGGGGAAGCTTGGC     2304

   201  ACAACATCATGCTCTCCTGCCTCAGCGGGAAGCCGTGCGACAAGAACTCG      250
        ||||||||||||| |||||||||||||||| ||||| || ||||||||
  2305  ACAACATCATGCTTTCCTGCCTCAGCGGGAAACCGTGTGATAAGAACTCT     2354

   251  GGGATCCTCACGGCT-GACTGCGGCAACGAGTTCGCGTACTTCTACTTCG      300
        || ||||| ||  |  || || ||||| || || || || || ||||| |
  2355  GGCATCCTGACT-CGAGAGTGTGGCAATGAATTTGCTTATTTTTACTTTG     2404

   301  TTTCTTTTATCTTCCTTTGCTCCTTTCTGATGCTGAATCTCTTTGTC...      350
        |||| || |||||||| ||||| |||||||||||||||||||||||
  2405  TTTCCTTCATCTTCCTCTGCTCGTTTCTGATGCTGAATCTCTTTGTC?R.     2454
```

Figure 3-6: cDNA Sequence Homology Of PNEC 345bp "P" Band With GenBank S76537

The PNEC "P" band has 87% sequence homology with GenBank S76537.

PART IV: CHANGES IN THE EXPRESSION LEVEL OF VOCC IN RESPONSE TO NICOTINE, NNK OR HYPOXIA AS ASSESSED BY RELATIVE QUANTITATIVE RT-PCR

Chapter 1: Abstract

Ligand binding of tobacco specific nicotinic agonists to the cell surface α_7-nAChR of SCLC and PNEC stimulates release of the autocrine growth factor 5-HT. The release and reuptake of 5-HT leads to cell proliferation. Thus, nicotinic agonists acting at the cell surface α_7-nAChR initiate a mitogenic autocrine loop with growing evidence of downstream activation of intracellular kinase-driven signaling cascades involving the raf kinases . The initiation of this growth promotion by agonist binding to the α_7-nAChR Ca^{2+} channel and the central role of Ca^{2+} as a second messenger in kinase-driven signaling pathways strongly suggests that cellular tools for controlling Ca^{2+} movement, such as VOCC, are upregulated in SCLC cells derived from chronic smokers. It was shown using flow cytometry that nicotine and NNK treatment of NCI-H69 cells stimulated the influx of extracellular Ca^{2+} through the α_7-nAChR followed by Ca^{2+} movement through VOCCs. It was demonstrated, using reverse transcription - polymerase chain reaction (RT-PCR), high expression levels by untreated NCI-H69 cells of all three "L, N, and P" VOCC subtype cDNA targets examined. In contrast, fetal hamster PNEC demonstrated a complete lack of the "N" type VOCC band and significantly less intense bands for "L" and "P" subtypes.

The present study used relative quantitative (RQ) RT-PCR to compare the VOCC subtype expression levels of NCI-H69 cells to fetal hamster PNEC following subchronic one week treatments with 1μM nicotine, 100pM NNK or hypoxic conditions with 10% atmospheric CO_2. NCI-H69 demonstrated much higher levels of expression of all three "L, N, and P" VOCC subtype cDNA targets than PNEC. In addition, the NCI-H69 responded to the treatments by altering their VOCC expression in a subtype dependent manner. PNEC expressed significant levels of only the "P" subtype and did not express the "N" subtype.

These findings strongly support the hypothesis that cell lines derived from human SCLC, all of which are from patients who were chronic smokers, demonstrate a massively upregulated ability to manipulate their Ca^{2+} levels using the α_7-nAChR Ca^{2+} channel and VOCCs. This ability would facilitate the use of Ca^{2+} as a second messenger in the serotonergic mitogenic signaling pathways including the downstream *raf* kinases .

Chapter 2: Introduction

The post-therapeutic regrowth and fatal metastatic spread (Hansen and Rorth 1997) of human small cell lung carcinoma (SCLC) is due to the remarkable growth promoting effects of smoking and the concurrent hypoxia of chronic lung disease. The mechanism by which these factors promote the growth of this "smoking specific" (Weiss 1991) neoplasm and their non-neoplastic pulmonary neuroendocrine cell (PNEC) counterparts involves the autocrine growth factor serotonin (5-HT) (Cattaneo et al. 1993, Schuller and Hegedus 1989). The secretion of 5-HT by SCLC in human patients (Gazdar 1994) has been simulated experimentally by treating the cells in vitro with nicotine (Cattaneo et al. 1993). Pulmonary cells of neuroendocrine phenotype, such as SCLC (Linnoila 1990) , utilize a unique cell membrane oxygen binding protein to respond to changes in oxygenation (Youngson et al. 1993) by becoming hyperplastic and increasing their 5-HT secretion (Youngson et al. 1993, Johnson and Georgieff 1989, Guyton and Hall 1996). The combined growth promoting influence of hypoxia with nicotine or nicotine-derived nitrosamines is currently under investigation.

The experimental growth promotion of SCLC in hamsters is driven by a mitogenic autocrine serotonergic loop that begins with the activation of the cell

surface membrane α-BTX -sensitive α_7-nAChR by simultaneous exposure to carcinogenic nitrosamines and hyperoxic lung injury (Schuller et al. 1988, Schuller et al. 1990) or to nicotine and hyperoxic lung injury (Schuller at al. 1995). In vitro growth promotion of cell lines derived from human SCLC in response nicotine or the structurally related NNK was further potentiated by simultaneous exposure to elevated atmospheric CO_2 (Schuller 1989, Schuller and Hegedus 1989) and blocked by 5-HT receptor antagonists and PKC inhibitors (Schuller 1994). Proliferation was also blocked in the presence of the α_7-nAChR antagonists α-BTX and hexamethonium, a broad spectrum blocker of all neuronal nicotinic receptors (Schuller 1989, Schuller and Hegedus 1989). Together these findings implicated an initial interaction of nicotine and/or NNK at the cell surface α_7-nAChRs of SCLC and the subsequent role of 5-HT in a kinase driven signaling pathway.

It was demonstrated using flow cytometry (Dissertation Part II) that the movement of Ca^{2+} into normal and neoplastic PNEC treated with nicotine and the nicotine-derived carcinogenic nitrosamine NNK. Ca^{2+} movement required agonist binding to the cell surface α_7-nAChR of SCLC thereby allowing initial Ca^{2+} entry through the α_7-nAChR Ca^{2+} channel. Subsequent movement of Ca^{2+} also required VOCC as evidenced by the blockage using the VOCC antagonist ω-CTX GVIA. Characterization of the VOCC expression of NCI-H69 cells and fetal hamster PNEC using RT-PCR to detect the presence of mRNA for specific GenBank

VOCC subtype cDNA sequences has recently been performed (Dissertation Part III). This work demonstrated that NCI-H69 had high levels of expression of the "L, N, and P" VOCC subtype cDNA sequences examined. In contrast, fetal hamster PNEC did not express the "N" subtype and gave lower levels of expression of the "L and P" subtypes upon visual comparison of band brightness between the two cell populations.

These findings strongly support the hypothesis that cell lines derived from human SCLC, all of which are from patients who were chronic smokers, demonstrated a massively upregulated ability to manipulate their Ca^{2+} levels using the α_7-nAChR Ca^{2+} channel and VOCCs. This ability would facilitate the use of Ca^{2+} as a second messenger in the serotonergic mitogenic signaling pathways including downstream *raf* kinases (Jull and Schuller, unpublished).

The next logical step is a quantitative examination of the mRNA expression levels for the VOCC subtypes in SCLC cells exposed to nicotine, tobacco-derived nitrosamines such as NNK, and hypoxic conditions simulating chronic lung disease. These three treatments represent the three factors believed to promote growth and recurrence of SCLC via the serotonergic mitogenic pathway. Comparison of the expression levels of fetal hamster PNEC , as the nonneoplastic PNEC counterpart to the SCLC, to that of SCLC may reveal which VOCC subtypes

of SCLC demonstrate altered expression and how this expression responds to the three treatments. The central hypothesis of this work is that nicotine and the nicotine-derived carcinogenic nitrosamine NNK act at the α_7-nAChR of normal and neoplastic pulmonary neuroendocrine cells to stimulate growth by a mechanism that moves Ca^{2+}. **The specific hypothesis to be tested in Part IV is that VOCC subtype expression is upregulated in neoplastic PNEC derived from SCLC of chronic smokers relative to normal fetal PNEC.** This process will be examined by assessing differences in the expression of specific cDNA sequences for VOCC subsets in the two cell populations in response to subchronic exposure to nicotine, NNK or hypoxia using relative quantitative (RQ) RT-PCR. The objective is to demonstrate differences in the expression pattern of specific genetic VOCC subtypes in the two cell populations and alterations in the expression levels in response to treatment with nicotine, NNK or hypoxia. This objective will be achieved by demonstrating differences in the respective band intensities upon analysis of phosphorimages of the RQ RT-PCR reaction products.

Chapter 3: Materials and Methods

NCI- H69 Cell Line: NCI-H69 cells from a human SCLC were purchased from the American Cell Type Culture Collection (Rockville, Maryland). Cells were grown at 37° in an atmosphere of 5% CO_2 and RPMI media supplemented with fetal bovine serum (10%, v/v), L-glutamine (2mM), penicillin (100U/ml) and streptomycin (100μg).

PNEC: Cultures of fetal hamster PNEC were established from fetal hamster lung periphery harvested on day 15 of gestation and maintained in an atmosphere of 10% CO_2, a condition which selectively promotes the growth of PNEC (Schuller 1994). The cells were routinely maintained in RPMI medium supplemented with fetal bovine serum (10%, v/v), L-glutamine (2mM), and gentamycin sulfate (50mg/ml).

RELATIVE QUANTITATIVE RT-PCR

Treatment Groups: NCI-H69 groups included control (5 %CO_2 , 7 days) , 1μM

nicotine (5 %CO_2, 7days), 100ρM NNK (5 %CO_2, 7 days) and 10% CO_2 (7 days). PNEC groups included control (10% CO_2, 7 days) and 1μM nicotine (10% CO_2, 7 days) and 100ρM NNK (5 %CO_2, 7days). Cells receiving nicotine or NNK treatments were dosed every other day immediately after being given fresh media.

RNA Isolation : RNA was isolated from NCI-H69 and PNEC using the guanidine isothiocyanate (GIT)/cesium chloride (CsCl) overnight ultracentrifugation method (MacDonald et al. 1987). The floating NCI-H69 and adherent PNEC cells were removed from their culture flasks by pouring and scraping, respectively, and placed in a 50 ml conical tube. The cells were centrifuged (1900x, 3 min) and the media from above the cell pellet was discarded. The cells were resuspended in 25 ml of PBS, centrifuged (1900x, 3 min), and PBS from above the cell pellet was discarded. A GIT buffer solution was prepared by adding 47.2 g (4M final) GIT and 1mL 3M sodium acetate pH 7 to a final volume of 100ml of sterile water. The GIT buffer solution was sterile filtered (0.2 μm filter) and 1ml 2-mercaptoethanol was added under a fume hood. The cell pellet was dissolved in 8 ml GIT buffer . The cell pellet was passed through a 20 gauge needle on a 30ml syringe three times in order to shear the DNA. A CsCl buffer solution was prepared by adding 95.97 g (5.7M final) CsCl, 1ml 3M sodium acetate pH 7 and 2ml 0.5M EDTA pH 8.0 to a final volume of 100ml sterile water. The CsCl buffer solution was sterile filtered (0.8 μm filter). For each cell sample, a seton tube (Seton Scientific, Los Gatos, CA) was

partially filled with 4 ml of the CsCl buffer solution. The sheared DNA solution was carefully placed in the seton tube on top of the CsCl buffer solution by expelling the DNA solution from the syringe along the inner wall of the seton tube above the level of the CsCl buffer solution. The total fluid level reached completely to the top of tube in order to avoid potential collapsing of the tube during the overnight centrifugation. The seton tubes were placed in a swinging bucket rotor in a balanced arrangement and centrifuged overnight (32,000 RPM, 19°). Following centrifugation, each seton tube was carefully removed from the rotor under a RNA-PCR hood. For each tube, the supernatant was removed using an autoclaved RNA pipette until the remaining supernatant was within 0.5 cm of tube base. The cup-like tube base containing the RNA pellet was separated from the remainder of the seton tube by cutting the tube with a sterile razor blade 5mm above the level of the remaining supernatant. All remaining supernatant was removed from the free cup-like seton tube base using a P-1000 pipette and care was taken not to disturb the small translucent RNA pellet. The RNA pellet was resuspended in 400µl sodium acetate by flushing and scraping at the pellet with the solution and pipette tip. The RNA solution was transferred to a 1ml Eppendorf tube and the tube was placed on ice. The RNA was precipitated by adding 1ml of 100% ethanol to the tube followed by freezing (80°, 15 min). The tube containing the frozen precipitated RNA was centrifuged (14,000 RPM, 4°, 10 min) and the supernatant was discarded. The RNA pellet was washed by adding 100µl of 80% ethanol and then centrifuged

(14,000 RPM, 4°, 5 min). The RNA pellet was dissolved by adding 50µl nuclease free water. The RNA concentration of this final RNA solution was determined by measuring the optical density of 3µl of sample in 297µl water at 260 and 280 nm using a UV-160 UV-Visible Recording Spectrophotometer (Shimadzu Corp., Kyoto, Japan).

DNase I/ Reverse Transcription (RT) :. RNA was purified of any potential contamination by genomic DNA by using DNase I according to the technique described by Ambion (Austin, TX, Bauer et al. 1997, Dixon et al. 1998). Each reaction began with 2ug RNA obtained by the GIT/CsCl method. The RNA, 1µl of DNase I 10x buffer and1µl DNase I were added to a 10ul total of nuclease free water. The mixture was incubated at room temperature (15 min). The reaction was stopped by adding 1µl of 25mM EDTA to the tube followed by a 65 ° incubation for 10 minutes.

Purified RNA was reverse transcribed into cDNA using the RETROscript™ kit (Ambion) according to the technique described by Ambion (Farrell 1997, Farrell 1993, Innis et al. 1990). Each reverse transcription (RT) reaction began with 2ug of DNase I-treated RNA which was in a 10µl volume following the DNase I treatment. 2ul (50mM) of random decamer primers (Ambion) were added to the 10µl RNA solution. The solution was heated to 82C for 3 minutes and then placed

on ice. To the iced mixture was added 1µl (0.5mM) each of dGTP, dATP, dCTP and dTTP, 2µl DTT, 2µl of 10x buffer (100mMTris-HCl pH 8.3, 500mM Kcl, 15mM MgCl2), 1µl (40U) RNasin ribonuclease inhibitor (Promega, Madison, WI) and 1µl (200U) M-MLV reverse transcriptase (Gibco, Gaithersburg, MD) yielding a final volume of 20ul. Tubes to be used as the negative control RT reactions in which cDNA copies would not be made from RNA contained 1µl water substituted for the 1µl M-MLV, thereby creating a reaction lacking the reverse transcriptase enzyme. The total mixture was incubated (1hour, 37°) and then heated (10 min, 92°). The final product was used immediately for PCR or frozen at -20° for later use.

Relative Quantitative Polymerase Chain Reaction (RQ RT-PCR): The amplification of cDNA was performed using the QuantumRNA™ kit (Ambion) according to the technique described by Ambion (Farrell 1997, Farrell 1993, Innis et al. 1990). Each PCR reaction began with 5ul of the cDNA product from the DNase I/RT procedure. The cDNA was added to 4µl (0.2mM) dNTPs, 0.75µL α^{32}P-dCTP and 5ul 10x PCR buffer (100mM Tris-HCl pH 8.3, 500 mM KCl, 15mM $MgCl_2$). Each reaction tube received 4 µl of a 10µM gene specific primer mixture and 4µl of the 18S ribosomal primer/competimer mixture provided by Ambion as an internal control for amplification of the abundant 18S ribosomal RNA (Finnegan et al. 1993). Two tubes serving as controls for measuring

phosphorimager background volume density were given only the gene specific primer pair or the 18S primer/competimer mixture. All tubes were supplemented with 0.25µl (1.25U) SuperTaq polymerase (Ambion). Nuclease free water was added to bring the final volume of each reaction to 50ul. Gene specific primers used were as follows:S76537 "P/Q" type from human SCLC forward GCT TAT GTC TGT CTG CTG ATC G and reverse GAC AAA GAG ATT CAG CAT CAG (Barry et al. 1995); M94172 and M94173 "N" type splice variants from human neuroblastoma forward GTC GCC AAC AGC TGG CCA GGA GC and reverse CGA AAG TGA GCG TGT CCT CAG GC (Williams et al. 1992a) ; and M76558 "L" type from human neuroblastoma forward GTG CCC TGC ACA CAG TAG TCG C and reverse GGC GCG GGC AGG TCG GCT GTT GG (Williams et al. 1992b). Anticipated cDNA band sizes for each primer pair based on the number of bases separating the primers in the GenBank sequences were 345 bp ("P" type, Barry et al. 1995), 200 and 392 bp ("N" type splice variants, Williams et al. 1992a), and 354 bp ("L" type, Williams et al. 1992b). The 18S primers provided by Ambion were designed to amplify a 488 bp DNA product in humans and mice (QuantumRNA™ Instruction Manual, Ambion). A common annealing temperature of 60° for 90 seconds was used for all the gene specific primers and the 18S primer/competimer mixture. The PCR program consisted of preheating (94°, 120 sec), melting (94°, 60 sec), annealing and extension (72°, 90 sec). The melting, annealing and extension cycle was repeated 32 additional times. There was a final

extension (72°, 5 minutes) after which the product was chilled at 4° until removal from the DNA Machine PTC-200 Peltier Thermal Cycler (MJ Research, Watertown, MA).

Radioactive 100bp DNA Ladder Preparation: A 100bp DNA ladder (Gibco) was labeled with γ^{32}P-ATP (Dupont NEN, Wilmington, DE) according a protocol provided by Gibco (Chaconas and Van de Sande 1980). In a 0.5ml microcentrifuge tube the following components were incubated (30 min, 37°): 13.5µl autoclaved nuclease free water, 5µl (5µg) 100bp DNA ladder (Gibco), 5µl 5x exchange reaction buffer (for T_4 polynucleotide kinase), 3µl of 10µCi/µl $\lceil\gamma\text{-}^{32}P\rceil$ ATP (Dupont) and 1µl 10µCi/µl T_4 polynucleotide kinase (Gibco) to a total volume of 27.25µl. The reaction was stopped by adding 1µl of 0.5M EDTA and centrifuging (10 sec, 14,000 rpm). Approximately 1×10^5 CPM of the labeled ladder was used in each PAGE gel lane. The labeled ladder was diluted to the necessary CPM per 1µl by adding sterile water and counting 1µl on scintillation counter. The radioactive ladder was frozen at -20° until needed.

Polyacrylamide Gel Electrophoresis (PAGE) : Aliquots of the radioactive RT/PCR products were visualized using a denaturing 5% PAGE gel. Each gel lane was loaded with 10 µl of a mixture consisting of 25µl of the radioactive PCR product and 2.5 µl of loading buffer (5Prime→3Prime, Inc., Boulder, CO). A marker lane was loaded with a mixture consisting of 1µl of the radioactive 100bp

DNA ladder , 2.5µl loading buffer and 7µl water. Gel electrophoresis was performed at 200 volts in 1X TBE buffer for 45 minutes or until the second dye front reached the bottom of the gel. The gels were dried on 3 mm Whatman chromatography paper (Whatman International Ltd, Maidstone, England) and placed on a phophorimager screen overnight. The phosphorimage was scanned using a PhosphorImager 445 SI (Molecular Dynamics, Sunnyvale, CA) and saved into the ImageQuant program. The band densities were analyzed using Microsoft Excel.

Cycle Studies: To determine the number of cycles during which the gene specific primers were amplifying within the linear range, cycle studies were performed in which the 18S primer/competimer pair was excluded and samples were taken following odd numbered PCR cycles from cycle 14 to cycle 35 for each gene specific primer. Band density quantification across cycles was determined and comparisons used to identify the linear range. A suitable cycle number applicable universally for all three gene specific primer pairs was chosen. Once the cycle number was chosen, a study was performed excluding the gene specific primers and using the 18S primer/competimers at ratios of 1:9, 2:8 and 3:7 for the chosen number of cycles. Band density quantification was utilized to identify the ratio yielding a band of similar density to the expected density range for the gene specific primer bands in previous studies at the determined cycle number. A

suitable 18S primer/competimer ratio applicable universally for all three gene specific primer pairs was chosen. A final study was performed to verify that the 18S primer/competimer at the chosen ratio was amplifying within the linear range at the chosen cycle number. This was determined by a cycle study excluding the gene specific primers and including the 18S primer/competimer at the chosen ratio with samples taken following odd numbered cycles from cycle 14 to cycle 35. Density comparisons to determine the linear range were performed as described for the gene specific primer cycle studies. The above described sequence of studies was performed separately on cDNA from both cell populations (NCI-H69 and PNEC) as the gene specific band densities varied for the two populations. It was crucial to determine cycle numbers and 18S primer/competimer ratios that could be universally applied to both populations in order to allow even casual comparison of expression levels between the two cell populations. Specific gene primer pair studies concentrated on the examination of bands that were known to be Ca^{2+} channels as determined by cDNA sequencing in Part III of this dissertation.

Relative Quantification Of Target Bands In Treatment Groups: The final experiments to achieve relative-quantification of band density for bands known to represent Ca^{2+} channels used cDNA from the control and treatment groups of both cell populations in the presence of one gene specific primer pair in combination with the 18S ribosomal primer/competimer pair at the chosen ratio for the chosen

number of PCR cycles. Two lanes to be used for background measurement contained reactions performed using cDNA of the untreated NCI-H69 group with either the gene specific primer or the 18S primer/competimer pair.

Individual treatment group band densities were analyzed by dividing the density of the gene specific band by the density of the 18S band for that treatment group. Background densities were calculated by dividing the density of the empty space in a lane without the gene specific primer by the density of the gene specific band for the untreated NCI-H69 group because this group had consistently yielded the densest band in the previous studies. The density of each treatment group was then expressed as a percent of the NCI-H69 control group in order to allow comparison to this group across all other treatment groups.

Chapter 4: Results

Phosphorimages using the 18S primer/competimers in addition to the gene specific primers for "L, N, and P" are shown in Figure 4-1, 4-2 and 4-3(1), respectively. The image in part "b" of each figure is supplemented with the uniformly sized rectangle used for volume densitometry of each band and background. The volume densities in raw data form are listed in Table 4-1 by rectangle numbers corresponding the numbering of rectanges shown in Figures 4-1, 4-2 and 4-3.

A comparison of the untreated control groups for NCI-H69 and PNEC using the three gene specific primers is shown in Figure 4-4 (Table 4-2). The expression level of the "L, N, and P" mRNA was much greater for the NCI-H69 cells than for the PNEC. The only PNEC VOCC subtype mRNA expressed at a level notably greater than that of the background is the "P" type which generated a band density volume 68% that of the untreated NCI-H69.

A comparison of the untreated NCI-H69 and PNEC groups with the treated groups using the "L" primer is shown in Figure 4-5 (Table 4-3). NCI-H69

---

1 All Tables and Figures are located within the Appendix at the end of Part IV.

expression of the "L" type VOCC subtype mRNA was reduced to approximately 60% for all three treatment groups. The untreated PNEC expression level (5%) was similar to the background level (1%) and was minimally changed by treatment with NNK (2.6%) or nicotine (6.7%).

A comparison of the untreated NCI-H69 and PNEC groups with the treated groups using the "N" primer is shown in Figure 4-6 (Table 4-4). NCI-H69 expression of the "N" type VOCC subtype mRNA was not the same for each treatment group. NCI-H69 demonstrated significantly less "N" expression in the NNK (52%) and nicotine (37%) groups but virtually no change in the hypoxic group (98%). The untreated PNEC expression level (5%) was similar to the background level (2.3%) and minimally changed by treatment with NNK (3.6%) and nicotine (4.3%).

A comparison of the untreated NCI-H69 and PNEC with the treated groups using the "P" primer is shown in Figure 4-7 (Table 4-5). NCI-H69 expression of the "P" type VOCC subtype mRNA was unchanged by treatment with nicotine and hypoxia but reduced for NNK (68%). The untreated PNEC expression level (6.8%) was unchanged by treatment with NNK (6.3%) and nicotine (6.6%).

The most important trends and findings are summarized in Tables 4-6, 4-7 and

4-8 and the corresponding Figures 4-8, 4-9, and 4-10. The NCI-H69 expression level for each treatment group is shown summarized for all three gene specific primers in Figure 4-8 (Table 4-6). The untreated NCI-H69 expressed all three VOCC subtypes at a level much higher than the background level. NNK treatment reduced expression of all three VOCC subtypes. Nicotine treatment reduced expression of the "L and N" VOCC subtypes. Hypoxia reduced expression of only the "L" subtype.

The PNEC expression level for each treatment group is shown summarized for all three gene specific primers in Figure 4-9 (Table 4-7). The untreated PNEC expressed the "L and N" VOCC subtypes at minimal levels that are nearly equal to the background. In contrast, untreated PNEC expressed the "P" VOCC subtype at 68% of the untreated NCI-H69 level which is significantly greater than the background. Expression levels by PNEC exposed to NNK (63%) or nicotine (66%) were similar to the untreated level (68%). The significant levels of PNEC expression across treatment groups for only the "P" VOCC subtype are shown by themselves in Figure 4-10 (Table 4-8) which emphasizes the magnitude of expression and the lack of change across treatment groups.

Chapter 5: Discussion

The specific hypothesis to be tested in Part IV was that VOCC subtype expression is upregulated in neoplastic PNEC phenotype cells derived from SCLC of chronic smokers relative to normal fetal PNEC. The objective was to demonstrate differences in the expression pattern of specific genetic VOCC subtypes in the two cell populations and alterations of expression levels by exposure to nicotine, NNK and hypoxia. It is strikingly apparent from our RQ RT-PCR findings that NCI-H69 had far greater expression of every VOCC subtype examined than did their non-neoplastic fetal counterparts. The only VOCC subtype expressed by the fetal PNEC at an appreciable, albeit reduced, level was the "P" type. This strongly supports the hypothesis that chronic nicotine exposure during years of smoking has greatly altered the ability of the neoplastic cells to manipulate their Ca^{2+} levels. The present evidence suggests that this phenomenon predominantly involved enhanced expression of the "L and N" VOCC subtypes. Such an enhanced feature would facilitate the generalized upregulation of the serotonergic mitogenic pathway from its initiation by the binding of nicotine or nicotine-derived carcinogenic nitrosamines such as NNK to the cell surface α_7-nAChR Ca^{2+} channel to its perpetuation within the *raf* kinase signaling machinery. Nicotine, structurally similar tobacco-derived nitrosamines such as NNK, and

hypoxia would have, therefore, a tremendous growth promotional effect on human SCLC as is observed clinically in the aggressive recurrence of this tumor type.

The NCI-H69, as neoplastic cells, demonstrated an ability to modify the expression levels of the VOCC subtypes in response to treatments, however, this ability was not observed for the non-neoplastic fetal PNEC. Fetal PNEC did not alter their expression levels of the "P" VOCC subtype when treated with NNK or nicotine. In contrast, exposure of NCI-H69 to NNK was associated with reduced levels of expression of all three VOCC subtypes and nicotine reduced the expression levels of both the "L and N" VOCC subtypes. Such a reduction was also detected in "L" VOCC subtype expression following a week in hypoxic conditions.

The adaptive character of expression of the "L and N" VOCC subtypes in the neoplastic cells indicates that the intracellular machinery of the NCI-H69 was actively responding to subchronic binding of nicotine or NNK to the α_7-nAChR Ca^{2+} channel and subchronic stimulation of the PNEC oxygen sensing receptor. The subchronic decreased mRNA expression associated with a constant exposure to nicotine, NNK or hypoxia for one week appears to be a phenomenon separate from the chronic upregulation of VOCC observed for the NCI-H69. The chronic upregulation of VOCC expression by neoplastic cells was a response to a chronic

pattern of frequent, rather than continuous, large spikes in blood nicotine or NNK levels as would occur during cigarette smoking. Each individual cigarette smoked would provide a brief but large dose of nicotine or nicotine-derived carcinogenic nitrosamines. By experimentally subchronically exposing the cells to a constant level of nicotine, NNK or hypoxia for one week, we provided constant uninterrupted exposure to an agonist thereby resulting in downregulation of the receptor. Alteration in the level of mRNA expression following subchronic hypoxia does not necessarily indicate that the cells were becoming desensitized to receptor ligation. Rather, decreased expression associated with hypoxia may have been associated with a heightened affinity or increased sensitivity of the receptors to the ligands. This was supported by the flow cytometry finding that subchronically hypoxic NCI-H69 treated with a single dose of NNK demonstrated only a small reduction in the amount of Ca^{2+} influx when compared to nonhypoxic cells.

Based on these findings, the VOCC appear to have promise as novel diagnostic and therapeutic targets in the fight against human SCLC. The target search may concentrate on the "L" VOCC subtype in consideration of the high expression levels and responsiveness to all treatments observed for the specific "L" subtype cDNA measured.

APPENDIX

Table 4-1: Relative Quantitative Reverse Transcriptase-Polymerase Chain Reaction (RQ RT-PCR): NCI-H69 and PNEC: Phosphorimager Volume Density Report Raw Data By Rectangle (Figures 4-1, 4-2 and 4-3).

Rectangle size 49x21mm

Rectangle Number	Cell Type	Treatment Group	Band Type	Volume (Millions)
1	NCI-H69	Background	18S	1.02
2	NCI-H69	Untreated	18S	36.04
3	NCI-H69	NNK	18S	47.07
4	NCI-H69	Nicotine	18S	45.79
5	NCI-H69	10% CO_2	18S	44.44
6	PNEC	Untreated	18S	43.76
7	PNEC	NNK	18S	37.64
8	PNEC	Nicotine	18S	42.08
9	NCI-H69	Background	L	0.51
10	NCI-H69	Untreated	L	35.62
11	NCI-H69	NNK	L	28.36
12	NCI-H69	Nicotine	L	27.09
13	NCI-H69	10% CO_2	L	26.55
14	PNEC	Untreated	L	2.20
15	PNEC	NNK	L	0.95
16	PNEC	Nicotine	L	2.79
17	NCI-H69	Background	18S	1.43
18	NCI-H69	Untreated	18S	40.34
19	NCI-H69	NNK	18S	42.07
20	NCI-H69	Nicotine	18S	38.83
21	NCI-H69	10% CO_2	18S	49.27
22	PNEC	Untreated	18S	38.14
23	PNEC	NNK	18S	35.88
24	PNEC	Nicotine	18S	34.25
25	NCI-H69	Background	N	0.67
26	NCI-H69	Untreated	N	30.88
27	NCI-H69	NNK	N	16.83
28	NCI-H69	Nicotine	N	11.03
29	NCI-H69	10% CO_2	N	36.79

Table 4-1: (Continued)

Rectangle Number	Cell Type	Treatment Group	Band Type	Volume (Millions)
30	PNEC	Untreated	N	1.46
31	PNEC	NNK	N	0.99
32	PNEC	Nicotine	N	1.13
33	NCI-H69	Background	18S	2.30
34	NCI-H69	Untreated	18S	66.54
35	NCI-H69	NNK	18S	62.44
36	NCI-H69	Nicotine	18S	62.00
37	NCI-H69	10% CO_2	18S	60.26
38	PNEC	Untreated	18S	59.27
39	PNEC	NNK	18S	54.75
40	PNEC	Nicotine	18S	51.27
41	NCI-H69	Background	P	0.97
42	NCI-H69	Untreated	P	79.28
43	NCI-H69	NNK	P	50.46
44	NCI-H69	Nicotine	P	74.09
45	NCI-H69	10% CO_2	P	72.04
46	PNEC	Untreated	P	48.02
47	PNEC	NNK	P	41.10
48	PNEC	Nicotine	P	40.07

Table 4-2: RQ RT-PCR: Comparison Of "L, N and P" Type Calcium Channel Expression In Untreated PNEC And Untreated NCI-H69 Expressed Relative To Untreated NCI-H69 (Figure 4-4)

	X Labels	A	B	C	D
	Primer	Bkgd: 18S	Bkgd: gene	NCI-H69	PNEC
	X	Y	Y	Y	Y
1	L	0.022538	0.011269	1.000000	0.050867
2	N	0.048109	0.022541	1.000000	0.050007
3	P	0.031135	0.013131	1.000000	0.679996

Table 4-3: RQ RT-PCR: Comparison Of "L" Type Calcium Channel Expression In NCI-H69 And PNEC Treated With Nicotine, NNK Or Hypoxia Expressed Relative To Untreated NCI-H69 (Figure 4-5)

	X Labels	A	B	C	D	E	F	G	H	I
	Primer	Bkgd: 18S	Bkgd: gene	NCI-H69	H69:NNK	H69:Nic	H69:CO2	NCI-PNEC	PNEC:NNK	PNEC:Nic
	X	Y	Y	Y	Y	Y	Y	Y	Y	Y
1	L	0.022538	0.011269	1.000000	0.609611	0.598590	0.604479	0.050867	0.025537	0.067084

Table 4-4: RQ RT-PCR: Comparison Of "N" Type Calcium Channel Expression In NCI-H69 And PNEC Treated With Nicotine, NNK Or Hypoxia Expressed Relative To Untreated NCI-H69 (Figure 4-6)

	X Labels	A	B	C	D	E	F	G	H	I
	Primer	Bkgd: 18S	Bkgd: gene	NCI-H69	H69:NNK	H69:Nic	H69:CO2	PNEC	PNEC:NNK	PNEC:Nic
	X	Y	Y	Y	Y	Y	Y	Y	Y	Y
1	N	0.048109	0.022541	1.000000	0.522601	0.371079	0.975452	0.050007	0.035863	0.043100

Table 4-5: RQ RT-PCR: Comparison Of "P" Type Calcium Channel Expression In NCI-H69 And PNEC Treated With Nicotine, NNK Or Hypoxia Expressed Relative To Untreated NCI-H69 (Figure 4-7)

	X Labels	A	B	C	D	E	F	G	H	I
	Primer	Bkgd: 18S	Bkgd: gene	NCI-H69	H69:NNK	H69:Nic	H69:CO2	PNEC	PNEC:NNK	PNEC:Nic
	X	Y	Y	Y	Y	Y	Y	Y	Y	Y
1	P	0.031135	0.013131	1.000000	0.678271	1.002968	1.003376	0.679996	0.630053	0.655957

Table 4-6: RQ RT-PCR: Comparison Of "L, N and P" Type Calcium Channel Expression In NCI-H69 Treated With Nicotine, NNK Or Hypoxia Expressed Relative To Untreated NCI-H69 (Figure 4-8)

	X Labels	A	B	C	D	E	F
	Primer	Bkgd: 18S	Bkgd: gene	NCI-H69	H69:NNK	H69:Nic	H69:CO2
	X	Y	Y	Y	Y	Y	Y
1	L	0.022538	0.011269	1.000000	0.609611	0.598590	0.604479
2	N	0.048109	0.022541	1.000000	0.522601	0.371079	0.975452
3	P	0.031135	0.013131	1.000000	0.678271	1.002968	1.003376

Table 4-7: RQ RT-PCR: Comparison Of "L, N and P" Type Calcium Channel Expression In PNEC Treated With Nicotine or NNK Expressed Relative To Untreated NCI-H69 (Figure 4-9)

	X Labels	A	B	C	D	E
	Primer	Bkgd: 18S	Bkgd: gene	PNEC	PNEC:NNK	PNEC:Nic
	X	Y	Y	Y	Y	Y
1	L	0.022538	0.011269	0.050867	0.025537	0.067084
2	N	0.048109	0.022541	0.050007	0.035863	0.043100
3	P	0.031135	0.013131	0.679996	0.630053	0.655957

Table 4-8: RQ RT-PCR: Comparison Of "P" Type Calcium Channel Expression In PNEC Treated With Nicotine or NNK Expressed Relative To Untreated NCI-H69 (Figure 4-10)

	X Labels	A	B	C	D	E
	Primer	Bkgd: 18S	Bkgd: gene	PNEC	PNEC:NNK	PNEC:Nic
	X	Y	Y	Y	Y	Y
1	P	0.031135	0.013131	0.679996	0.630053	0.655957

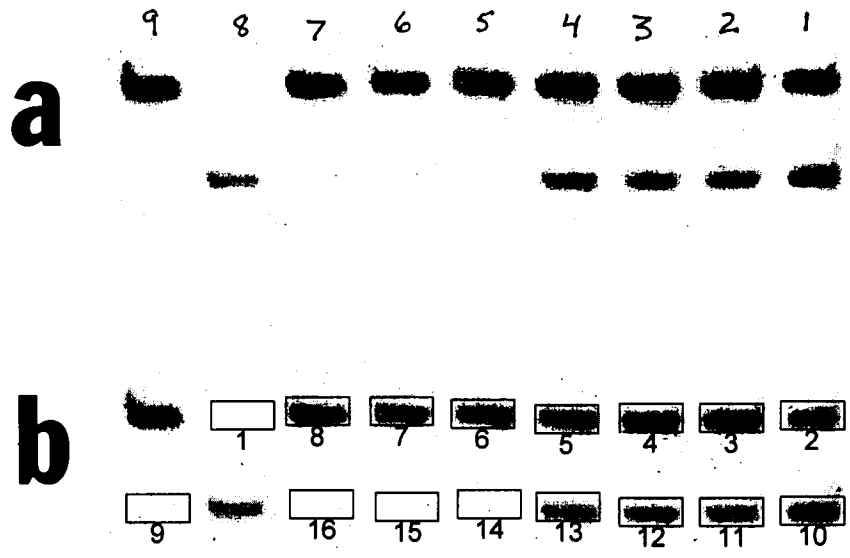


Figure 4-1: Relative Quantitative Reverse Transcriptase Polymerase Chain Reaction (RQ RT-PCR): Comparison Of Expression Levels of "L" Type VOCC by NCI-H69 And PNEC Treated With Nicotine, NNK And Hypoxia Using "L" Type Primers And A 2:8 Ratio Of 18S Primer/Competimer (Table 4-1)

Lanes are as follows: 1. Untreated NCI-H69, 2. NCI-H69 (100pM NNK , 1 week), 3. NCI-H69 (1μM nicotine, 1 week), 4. NCI-H69 (10% CO_2, 1 week), 5. PNEC untreated, 6. PNEC (100pM NNK, 1week), 7. PNEC (1μM nicotine, 1 week), 8. Untreated NCI-H69, L primer only, 9. Untreated NCI-H69, 18S primer/competimer only. Rectangles in part "b" are for volume density quantifications.

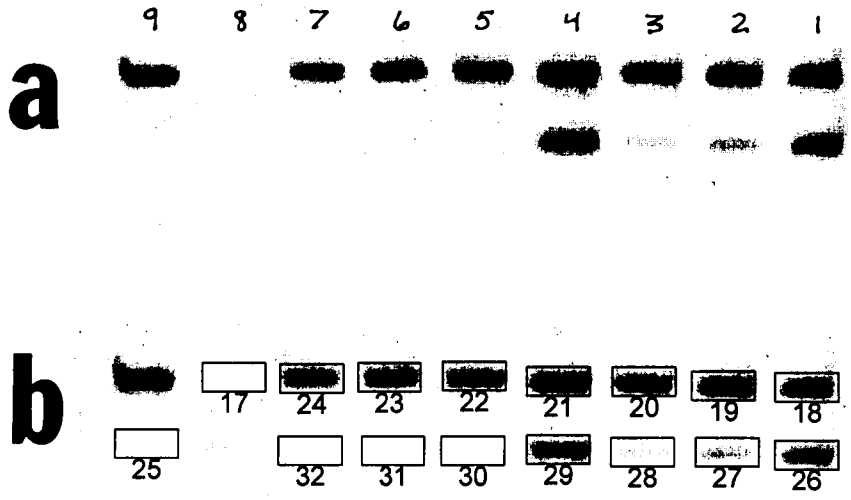


Figure 4-2: RQ RT-PCR: Comparison Of Expression Levels of "N" Type VOCC by NCI-H69 And PNEC Treated With Nicotine, NNK And Hypoxia Using "N" Type Primers And A 2:8 Ratio Of 18S Primer/Competimer (Table 4-1)

Lanes are as follows: 1. Untreated NCI-H69, 2. NCI-H69 (100pM NNK , 1 week), 3. NCI-H69 (1μM nicotine, 1 week), 4. NCI-H69 (10% CO_2, 1 week), 5. PNEC untreated, 6. PNEC (100pM NNK, 1week), 7. PNEC (1μM nicotine, 1 week), 8. Untreated NCI-H69, N primer only, 9. Untreated NCI-H69, 18S primer/competimer only. Rectangles in part "b" are for volume density quantifications.

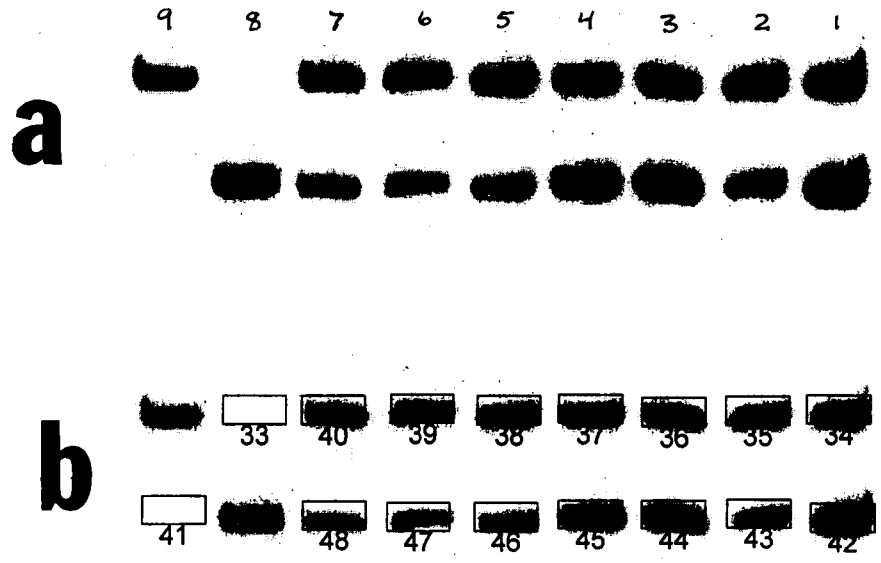


Figure 4-3: RQ RT-PCR: Comparison Of Expression Levels of "P" Type VOCC by NCI-H69 And PNEC Treated With Nicotine, NNK And Hypoxia Using "P" Type Primers And A 2:8 Ratio Of 18S Primer/Competimer (Table 4-1)

Lanes are as follows: 1. Untreated NCI-H69, 2. NCI-H69 (100pM NNK , 1 week), 3. NCI-H69 (1μM nicotine, 1 week), 4. NCI-H69 (10% CO_2, 1 week), 5. PNEC untreated, 6. PNEC (100pM NNK, 1week), 7. PNEC (1μM nicotine, 1 week), 8. Untreated NCI-H69, P primer only, 9. Untreated NCI-H69, 18S primer/competimer only. Rectangles in part "b" are for volume density quantifications.

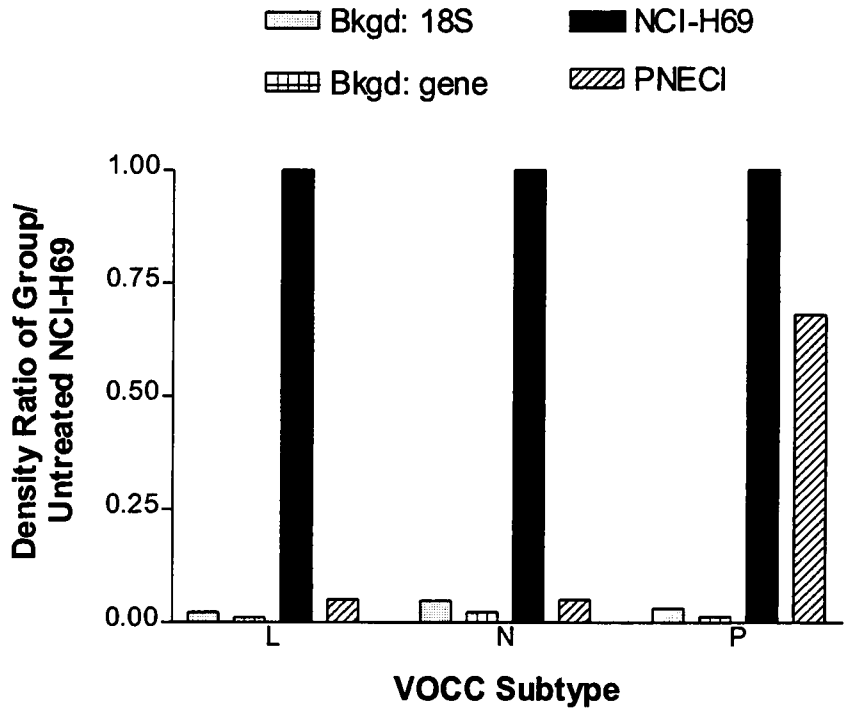


Figure 4-4: RQ RT-PCR: Comparison Of "L, N and P" Type Calcium Channel Expression In Untreated PNEC And Untreated NCI-H69 Expressed Relative To Untreated NCI-H69 (Table 4-2)

NCI-H69 cells had high levels of expression of all three VOCC subtypes. Fetal hamster PNEC had significant expression of only the "P type VOCC subtype.

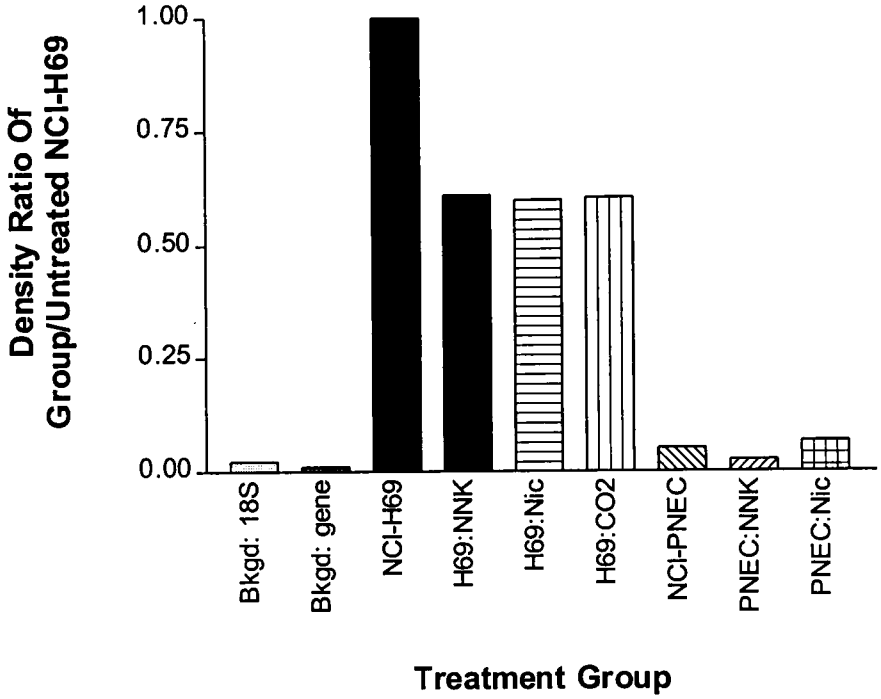


Figure 4-5: RQ RT-PCR: Comparison Of "L" Type Calcium Channel Expression In NCI-H69 And PNEC Treated With Nicotine, NNK Or Hypoxia Expressed Relative To Untreated NCI-H69 (Table 4-3)

NCI-H69 demonstrated reduced expression of the "L" VOCC subtype when exposed to nicotine, NNK or 10% CO_2. Fetal hamster PNEC did not have significant expression of the "L" VOCC subtype.

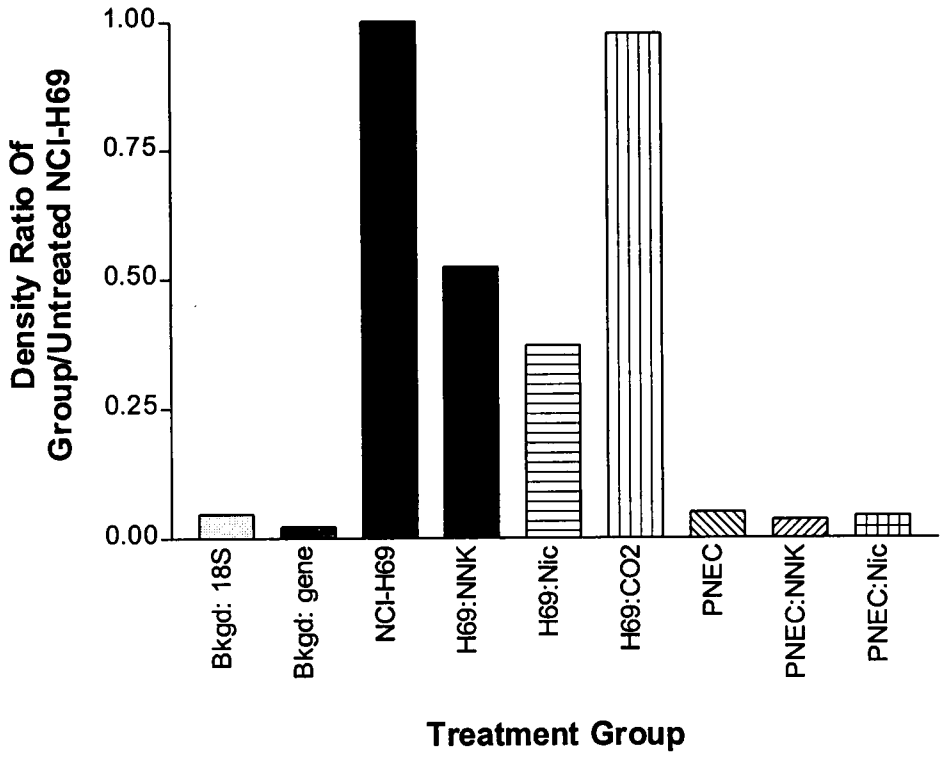


Figure 4-6: RQ RT-PCR: Comparison Of "N" Type Calcium Channel Expression In NCI-H69 And PNEC Treated With Nicotine, NNK Or Hypoxia Expressed Relative To Untreated NCI-H69 (Table 4-4)

NCI-H69 demonstrated reduced expression of the "N" VOCC subtype when exposed to NNK or nicotine but not 10% CO_2. Fetal hamster PNEC did not have significant expression of the "P" VOCC subtype.

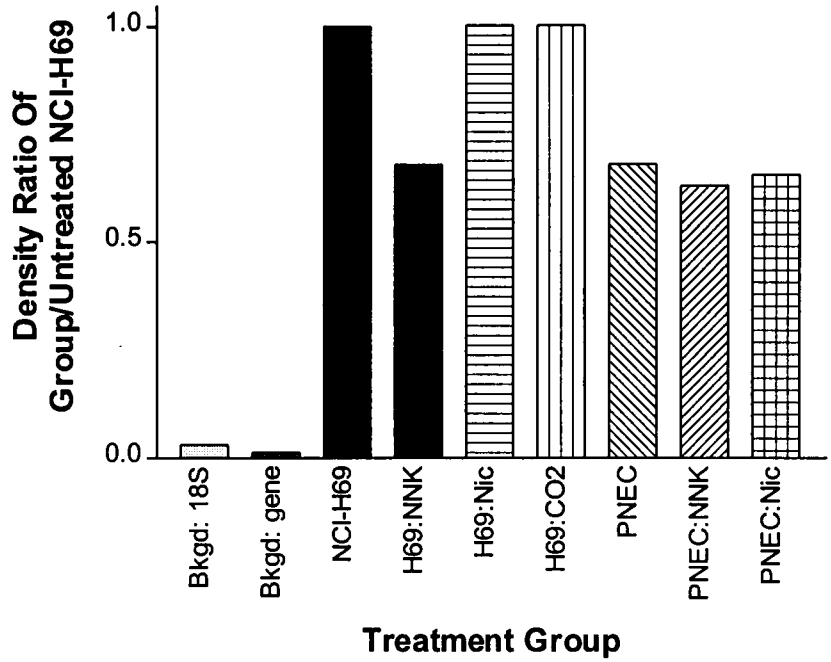


Figure 4-7: RQ RT-PCR: Comparison Of "P" Type Calcium Channel Expression In NCI-H69 And PNEC Treated With Nicotine, NNK Or Hypoxia Expressed Relative To Untreated NCI-H69 (Table 4-5)

NCI-H69 demonstrated reduced expression of the 'P" VOCC subtype when exposed to NNK but not nicotine or 10% CO_2. Fetal hamster PNEC had significant expression of the "P" VOCC subtype but it was not altered by exposure to NNK, nicotine or 10% CO_2.

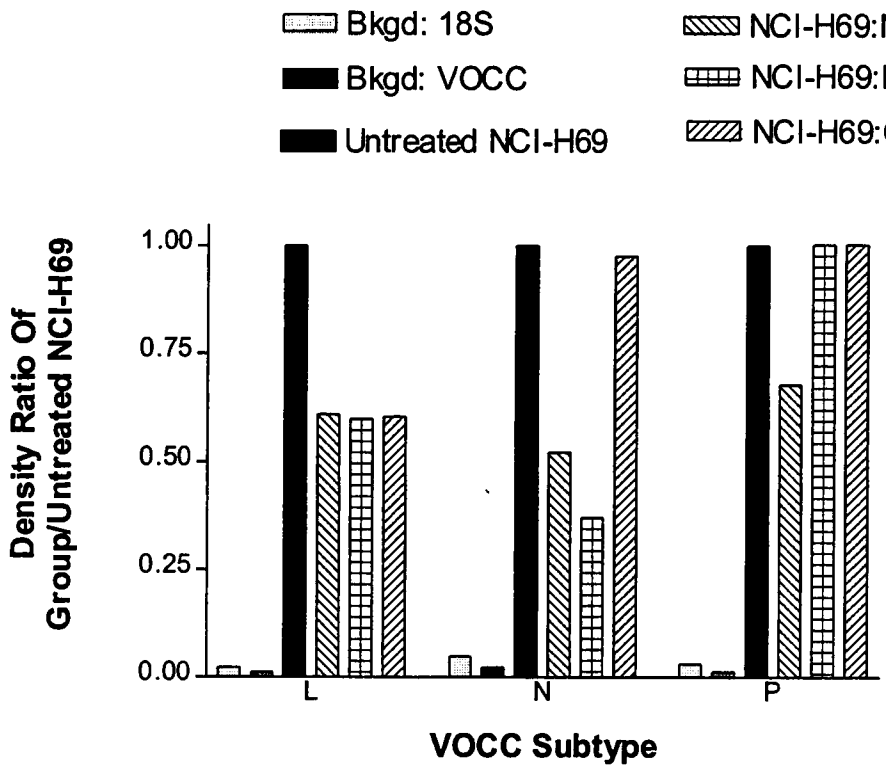


Figure 4-8: RQ RT-PCR: Comparison Of "L, N and P" Type Calcium Channel Expression In NCI-H69 Treated With Nicotine, NNK Or Hypoxia Expressed Relative To Untreated NCI-H69 (Table 4-6)

NCI-H69 demonstrated reduced expression of the "L, N and P" VOCC subtypes when exposed to NNK. NCI-H69 demonstrated reduced expression of the "L and N" VOCC subtypes when exposed to nicotine. NCI-H69 demonstrated reduced expression of only the "L" VOCC subtype when exposed to 10% CO_2.

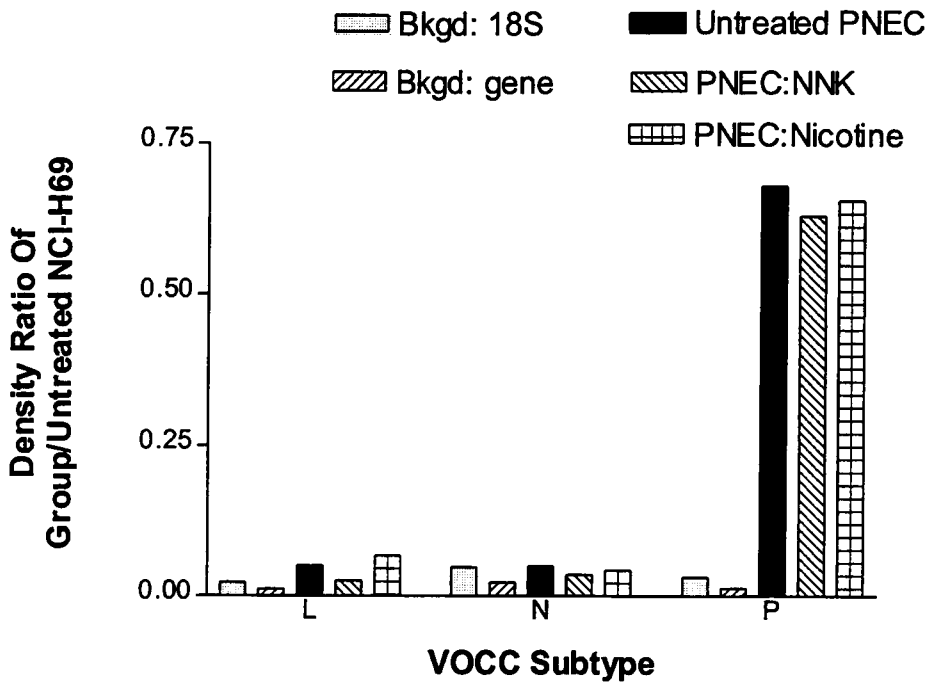


Figure 4-9: RQ RT-PCR: Comparison Of "L, N and P" Type Calcium Channel Expression In PNEC Treated With Nicotine or NNK Expressed Relative To Untreated NCI-H69 (Table 4-7)

Fetal hamster PNEC demonstrated significant expression of only the "P" VOCC subtype. Expression of the "P" VOCC subtype was not altered by exposure to NNK, nicotine or 10% CO_2.

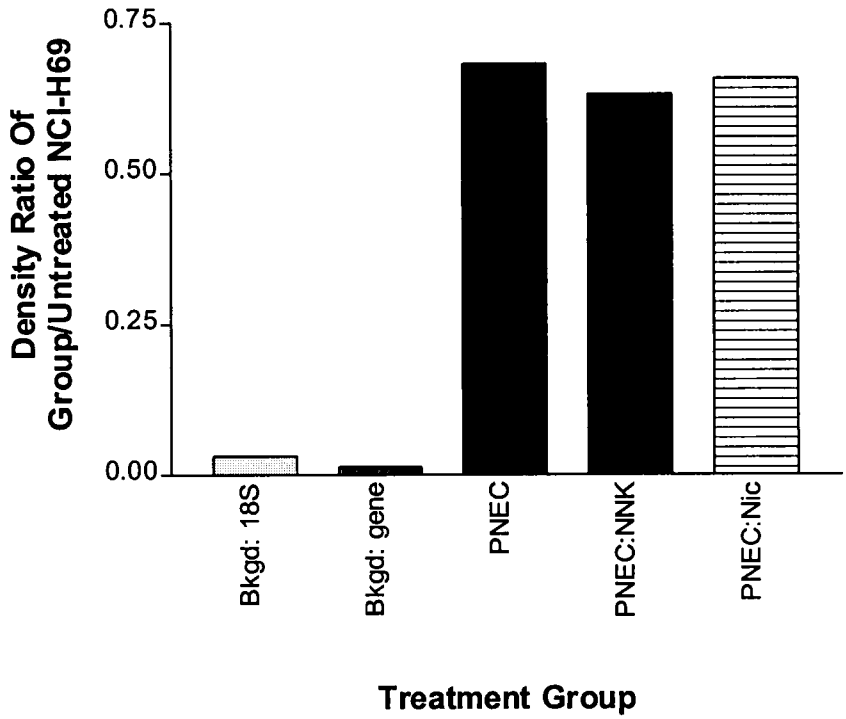


Figure 4-10: RQ RT-PCR: Comparison Of "P" Type Calcium Channel Expression In PNEC Treated With Nicotine or NNK Expressed Relative To Untreated NCI-H69 (Table 4-8)

Fetal hamster PNEC expression of the "P" VOCC subtype was not altered by exposure to NNK, nicotine or 10% CO_2.

PART V: OVERALL SUMMARY

Chapter 1: Summary

The research findings described in Parts II, III and IV have supported the specific and central hypotheses of the dissertation. The central hypothesis was that nicotine and the nicotine-derived carcinogenic nitrosamine NNK act at the α_7-nAChR of normal and neoplastic PNEC to stimulate growth by a mechanism that moves Ca^{2+}. The first specific hypothesis, supported by flow cytometry in Part II, was that the stimulation of normal and neoplastic PNEC by nicotine or NNK results in the influx of extracellular Ca^{2+} through the α_7-nAChR Ca^{2+} channel. The second specific hypothesis, successfully demonstrated using molecular genetics in Parts III and IV, was that VOCC subtype expression is upregulated in neoplastic PNEC derived from SCLC of chronic smokers relative to normal fetal hamster PNEC. Highlights of each Part are combined in the following overall summary in order to create a cohesive picture of what has been found and the potential therapeutic and diagnostic significance.

It was demonstrated that stimulation of normal and neoplastic PNEC by nicotine and NNK resulted in the influx of extracellular Ca^{2+} through the α_7-nAChR Ca^{2+} channel. Using flow cytometry, a large influx of extracellular Ca^{2+} occurred when NCI-H69 cells were treated with the comparatively high dose of 1μM and not with lower doses. The source of Ca^{2+} was clearly extracellular rather than representing release from intracellular stores because the response was

quenched in the absence of extracellular buffer Ca^{2+}. Substantial but not complete blockage of the response to 1 μM nicotine by pretreatment with α-BTX identified one unique channel through which most of the Ca^{2+} entered as the α_7-nAChR Ca^{2+} channel based on the known specificity of α-BTX. The snake venom α-BTX binds with high affinity only to the small subset of neuronal nicotinic receptors (Gopalakrishnan et al. 1995 and 1996) having the α_7 and α_8 subunits which are expressed primarily in the brain and retina, respectively (Chini et al. 1993, Lindstrom et al. 1995). While most of the Ca^{2+} entered via stimulated α_7-nAChR Ca^{2+} channels, nicotine must also have stimulated Ca^{2+} movement through additional channels. These additional channels could have included neuronal nicotinic receptors having α subunits other than α_7. Indeed, NCI-H69 cells have recently been shown to also express nAChRs with the α_3 and α_5 subunits (Schuller unpublished).

The NCI-H69 responded maximally to the much smaller dose of 100pM NNK compared to 1μM nicotine , however, they experienced a much smaller amount of Ca^{2+} influx. The NNK response was completely blocked by pretreatment with α-BTX. Together these findings indicated that NNK stimulated the influx of Ca^{2+} exclusively via the α_7-nAChR Ca^{2+} channel and that NNK was a much more potent activator of this channel than was nicotine. This increased sensitivity to NNK was supported by recent binding studies. The affinity of NNK to the α_7 receptor was

shown to be 1,300 times greater than that of nicotine and 3,500 times greater than that of the nicotine-derived carcinogenic nitrosamine NNN (Schuller and Orloff 1998). In addition, the NNK-induced cell proliferation and DNA synthesis measured by incorporation of ^{3}H-thymidine was completely inhibited by α-BTX (Schuller and Orloff 1998). It has also been shown that cell lines derived from SCLC cannot metabolize NNK and, therefore, cannot generate the metabolites which are believed to cause the ki-*ras* mutations that are a common finding in non-small cell carcinomas. Ki-*ras*, which plays a key role in the signal transduction pathway utilized by many growth factors (Segar and Krebs 1995), is frequently mutated in human PAC derived from the bronchiolar Clara cells (Linnoila 1990). Exposure of laboratory rodents to the tobacco-specific carcinogenic nitrosamine NNK resulted in the formation of PAC of a Clara cell phenotype (Hecht and Hoffman 1988; Schuller et al. 1990). These PAC cells had a high incidence of Ki-*ras* gene mutation (Mitsudomi et al. 1991) which was most commonly a point mutation at codon 12 (Mitsudomi et al. 1991, Yesner 1993). Formation of this mutation was highly correlated with the metabolism of NNK to O^{6}-methylguanine (Belinsky et al. 1989) indicating that metabolism of NNK by the PAC cells preceded mutation of the Ki-*ras* gene. In contrast, SCLC cells were unable to metabolize NNK (Falzon et al. 1986a) due to a lack of the necessary enzyme profile (Falzon et al. 1986b), thereby making them unable to generate the NNK metabolite, O^{6}-methylguanine, associated with mutation of the Ki-*ras* gene. In light of the inability of SCLC cells to metabolize NNK, any growth promotion effect of

NNK on SCLC must utilize a separate mechanism. This mechanism was most likely direct stimulation of the α_7-nAChR Ca^{2+} channel as supported by the flow cytometry findings.

The subchronic culturing of NCI-H69 cells for one week in a hypoxic incubator at 10% atmospheric CO_2 resulted in a small reduction in the responsiveness of the cells to NNK. The response to NNK was completely blocked by pretreatment with the α_7-nAChR antagonist α-BTX or the VOCC ligand ω-CTX GVIA. This was consistent with previous findings that NNK-induced SCLC cell line proliferation was blocked in the presence of the α_7-nAChR antagonists α-BTX and hexamethonium, a broad spectrum blocker of all neuronal nicotinic receptors (Schuller 1989, Schuller and Hegedus 1989). Collectively these flow cytometry findings elucidate a pattern of NNK-induced Ca^{2+} influx that begins with ligation of the α_7-nAChR and is propagated by subsequent activation of VOCC.

The findings demonstrated that VOCC subtype expression is upregulated in untreated NCI-H69 derived from SCLC of chronic smokers relative to normal fetal PNEC. Differences were also demonstrated in the expression pattern of specific genetic VOCC subtypes in the two cell populations and alterations of expression levels by subchronic continuous exposure to nicotine, NNK and hypoxia. It is strikingly apparent from our RQ RT-PCR findings that NCI-H69 had far greater expression of every VOCC subtype examined than did their non-neoplastic fetal

counterparts. The only VOCC subtype expressed by the fetal PNEC at an appreciable, albeit reduced, level was the "P" type. This strongly supports the hypothesis that chronic nicotine exposure during years of smoking has greatly altered the ability of the neoplastic cells to manipulate their Ca^{2+} levels. The present evidence suggests that this phenomenon predominantly involved enhanced expression of the "L and N" VOCC subtypes. Such an enhanced feature would facilitate the generalized upregulation of the serotonergic mitogenic pathway. This upregulation could extend from the pathways initiation by the binding of nicotine or nicotine-derived carcinogenic nitrosamines such as NNK to the cell surface α_7-nAChR Ca^{2+} channel to its perpetuation within the *raf* kinase signaling machinery. Nicotine, structurally similar tobacco-derived nitrosamines such as NNK, and hypoxia would have, therefore, a tremendous growth promotional effect on human SCLC as is observed clinically in the aggressive recurrence of this tumor type.

The hypoxic conditions imposed on the lung during chronic lung disease could result in the upregulation of the serotonergic mitogenic pathway due to the unique ability of SCLC to respond to atmospheric hypoxia. Normal PNEC and SCLC, as cells of neuroendocrine origin (Linnoila 1996), possess a cell membrane oxygen binding protein that responds to changes in the relative proportions of the intrapulmonary gases O_2 and CO_2 (Youngson et al. 1993). Under conditions of decreased lung oxygenation such as in the normal neonatal lung or the pathologic predicament of chronic lung diseases, PNEC exhibited a hyperplastic response and

enhanced secretion of the biogenic amine 5-HT (Youngson et al. 1993, Johnson and Georgieff 1989, Guyton and Hall 1996). The classic pulmonary physiological consequences of 5-HT release are constriction of bronchial smooth muscle and concentration dependent vasodilation or vasoconstriction (Garrison 1990), however, 5-HT was also an autocrine growth factor for PNEC (Cattaneo et al. 1993, Schuller and Hegedus 1989. These findings collectively suggested that growth promotion occurring during the recurrence phase of human SCLC involves a combination of factors including 5-HT, nicotine or nicotine-derived metabolic products, and chronic hypoxia associated with chronic lung disease.

Upregulation of VOCC subtypes involved in the serotonergic mitogenic pathway could have been potentiated by exposure of SCLC to hypoxia in combination with nicotine or nicotine-derived nitrosamines. The proliferation of neuroendocrine cell lines derived from lung carcinoid tumors or SCLC (Schuller 1994) treated with nicotine or the structurally related NNK was potentiated by simultaneous exposure to elevated atmospheric CO_2 (Schuller 1989, Schuller and Hegedus 1989). This proliferation was blocked by 5-HT/MB receptor antagonists and PKC inhibitors (Schuller 1994). The nicotine and NNK-induced cell proliferation occurred at 10% but not 5% atmospheric CO_2 in one dose exposure experiments (Maneckjee and Minna 1990, Schuller 1994). This is important because the intrapulmonary concentration of CO_2 in the healthy adult lung is 5% whereas a CO_2 concentration of 10% simulates the intrapulmonary levels of this

gas in a mildly diseased lung (Guyton and Hall 1996). Therefore, growth promotion in response to nicotine and NNK was most remarkable under the hypoxic conditions of a chronically diseased lung which is in agreement with the high incidence of SCLC in smokers with chronic lung disease.

Given that differences in VOCC expression levels between the NCI-H69 and fetal hamster PNEC have been detected, does this provide insight into which VOCC subtype or subtypes might serve as a therapeutic target? If the fetal hamster PNEC are considered to be the "normal" or "unstimulated" PNEC counterpart to the SCLC cells, then the greatly enhanced "L and N" expression by the NCI-H69 as measured by RQ RT-PCR must represent a type of adaptation to conditions experienced by the neoplastic cells. The hypothesis was that the NCI-H69 cell line, which is derived from a chronic smoker, overexpressed the VOCC subtypes examined as a result of the chronic overstimulation and subsequent massive upregulation of the serotonergic mitogenic signaling pathway. The source of overstimulation would have been due to a combination of nicotine or nicotine-derived nitrosamine binding at the α_7-nAChR Ca^{2+} channel and hypoxia. Although the exposure to nicotine and NNK for the smoker would have been chronic, each cigarette would have provided a large but brief exposure to both compounds. Based on the findings, the character of this exposure appears to have encouraged the upregulation of receptors in the NCI-H69, whereas, continuous exposure to a constant dose for one week resulted in downregulation. It was found

that fetal hamster PNEC treated with a single dose of nicotine or NNK demonstrated much smaller amounts of Ca^{2+} movement using flow cytometry than did the NCI-H69. Complete blockage of the fetal hamster PNEC response to NNK by pretreatment with either α-BTX or the broad spectrum neuronal nAChR blocker hexamethonium suggested that the PNEC response to NNK was completely mediated by α_7-nAChRs in a fashion similar to NCI-H69 but that PNEC had a lesser ability to respond. This lesser ability to respond was supported by our RQ RT-PCR findings that the PNEC had significantly less expression of the "L and N" VOCC subtypes.

It was found that a pharmacological approach for characterization of VOCC subtype expression using classic radioligand binding studies did not produce informative saturation or competition curves. The delicate character of the neoplastic cells may have made them susceptible to physical damage during experimental manipulation of the cells or resulted in toxicity at higher ligand concentrations. This would have exposed additional surface proteins which contributed to the high levels of nonspecific binding. The ligands, although demonstrating a predilection for certain channel subtypes, may have been less specific than desired when used on neoplastic cells with such high expression levels of each VOCC subtype. Slight variations in the amino acid sequences of the α_1 subunit transmembrane α-helices and intervening loops are responsible for the antagonist/agonist sensitivites of each pharmacologically-defined VOCC family

(De Waard et al. 1996, McClesky 1994, Stea et al. 1995, Tsien et al. 1991, Uchitel 1997). The predilection of these antagonists and agonists to target a specific VOCC subtype is based on small differences in the physical structure of the VOCC subtypes and does not disallow binding to other VOCC subtypes or other types of ion channels. Among the DHP-insensitive VOCC subtypes, sensitivity differences may be most effective in discriminating "N" from the "P" and "Q" subtypes. Due to the structural similarity of all ion channel types and the high level of sequence homology within the VOCC, agonists and antagonists are able to display a predilection for a VOCC subtype but are unlikely to exclusively interact with only one specific ion channel subtype. The high levels of expression of multiple VOCC subtypes by the NCI-H69 and possible damage-associated exposure of additional receptors were probably responsible for the large amounts of nonspecific binding detected.

An additional feature of NCI-H69, detected by RQ RT-PCR, was their downregulation of VOCC subtypes in response to subchronic constant uninterrupted exposure to agonists. The NCI-H69, as neoplastic cells, demonstrated an ability to modify the expression levels of the VOCC subtypes in response to subchronic exposure to nicotine, NNK or hypoxia. This ability was not observed for the non-neoplastic fetal PNEC. Fetal PNEC did not alter their expression levels of the "P" VOCC subtype when treated with NNK or nicotine. In contrast, exposure of NCI-H69 to NNK was associated with reduced levels of

expression of all three VOCC subtypes and nicotine reduced the expression levels of both the "L and N" VOCC subtypes. Such a reduction was also detected in "L" VOCC subtype expression following a week in hypoxic conditions. Following a week of hypoxia, NCI-H69 had a reduction to 60% in the "L" VOCC subtype cDNA expression level as indicated by RQ RT-PCR. However, subchronically hypoxic NCI-H69 had only a small reduction in NNK-induced Ca^{2+} movement measured by flow cytometry. Together these findings may suggest that the "L" type VOCC channels had increased in sensitivity or that the "N or P" type channels were responsible for most of the NNK-induced Ca^{2+} movement.

The adaptive character of expression of the "L and N" VOCC subtypes in the neoplastic cells indicates that the intracellular machinery of the NCI-H69 was actively responding to subchronic binding of nicotine or NNK to the α_7-nAChR Ca^{2+} channel and subchronic stimulation of the PNEC oxygen sensing receptor. The subchronic decreased mRNA expression associated with a constant exposure to nicotine, NNK or hypoxia for one week appears to be a phenomenon separate from the chronic upregulation of VOCC observed for the NCI-H69. The chronic upregulation of VOCC expression by neoplastic cells was a response to a chronic pattern of intermittent, rather than continuous, large spikes in blood nicotine or NNK levels as would occur during cigarette smoking. Each individual cigarette smoked would provide a brief but large dose of nicotine or nicotine-derived carcinogenic nitrosamines. By experimentally subchronically exposing the cells to

a constant level of nicotine, NNK or hypoxia for one week, we provided constant uninterrupted exposure to an agonist thereby resulting in downregulation of the receptor. Alteration in the level of mRNA expression following subchronic hypoxia does not necessarily indicate that the cells were becoming desensitized to receptor ligation. Rather, decreased expression associated with hypoxia may have been associated with a heightened affinity or increased sensitivity of the receptors to the ligands. This was supported by the flow cytometry finding that subchronically hypoxic NCI-H69 treated with a single dose of NNK demonstrated only a small reduction in the amount of Ca^{2+} influx when compared to nonhypoxic cells.

Based on these findings, VOCCs appear to have promise as novel diagnostic and therapeutic targets in the fight against human SCLC. The target search may concentrate on the "L" VOCC subtype in consideration of the high expression levels and subchronic responsiveness to all treatments observed for the specific "L" subtype cDNA measured. We have examined the expression levels of one GenBank cDNA sequence for the "L" subtype VOCC, however, there are many additional "L" cDNA sequences that could be examined. Given the rapidly growing knowledge base within both the pharmacological and genetic fields regarding VOCC subtypes, there exists enormous potential to therapeutically target VOCCs when unique characteristics of their expression by SCLC are further elucidated.

PART VI: REFERENCES CITED

Barry, E.L. Viglione, M.P., Kim, Y.I. and Froehner, S.C. (1995). Expression and antibody inhibition of P-type calcium channels in human small-cell lung carcinoma cells. J. Neurosci., **15(1)**, 274-283.

Bauer, P. Rolfs, A., Regitz-Zagrosek, V., Hildebrandt, A. and Fleck, E. (1997). Use of manganese in RT-PCR eliminates PCR artifacts resulting from DNase I digestion. Biotechniques, 22(6), 1128-1132.

Belinsky, S.A., Devereux, R.R., Maranpot, R.R., Stoner, D.G., and Anderson, M. (1989). Relationship between the formation of promutagenic adducts and the activation of the ki-*ras* protooncogene in lung tumors from A/J mice. *Cancer Res*, **49**, 5305-5311.

Birnbaumer, L., Campbell, K.P., Catterall, W.A., Harpold, M.M., Hofmann, F., Horne, W.A., Mori, Y., Schwartz, A., Snutch, T.P., Tanabe, T., and Tsien, R.W., 1994. The naming of voltage-gated calcium channels. *Neuron,* **13**, 505-506.

Bunn, P.A, Jr., Chan, D., Steward, J., Gera, J., Tolley, R., Jewett, P., Tagawa, M., Alford, C., Machzuki, T., and Yanaihara, N. (1994). Effects of neuropeptide

analogues on calcium flux and proliferation in lung cancer cell lines. *Cancer Res,* **54**, 3602-3610.

Cassola, A.C. and Afeche S.C. (1996). Use of neurotoxins to study Ca^{2+} channel functions. *Brazilian J. Med and Biol Res*, **29**, 1759-1763.

Cattaneo, M.G., Codignola, M., Vicenti, L.M., Clementi, F., and Sher, E. (1993). Nicotine stimulates a serotonergic autocrine loop in human small cell lung carcinoma. *Cancer Res*, **35**, 5566-5568.

Cattaneo, M.G., D'Atri, F., and Vicentini, L.M. (1997). Mechanisms of mitogen-activated protein kinase activation by nicotine in small-cell lung carcinoma cells. *Biochem. J.*, **328**, 499-503.

Chaconas, G. and Van de Sande, J.H. (1980). 5'-32P labeling of RNA and DNA restriction fragments. *Methods in Enzymology*, **65**, 75-85.

Chini, B., Raimond, E., Elgoyhen, A.B., Moralli, D., Balzaretti, M., and Heinemann, S. (1994). Molecular cloning and chromosomal localization of the human α_7 –nicotinic receptor subunit gene (CHRNA7). *Genomics*, **19**, 379-381.

Clapham, D.E. (1995). Calcium Signalling; Review. *Cell*, **80**, 259-268.

Clark, R. and Eichhorn, G. (1974). *Biochem*, **13**, 5098.

Cook, R.L., Miller, Y.E., and Bunn, P.A., Jr. (1993). Small cell lung cancer: etiology, biology, clinical features, staging, and treatment. *Curr Probl Cancer*, **17**, 71-141.

De Waard, M., Pragnell, M., and Campbell, K.P., 1994. Calcium channel regulation by a conserved β subunit domain. *Neuron* **13**, 495-503.

De Waard, M., Gurnett, C.A., and Campbell, K.P. (1996). Chapter 2: Structural and functional diversity of voltage-activated calcium channels. In *Ion Channels*, T. Narahashi (ed.), Plenum Press, New York, **4**, 41-87.

Dixon, D.A., Vaitkus, D.L. and Prescott, S.M. (1998). DNase I treatment of total RNA improves the accuracy of ribonuclease protection assay. *Biotechniques*, **24(5)**, 732-734.

Dubel, S.J., Starr, T.V.B. and Hell, J. (1992). Molecular cloning of the α-1 subunit of an ω-conotoxin-sensitive calcium channel. *Proc. Nat. Acad. Sci. U.S.A.*, **89**, 5058-5062.

Ellinor, P. T., Zhang, J. F., Randall, A.D., Zhou, M., Schwarz, T.L., Tsien, R.W., and Horne, W.A., 1993. Functional expression of a rapidly inactivating neuronal calcium channel. Nature, 363, 455-458

Ertel, S.I. and Ertel, E.A. (1996). Low-voltage-activated T-type Ca^{2+} channels. *TiPs*, **18(2)**, 37-42

Falzon, M., McMahon, J.B., Gazdar A.F., and Schuller H.M. (1986a). Preferential metabolism of N-nitrosodietylamine by two cell lines derived from human pulmonary adenocarcinomas. *Carcinogenesis*, **7**, 17-22.

Falzon, M., McMahon, J.B., and Schuller, H.M. (1986b). Xenobiotic-metabolizing enzyme activity in human non-small-cell derived lung cancer cell lines. *Biochemical Pharmacol*, **35**, 563-568.

Farrell, RE (1997). DNA amplification. *Immunol Invest*, **26(1-2)**, 3-7.

Farrell, R.E. (1993). *RNA Methodologies*, Academic Press, Inc. San Diego, CA.

Finnegan M., Goepel, J., Hancock, B.W. and Goyns, M.H. (1993). Investigation of the expression of housekeeping genes in non-Hodgkin's lymphoma. *Leukemia and Lymphoma*, **10(4-5)**, 387-393.

Fischer, S., Spiegelhalder, B., Eisenbarth, J., and Preussmann, R. (1990). Investigation on the origin of tobacco-specific nitrosoamines in mainstream smoke of cigarettes. *Carcinogenesis*, **11**, 723-730.

Fujita, Y., Mynlieff, M., Dirksen, R.T., Kim, M.S., Niidome, T., Nakai, J., Priedrich, T., Iwzbe, N., Miyata, T., Furuichi, T., Furutama, D., Mikoshiba, K., Mori, Y., and Beam, K.G. (1993). Primary structure and functional expression of the ω-conotoxin-sensitive N-type calcium channel from rabbit brain. *Neuron*, **10**, 585-598.

Garrison, J.C. (1990). Histamine, bradykinin, 5-hydroxytryptamine, and their antagonists. In A. Goodman Gilman, T.W. Rall, A.S. Nies, and P. Taylor (eds.). *The Pharmacological Basis of Therapeutics*. Pergamon Press, new York, pp. 575-599.

Gazdar, A.F. (1994). The biology of lung cancer. In K.L. Becker, A.F. Gazdar (eds.), *The Endocrine Lung in Health and Disease*, W.B. Saunders, Philadelphia, pp 448-459.

Gopalakrishnan, M., Buisson, B., Touma, E., Giordano, T., Campbell, J.E., Hu, I.C., Donnelly-Roberts, D., Arneric, S.P., Bertrand, D. and Sullivan, J.P. (1995).

Stable expression and pharmacological properties of the human alpha 7 nicotinic acetylcholine receptor. *Eur J Pharmacol.*, **290(3)**, 237-246.

Gopalakrishnan, M., Monteggia, L.M., Anderson, D.J., Molinari, E.J., Piattoni-Kaplan, M., Donnelly-Roberts, D., Arneric, S.P. and Sullivan, J.P. (1996). Stable expression, pharmacologic properties and regulation of the human neuronal nicotinic acetylcholine alpha 4 beta 2 receptor. *J. Pharmacol Exp Ther*, **276(1)**, 289-297.

Guyton, A.C. and Hall, J.E., (1996). Chapter 39: Principles of gaseous exchange; diffusion of oxygen and carbon dioxide across the respiratory membranes. In *Textbook of Medicial Physiology*. A.C. Guyton and J.E. Hall (eds), W.B. Saunders Company, Philadelphia, PA, Ninth Edition, 501-512.

Hansen, H.H. and Rorth, M. (1997). Chapter 20: Lung Cancer. In *Cancer Chemotherapy and Biological Response Modifiers Annual 17*, H.M. Pinedo, D.L. Longo and B.A. Chabner (eds), Elsevier Science B.V., 444-463.

Hecht, S.S. and Hoffmann, D. (1988). Tobacco-specific nitrosamines, an important group of carcinogens in tobacco and tobacco smoke. *Carcinogenesis*, **9**, 875-884.

Hui, A., Ellinor, P.T., Krizanova, O., Wang, J.J., Diebold, R.J. and Schwartz, A. (1991). Molecular cloning of multiple subtypes of a novel rat brain isoform of the α_1 subunit of the voltage-dependent calcium channel. *Neuron,* **7**, 35-44.

Hullin, R., Singer-Lahat, D., Freichel, M., Biel, M., Dascal, N., Hofmann, F., and Flockerzi, V., 1992. Calcium channel β subunit heterogeneity: Functional expression of cloned cDNA from heart, aorta and brain. *EMBO J.*, **11**, 885-890.

Innis, M., Gelfand, D., Sninsky, J., and White, T. (eds), (1990). *PCR Protocols, A Guide to Methods and Applications*, Academic Press, Inc., San Diego, CA.

Johnson, D.E., and Georgieff, M.K. (1993). Pulmonary perspectives: neuroendocrine cells in health and disease. *Amer Rev Resp Dis*, **140**, 1807-1812.

Kamphuis, W and Henriksen H. (1998). Expression patterns of voltage-dependent calcium channel alpha1 subunits (α_{1A}-α_{1E}) mRNA in rat retina. *Brain Res Mol Brain* Res, **55(2)**, 209-220.

Lindstrom, J., Peng, A.R., Gerzanich, V. (1995). Neuronal nicotinic receptors and function. In *Effects of Nicotine on Biological Systems II*, Clarke, P.B.S., Quick., M. Adlkofer, F., and Thurau, K. (eds.), Birhauser, Basel, 45-50.

Linnoila, I.R. (1990). Pathology of non-small cell lung cancer. *Hematol Oncol Clin North Amer*, **4**, 1027-1051.

Ma, W.J., Holz, W., and Uhler, M.D. (1992). Expression of a cDNA for a neuronal calcium channel α_1 subunit enhances secretion from adrenal chromaffin cells. *J. Biol Chem.*, **267**, 22728-22732.

MacDonald RJ, Swift, G.H., Przybyla, A.E. and Chirgwin, J.M. (1987). Isolation of RNA using guanidinium salts. *Meth Enzymol.*, **152**, 219-227.

Maneckjee, R. and Minna, J.D. (1990). Opioid and nicotinic receptors affect growth regulation of human lung cancer cell lines. *Proc Natl Acad Sci*, **87**, 3294-3298.

McCleskey, E.W. 1994). Calcium channels: cellular roles and molecular mechanisms. *Cur Opin Neurobiol*, **4**, 304-312.

Merryman, J.I., Park, P.G., and Schuller H.M. (1997). Carbon dioxide, an important messenger molecule for small cell lung cancer. *Chest*, **112**, 779-784.

Mikami, A., Imoto, K., Tanabe, T., Niidome, T., Mori, Y., Takeshima, H., Narumiya, S., and Numa, S. (1989). Primary structure and functional expression of the cardiac dihydropyridine-sensitive calcium channel. *Nature,* **340**, 230-233.

Miller, M.S., Fan, M., and Schuller, H.M. (1996). Induction of c-fos expression following stimulation of pulmonary neuroendocrine cell proliferation by alterations in CO_2/O_2 concentration. *Int J Oncol*, **8**, 423-438.

Mitsudomi, T., Viallet, J., Mulshine, J.L., Linnoila, I.R., Minaa, J.D., and Gazdar, A.F. (1991). Mutations of *ras* genes distinguish a subset of nonsmall cell lung cancer cell lines from small cell lung cancer cell lines. *Oncogene,* **6**, 1353-1362.

Mori, Y., Friedrich, T., Kim, M., Mikami, A., Nakai, J., Ruth. P., Bosse, E., Hofmann, F., Flockerzi, V., Furuichi, T., Mikoshiba, K., Imoto, K., Tanabe, T. and Numa, S. (1991). Primary structure and and functional expression from complementary DNA of a brain calcium channel. *Nature,* **350**, 398-402.

Murad, F. (1990). Drugs used for the treatment of angina: organic nitrates, calcium channel blockers and β-adrenergic antagonists. In A. Goodman Gilam, T.W. Rall, A.S. Nies, and P. Taylor (eds.). *The Pharmacological Basis of Therapeutics*. Pergamon Press, new York, pp. 764-783.

Niidome, T., Kim, M.S., Friedrich, T., and Mori, Y. (1992). Molecular cloning and characterization of a novel calcium channel from rabbit brain. *FEBS Lett.*, **308**, 7-13.

Novak E.J. and Rabinovitch P.S. (1994). Improved sensitivity in flow cytometric intracellular ionized calcium measurement using fluo-3/fura red fluorescence ratios. *Cytometry*, **17**, 135-141.

Phelps, M.R., Johnson, B.E., Ihde, D.C., Gazdar, A.F., Carbone, D.P., McClintock, P.R., Linnoila, I., Matthews, M.J., Bunn, P.A., Carney, D., Minna, J.D. and Mulshine, J.L. (1996). NCI-Navy medical oncology branch cell line data base. *J. Cellular Biochemistry Suppl.*, **24**,32-91.

Schuller, H.M. (1989). Cell type specific, receptor-mediated modulation of growth kinetics in human lung cancer cell lines by nicotine and tobacco-related nitrosamines. *Biochem Pharmacol*, **38**, 3439-3442.

Schuller, H.M. (1994). Carbon dioxide potentiates the mitogenic effects of nicotine and its carcinogenic derivative, NNK, in normal and neoplastic neuroendocrine lung cell. *Neurotoxicol*, **15**, 877-886.

Schuller, H.M., Becker, K.L., and Witschi, H.P. (1988). An animal model for neuroendocrine lung cancer. *Carcinogenesis*, **7**, 293-296.

Schuller, H.M., and Hegedus, T.J. (1989). Effects of endogenous and tobacco-related amines and nitrosamines on cell growth and morphology of a cell line derived from a human neuroendocrine lung cancer. *In Vitro Toxicol*, **3**, 37-43.

Schuller, H.M., Witschi H.P., Nylen E.S., Joshi P.A., Correa E., and Becker K.L. (1990). Pathobiology of lung tumors induced in hamsters by 4-(methylnitrosoamino)-1-(3-pyridyl)-1-butanone and the modulating effects of hyperoxia. *Cancer Res*, **50**, 1960-1965.

Schuller, H.M., Correa, E., Orlogg, M., and Reznik, G.K. (1990). Successful chemotherapy of experimental neuroendocrine lung tumors in hamsters with an antagonist of Ca^{2+}/calmodulin. *Cancer Res*, **50**, 1645-1649.

Schuller, H.M., McGavin M.D., Orlogg, M., Reichert, A. and Porter B. (1995). Simulataneous exposure to nicotine and hyperoxia causes tumors in hamsters. *Lab Invest*, **73(3)**, 448-456.

Schuller, H.M. and Orloff, M. (1998). Tobacco-specific carcinogenic nitrosamines. *Biochemical Pharmacology*, **55**, pp ?

Segar, R. and Krebs, E.G. (1995). MAP kinase signaling cascade. *FASEB J*, **9**, 726-735.

Seino, S., Chen, L., Seino, M., Blondel, O., Takeda, J., Johnson, J.H., and Bell, G.I. (1992). Cloning of the α1 subunit of a voltage-dependent calcium channels expressed in pancreatic β cells. *Proc. Natl. Acad. Sci. U.S.A.*, **89**, 584-588.

Snutch, T.P., Leonard, J.P., Gilbert, M.M., Lester, H.A., and Davidson, N., 1990. Rat brain expresses a heterogeneous family of calcium channels, *Proc Natl. Acad. Sci. USA*, **87**, 3391-3395.

Snutch, T.P., Tomlinson, W.J., Leonard, J.P., and Gilbert, M.M. (1991). Distinct calcium channels are generated by alternative splicing and are differentially expressed in the mammalian CNS. *Neuron,* **7**, 45-57.

Soong, T.W., Stea, A. and Hodson, C.D. (1993). Structure and functional expression of a member of the low voltage-activated calcium channels family. *Science, N.Y.*, **260**, 1133-1136.

Starr, T.V.B., Prystay, W., and Snutch, T.P. (1991). Primary structure of a calcium channel that is highly expressed in the rat cerebellum. *Proc. Nat. Acad. Sci. U.S.A.*, **88**, 5621-5625.

Stea, A., Dubel, S.J., Pragnell, M., Leonard, J.P., Campbell, K.P. and Snutch, T.P., 1993. A β-subunit normalizes the electrophysiological properties of a cloned N-type calcium channel α_1-subunit. *Neuropharmacology* **32**: 1103-1116.

Stea, A., Soong, T.W. and Snutch T.P. (1995). Voltage-gated calcium channels. In *Handbook of Receptors and Channels,* 113-150.

Tanabe, T., Mikami, A., Numa, S., and Beam, K.G., 1990 . Cardiac-type excitation-contraction coupling in dysgenic skeletal muscle injected with cardiac dihydropyridine receptor cDNA. *Nature,* **344**: 451-453.

Tsien, R.W., Ellinor, P.T., and Horne, W.A. (1991). Molecular diversity of voltage-dependent Ca^{2+} channels. *TiPS*, **121**, 349-354.

Uchitel, O.D. (1997). Review Article: Toxins affecting calcium channels in neurons. *Toxicon*, **35(8)**, 1161-1191.

Wagenaar, S.S. and Tazelaar, H.D. (1994). Ten years after the WHO classification of lung cancer: where are we? *Lung Cancer*, **11**, S39-S43.

Weiss, W. (1991). COPD and lung cancer. In N.S. Cherniak (ed), Chronic Obstructive Pulmonary Disease, W.B. Saunders, Philadelphia, pp. 344-347.

Wickman, K. and Clapham D.E. (1995). Ion channel regulation by G proteins. *Physiol Rev,* **75(4)**, 865-885.

Williams, M.E., Brust, P.F. Feldman, D.H, Patthi, S., Simerson, S., Maroufi, A., McCue, A.F., Velicelebi, G., Ellis, S.B., and Harpold, M. (1992a). Structure and functional expression of an ω-conotoxin-sensitive human N-type calcium channel. *Science, N.Y.*, **257**, 389-395.

Williams, M.E., Feldman, D.H., McCue, A.F., Brenner, R., Velicelebi, G., Ellis, S.B., and Harpold, M.M. (1992b). Structure and functional expression of α_1, α_2, and β subunits of a novel human neuronal calcium channel subtype. *Neuron,* **8**, 71-84.

Williams, M.E., Marubio, L.M., Deal, C.R., Hans, M., Brust, P.F., Philipson, L.H., Miller, R.J., Johnson, E.C., Harpold, M.M., and Ellis, S.B. (1994). Structural and functional characterization of neuronal α_{1E} Ca^{2+} channel subtypes. *J. Biol. Chem,* **269(35)**, 22347-22357.

Yesner, R. (1993). Lung cancer pathogenesis and pathology. *Clinics in Chest Med*, **14**, 17-30.

Youngson, C., Nurse, C., Yeger, H., and Cutz, E. (1993). Oxygen sensing in airway chemoreceptors. Nature, 365, 153-155.

VITA

Barbara Jane Sheppard was born in Washington, District of Columbia, USA on November 25, 1963. She graduated from the Virginia Polytechnic Institute & State University with a B.S. in Biology having an emphasis in biomedical engineering in 1986 and a M.S. in 1989. She was inducted into Phi Kappa Phi during graduate studies. She graduated with the Doctorate of Veterinary Medicine from the College of Veterinary Medicine, North Carolina State University in 1993 and was inducted into the veterinary honor society Phi Zeta. Following graduation, she worked for one year in private practice in Dover, Delaware performing a combination of small animal work in Dover for Governor's Avenue Animal Hospital and mobile equine duties throughout the Delmarva peninsula for Delmarva Equine Practice. The next two years, 1994-1996, were spent in an Anatomic and Surgical Pathology Residency at the College of Veterinary Medicine, University of Florida in Gainesville. Her resident's research project on FIV infection of feline astrocytes with Calvin Johnson, DVM, PhD was awarded a competitive resident research grant and she was honored as the Ancillary Resident of the Year by the graduating class. In 1999, she received a PhD in the Comparative and Experimental Medicine Program within the Department of Pathology at the College of Veterinary Medicine, University of Tennessee as a NIEHS Postdoctoral Trainee. The first year of the PhD was spent within the Mammalian Genetics Division of the Oak Ridge National Laboratory. Her PhD dissertation, guided by her major advisor Hildegard M. Schuller, DVM, PhD, examined the role of calcium in the nicotine stimulated

serotonergic autocrine mitogenic pathway of human small cell lung carcinoma.

In the spring of 1999, she moved to New Haven, Connecticut to the Department of Pathology in the College of Medicine at Yale University for a postdoctoral position in the laboratory of David Rimm, MD, PhD researching new molecular genetics approaches to diagnosing and studying neoplasia.